Modelling and simulation of a packed-bed heat-exhange process

MODELLING AND SIMULATION OF A PACKED-BED HEAT-EXCHANGE PROCESS

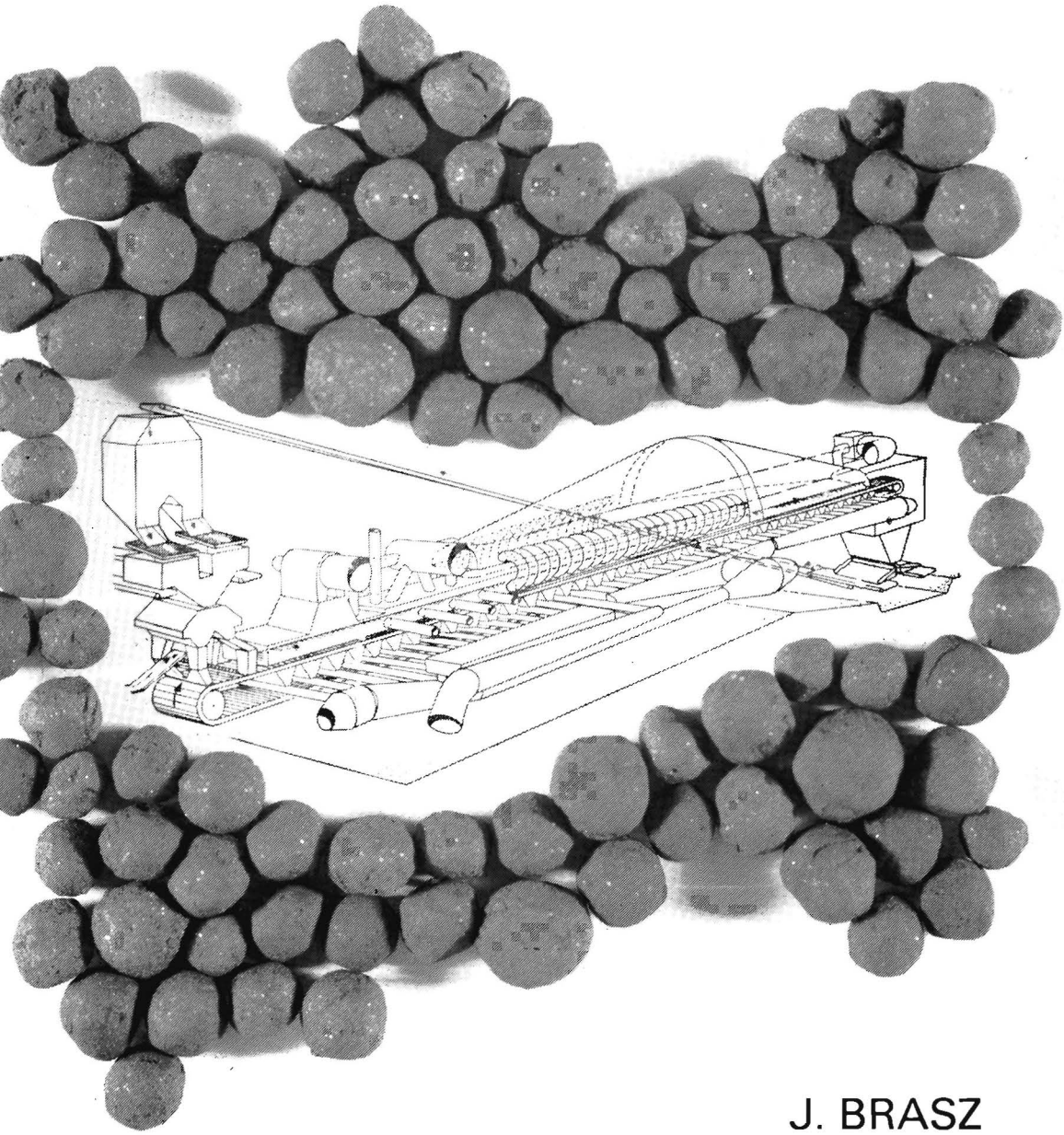

J. BRASZ

MODELLING AND SIMULATION OF A PACKED-BED HEAT-EXCHANGE PROCESS

MODELLING AND SIMULATION OF A PACKED-BED HEAT-EXCHANGE PROCESS

P R O E F S C H R I F T

ter verkrijging van de graad van doctor in de technische wetenschappen aan de Technische Hogeschool Eindhoven, op gezag van de rector magnificus, prof.dr. P. van der Leeden, voor een commissie aangewezen door het college van dekanen in het openbaar te verdedigen op vrijdag 11 maart 1977 te 16.00 uur

door

J O O S T B R A S Z

geboren te Amsterdam

DIT PROEFSCHRIFT IS GOEDGEKEURD
DOOR DE PROMOTOREN

Prof.ir. O. Rademaker

en

Prof. ir. J.E. Rijnsdorp

voor Ulla

C O N T E N T S

Chapter One

GENERAL INTRODUCTION

1.1 MOTIVATION OF THE STUDY

In the process industry various kinds of plants are encountered in which a bed of solid particles is treated by a stream of fluid flowing through it. When the bed of solid particles is fixed, the treatment of the fluid is of first importance, as e.g. in regenerators where the solid material is used to heat or cool gas, or in chemical reactors where the solid particles are used as carriers of the catalyst to enhance a desired reaction of the fluid. In moving-bed processes, when the bed is transported through an installation by a grate, the heat treatment of the solid particles by the fluid is usually of first importance. Examples of these processes are clinker coolers, sintering plants, pellet-drying and -indurating machines.

The Measurement and Control Group of the Department of Technical Physics of Eindhoven University of Technology was confronted with such moving-bed plants when studying the dynamics and control of a cement clinker cooler /55/ and a pellet-indurating plant /68/ [+]).

In principle, such moving-bed processes can be considered as gas-solid cross-flow heat exchangers where a horizontally moving bed of solid particles is cooled or heated by vertical gas streams (see Figure 1.1). The exchange of heat will cause a change of gas as well as solid temperatures and as a consequence other processes may take place like drying, sintering and chemical conversion.

The construction of a mathematical model of the heat and mass transfer behaviour of a moving bed process results in a set of coupled non-linear partial-differential equations with respect to in principle five independent variables, viz. time t, horizontal coordinates x and y, vertical position z and

[+]) see note at page 7

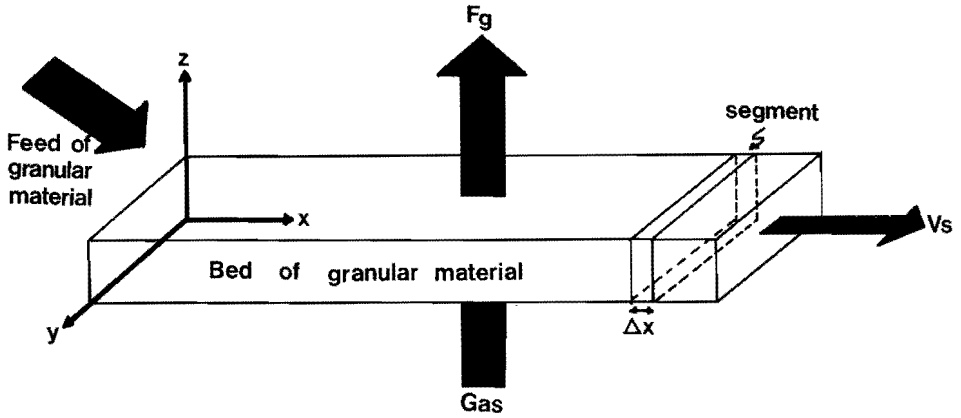

Figure 1.1 Diagrammatic representation of a gas-solid cross-flow heat exchanger

location r inside the solid particles. Irregular shapes and sizes of the particles may further complicate the analysis.

The study of this type of process is not only of practical value but also theoretically interesting. A search of the literature turns up many papers on modelling and simulation of fixed-bed processes like regenerators and chemical reactors, but very few about moving-bed processes. Recently, a static model of a pellet-indurating machine /44/ and a very simple dynamic model of a sinter strand process /14/ have been published.

Also, in contrast to co-current and counter-current heat exchangers, little is known about the dynamic behaviour of cross-flow heat exchangers: the few publications about this subject /5,45,50/ all deal with heat exchangers of a different type, viz. liquid-liquid /45,50/ and gas-liquid /5/ instead of gas-solid. Moreover, these publications consider only the effect of temperature variations, with the exception of the study of Bender /5/ that takes the effect of flow disturbances into account. In addition, in all simulations only one spatial dimension is considered. For a gas-solid cross-flow heat exchanger this simplification is not allowed, because of the large temperature gradients both horizontally and vertically.

Little has been published by other groups concerning the

dynamics and control of a pellet-indurating plant. In the only paper known to us, Henry and Smeaton /32/ offer only a few suggestions about computer-control possibilities without discussing the dynamics of the plant. For any fundamental control study a dynamic model is required of which a fast simulation (digital, analog or hybrid) can be obtained. Because of the fact that the basic physical laws of moving-bed processes result in a set of complicated partial-differential equations, the possibilities of model reduction beforehand, using overall quantities, has been investigated. Even after this model reduction, the resulting mathematical model was difficult to simulate. The model equations are different from the equations normally encountered in literature in that partial-differential equations with respect to three independent variables occur with only first-order differential quotients. A dynamic simulation on present-day computers shows the following characteristics: long computing times are used by digital machines, much hardware is needed by analog machines and much storage capacity is demanded by hybrid ones.

Therefore, the work described here aimed at developing more practicable simulation methods for the dynamic behaviour of moving packed-bed heat-exchange processes.

1.2 DESCRIPTION OF THE PROCESS

In ironmaking, blast furnace charges are more and more prepared by means of pellet-indurating plants instead of sintering installations because the use of pellets is more economical /23/. The object of iron-ore pelletising is to produce firm, hard balls (about 0.01 m in diameter) from finely ground ore. These pellets must have sufficient strength and suitable chemical properties to serve as blast furnace charge material. Therefore, after balling, the wet green pellets are indurated (heat hardened). In commercial practice a shaft furnace, a moving grate, or a moving grate and kiln combination are normally used for this induration process.

In this study, the pellet-indurating plant of the Royal Netherlands Blast Furnaces and Steelworks at IJmuiden in the

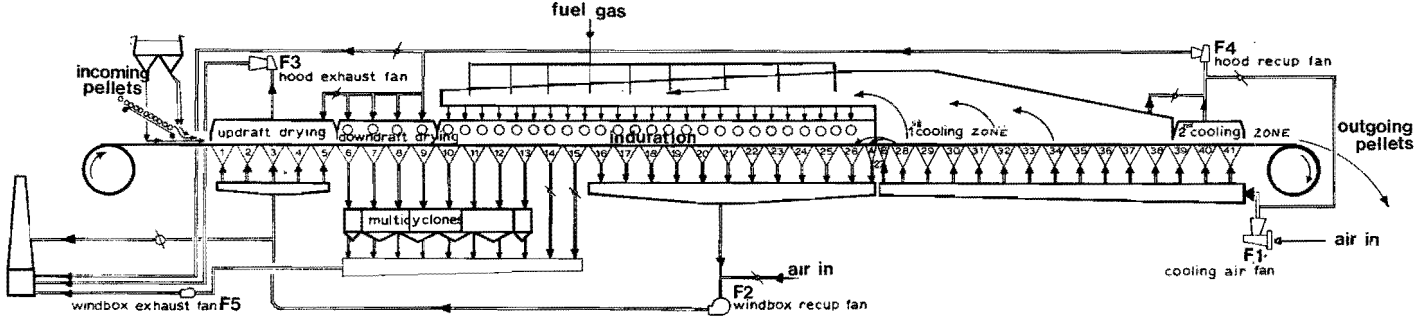

o o o o : gas-fired burners

	Number of boxes*	Location	Surface area (m^2)
Updraft-drying zone	5	1-5	52.5
Downdraft-drying zone	4	6-9	42
1st Induration zone (fan F5)	6	10-15	63
2nd Induration zone (fan F2)	11.5	16-27A	120.75
1st Cooling zone	11.5	27B-38	120.75
2nd Cooling zone	3	39-41	31.5

* Dimensions of one windbox - length: 3m width: 3.5m

Figure 1.2 Diagram of the pellet-indurating plant

Netherlands, a moving grate unit designed by Lurgi /42/, will be analysed. A sketch of the plant is given in Figure 1.2. The wet green pellets coming from the balling plant are loaded onto a moving grate via a roller-conveyor which screens out the smallest pellets, thus preventing blockage of the bed. The remaining pellets are deposited as a layer of about 0.3 m height on top of a so-called hearth-layer of 0.1 m height consisting of indurated pellets covering the grate for protection.

The grate with pellets moves through the various zones of the plant where the pellets are dried, indurated (fired) and cooled to obtain the required physical properties. The total length of the plant is 123 m, the width of the grate is 3.5 m, the speed normally 0.04 - 0.08 m s^{-1}. In the induration zones an exothermic reaction takes place converting the magnetite in the iron ore into hematite. For the production of good quality pellets all green pellets must achieve sintering temperatures during a prescribed period of time (more than 1300 ^{o}C for at least two minutes). But also, as the strength of the grate decreases rapidly with higher temperatures, care must be taken that the grate temperature does not exceed its maximum admissible value (650 ^{o}C). The division of the induration area in two zones connected to different fans, is a good device enabling to meet both the quality and the temperature requirements. As somewhere halfway the second induration zone enough heat has been transferred to the bed to obtain the required sintering temperature at the bottom of the layer of green pellets, the gas temperature in the remainder of this zone may be lowered. Having accomplished the induration, cooling is started and in order to prevent overheating of the grate an updraft blowing system is used.

Looking at the indurating machine from the gas side, two main streams can be distinguished. One flowing upwards through the second cooling zone, downwards through the downdraft-drying zone and, with the help of fan F5 (see Figure 1.2) to the stack. The other stream flows upwards

through the first cooling zone, downwards through the induration zone and fan F2, and again upwards through the updraft-drying zone. This stream is divided in the first part of the induration zone where part of the gas is blown to the stack. Ambient air is added to the hot exhaust gas stream leaving the second induration zone in order to protect fan F2 against overheating.

A great amount of heat is re-used. The air coming out of the first cooling zone is used as combustion air for the fuel in the induration section. The air coming out of the second cooling zone is used as a drying agent in the downdraft-drying zone. The gases leaving the last section of the induration zone are used for the updraft drying zone. Because of the repeated use of the same gas flow, disturbances occurring in one zone readily propagate into another zone. Because of the resulting interaction between zones in the indurating plant combined with the high operating costs, the indurating plant proved to be an interesting object for control studies. As

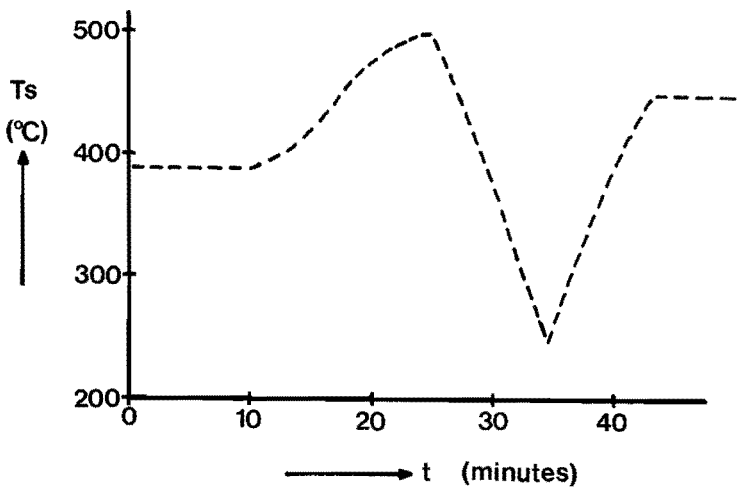

Figure 1.3 Pellet temperature response halfway the cooling section after a porosity step disturbance at $t = 0$.

an example of the consequences of the interactions between the various zones the pellet temperature response halfway the cooling section after a porosity step disturbance is shown in Figure 1.3. To understand the phenomena taking place in the pellet-indurating machine during transients a dynamic model must be constructed and solved.

1.3 OUTLINE OF THE THESIS

The outline of this thesis is as follows: After the general introduction of Chapter 1, the model-building activity is described in Chapter 2. Possible simulation strategies are reviewed in Chapter 3. Chapter 4 compares the effectiveness of various integral-transform methods for the simulation of a segment (a slice) of the pellet bed (see Figure 1.1). In Chapters 5 to 8 four different simulation methods for a whole bed or compartment, viz.:

- a digital simulation in the time domain,
- a digital simulation in the frequency or Laplace domain,
- a hybrid simulation,
- an RC-network simulation,

are applied to the cooling zone of the pellet-indurating plant.

Each of these methods lends itself as well to simulation of the induration zone (gas flowing downward) - if the ore contains little or no magnetite the chemical reaction can be ignored - coupled to the cooling zone (gas flowing upward), and changes in the bed porosity in the drying zone can also be taken into account.

Chapter 9 attempts to present a critical evaluation of the various methods: advantages and drawbacks of the different simulation techniques are summarised and the generality of the results is discussed in view of the underlying assumptions.

NOTE: In order to make a clear distinction all references to publications in which the auther was involved are identified in underlined italics whereas the references from already existing literature are denoted in roman types.

Chapter Two

MODELLING

2.1 INTRODUCTION

The word *model* is used in the sense of *mathematical model* by which we mean any collection of algebraic, differential and/or integral equations or inequalities which describe the behaviour of the process. *Modelling* or *model building* is defined as the activity of choosing and defining process variables and deriving mathematically expressed relationships between them /18/.

In extremis, two different approaches of the modelling activity may be distinguished /21/: on the one hand the *physical approach*, using laws of conservation of mass, energy and momentum, and physical and chemical relations like the kinetic equations for chemical reactions, or the equations describing phase changes, e.g. the transition of liquid to gas, and on the other hand the *black-box approach*, using input and output data collected from an operating process to estimate the model parameters of a priori postulated relationships between process variables. These parameters rarely have a physical meaning.

In practice, the physical approach tends to be used when theoretical knowledge of the process is available, when there are poor possibilities (or none at all!) to experiment and when the modelling is not too expensive. Advantages of the physical approach are that - in contrast to the black-box approach - it can be started before the actual plant exists, which may result in valuable design and start-up information, that it may lead to conclusions relevant to other, similar processes, that the influence of different physical parameters can be investigated, and that it may give deeper insight into the system, thereby serving as a valuable guide to the design, operation or improvement of the process. A disadvantage of

the physical approach is that it is generally computationally tedious.

As described above, the distinction is essential, but in practice both extremes are hardly ever used: mixed approaches abound. Even when it is undesirable from the point of view of continuous plant operation to do measurements on the process, some tests have to be performed in order to get an idea about the reliability of the physical model and, when necessary, appropriate corrections have to be made. Also, certain unknown interrelations may have to be determined experimentally. Conversely, when following the black-box approach certain model parameters may easier be obtained from elementary physical considerations than from identification experiments.

Because of the fact that there were few chances to do enough identification experiments in the industrial environment of the pellet-indurating plant and because, at first, the pellet plant was still only in the design stage and little was known about potential start-up problems, it was decided to follow the physical approach of model building.

In this approach, i.e. modelling the system from first principles for a particular purpose, many assumptions have to be made. Indeed, the art of the model building is to make assumptions such that the resulting model represents as accurately as desired and as simply as possible the principal process characteristics that we are interested in. The main assumptions used in model building the pellet-indurating plant are presented and discussed explicitly in Section 2.2. In Section 2.3 it will be shown that for a spherical particle, under the prevailing conditions, heat conduction inside the pellets is fast compared with heat exchange between gas and pellets, so that uniform internal temperatures come about. In this way the use of a model without internal pellet temperature gradients is justified and a considerable reduction of the complexity of the model is obtained. The resulting model equations for a segment moving along with the pellet bed are derived in Section 2.4. In Section 2.5 the

model equations will be extended to the whole bed.

2.2 *ASSUMPTIONS*

Studies about the static behaviour of the complete indurating plant /*69*/ showed that - within the normal range of operating conditions - changes in input variables of the drying zones do not influence overall plant behaviour considerably, whereas many input variables of the firing and cooling zones were found to play an important part. Therefore, it was decided to restrict the dynamic studies of the plant to the firing and cooling zones (i.e. Box 10 - 41 in Figure 1.2). The following assumptions are used:

Assumption 1: Pellet inlet conditions

As the wet green pellets have been dried sufficiently in the drying zones, they enter the first firing zone with zero moisture content, in spite of small variations in e.g. grate velocity or gas flow rate during transportation in the drying zones. The corresponding changes in pellet temperature at the inlet of the first firing zone are small compared with the temperature rise which the pellets undergo during the induration process. Therefore, as inlet conditions for the first firing zone the moisture concentration will be taken zero and the pellet temperatures will be considered as input variables independent of the conditions in the firing and cooling zones, but not independent of time and height.

Assumption 2: Uniform distribution of pellets over the bed

Because the transport of pellets on the moving grate is going on rather smoothly, any redistribution of pellets, for example in vertical direction with the big ones moving to the top and the small ones down to the bottom of the bed, will not take place. The effect of bursting or wastage of the pellets and dust from the pellets carried along by the gas flow on e.g. the porosity of the bed or the heat transfer between gas and pellets, is rather unlikely to be significant under the prevailing conditions and, hence, will be neglected.

Assumption 3: Rectangular pellet bed and constant overall dimensions

It is assumed that the height of the bed of pellets does not change during transport through the plant. Hardly any pellets are lost through the grate during transportation through the installation. Also the effect of shrinkage of the pellets on the height and the other dimensions of the pellet bed can be neglected, for the experiments of Ross and Ohno /59/ show that the shrinkage of briquettes of magnetite and hematite iron ore mixtures during induration is only a few percent.

Assumption 4: Interchange with environment

The grate on which the pellets are transported will be heated or cooled by the gas flow. It is described by the same equations as those of a layer of pellets, with adapted values for the heat capacity and the heat exchanging surface.

There are other interchanges of the pellet bed and the gas flow with the enviromment which usually result in loss of heat and/or mass at the boundaries of the bed. Owing to the large size of the bed and the design of the plant, only negligible quantities of heat and material will be lost compared with the total amount which is processed. Hence, these losses are neglected. Their incorporation will be briefly resonsidered in Chapter 9.

Assumption 5: Independence of the y direction

All (heat) transport phenomena are taken independent of the y direction (the pellet and gas streams flow in the x and z directions, respectively; see Figure 1.1 for the orientation of the spatial coordinates).

Assumption 6: Plug-flow gas stream

The gas flow in the bed can be described as forced transitional (i.e. between laminar and turbulent) flow. The presence of particles obliges the stream to undergo constant splitting and intermingling, so that the conditions of plug flow are better approached than for a stream with the same mean velocity in an empty tube /53/. No channeling effects have been observed in pot-test experiments. The compression term of the gas has been neglected because of the small pressure differences over the bed ($\Delta P \simeq 4 * 10^3\ Nm^{-2}$) and the

small changes in gas pressure. The plug-flow assumption does not imply that the gas flow rate is independent of the horizontal position x. On the contrary, due to its strong temperature dependence (see Assumption 8) the gas flow rate changes much with horizontal position. Moreover, its direction in the induration zones is downward whereas it is upward in the cooling zones.

Assumption 7: Neglection of the accumulation term in the heat balance of the gas

For a unit volume of the bed the heat capacity of the gas, given by

$$\mu g = \varepsilon \rho g \gamma g \tag{2.1}$$

with

γg = specific heat of the gas [J K^{-1} kg^{-1}]
ε = void fraction of the bed [-]
μg = heat capacity of the gas in the bed [J K^{-1} m^{-3}]
ρg = density of the gas [kg m^{-3}]

is small compared with the heat capacity of the pellets

$$\mu s = (1-\varepsilon) \rho s \gamma s \tag{2.2}$$

with

γs = specific heat of the pellet material [J K^{-1} kg^{-1}]
μs = heat capacity of the pellets in the bed [J K^{-1} m^{-3}]
ρs = density of the pellet material [kg m^{-3}].

Hence, the time constants of the gas temperatures can be neglected as compared with the pellet-temperature time constants.

Assumption 8: ΔP - Fg relation

Ergun /22/ confirmed by accurate experiments that a satisfactory relationship between the gas flow rate through an isothermal packed bed and the pressure difference over the bed under laminar, transitional and turbulent flow conditions is given by the expression

$$A_1 \eta g \, Fg + A_2 \, Fg^2 = - \frac{\rho g \, \Delta P}{Z} \tag{2.3}$$

where

Fg = gas flow rate [kg m^{-2} s^{-1}]

Z = height of the bed [m]

ΔP = pressure drop over the bed [N m^{-2}] = [kg m^{-1} s^{-2}]

ηg = viscosity of the gas [kg m^{-1} s^{-1}]

while the constants A_1 and A_2, which are independent of temperature, pressure drop, gas flow rate and height of the bed, are defined as

$$A_1 = \frac{150(1-\varepsilon)^2}{(\phi\ dp)^2 \varepsilon^3} \quad \text{and} \quad A_2 = \frac{1.75(1-\varepsilon)}{(\phi\ dp)\ \varepsilon^3}$$

with

dp = diameter of the pellets [m]

ϕ = shape factor (which is 1 for spherical particles) [-]

The first term of (2.3) is the viscous term which is predominant for laminar flow and the second term is the friction term which prevails in turbulent flow.

In the strongly non-isothermal pellet bed, the Ergun relation is not valid as both the density and the viscosity of the gas are temperature dependent. Therefore, use has been made of the extended Ergun relationship of Szekely and Carr /65/ which is reported to agree fairly well with measurements in such situations

$$\frac{Fg^2}{2\varepsilon^2} \ln \frac{\rho g_{in}}{\rho g_{out}} + \int_0^Z (A_1\ \eta g\ Fg + A_2\ Fg^2) dz = -\int_{P(0)}^{P(Z)} \rho g\ dP \qquad (2.4)$$

where ρg_{in} is the inlet density of the gas at $z=0$ and ρg_{out} the outlet density at $z=Z$.

There are two differences between (2.3) and (2.4): firstly, because of the large change in density of the gas when passing through the bed, a kinetic energy term has been added, viz. the first term at the left hand side of (2.4) and, secondly, the differential form of the mechanical energy balance (2.3) has been used to take the temperature dependence of ηg and ρg into account.

The integrals in (2.4) have to be determined numerically,

e.g. by division of a segment (see Figure 2.2) into N layers

$$Fg^2\{\sum_{n=1}^{N} \frac{1}{\rho g_n}\frac{1}{2\varepsilon^2}\ln\frac{\rho g_{n-1}}{\rho g_n} + A_2\Delta z\} + Fg\{\sum_{n=1}^{N}\frac{A_1\,\eta g_n}{\rho g_n}\Delta z\} = -\Delta P \quad (2.5)$$

where the index n refers to the local situation at layer n. Hence, given the pressure difference over the bed and the vertical gas temperature profile (necessary to evaluate ρg and ηg at various heights in the bed), the gas flow rate can be found from the quadratic relation (2.5). Because of the strong pellet- and gas-temperature dependence on the horizontal position x, the gas flow rate also depends on x.

Assumption 9: Heat transport

In the horizontal x direction heat transport is primarily governed by advection owing to the moving bed of pellets. All other horizontal heat transport mechanisms, such as transport of heat between pellets by conduction or radiation, and advective heat transport by horizontal dispersion of the vertical gas stream as a result of the constant splitting and intermingling of the gas through the pellet bed, are neglected.

Similarly, it is assumed that in the vertical z direction heat is transported only by advection owing to the gas stream. Again, all radiative, conductive and dispersive contributions may be neglected. Experimental support is given in /22a/.

Assumption 10: Heat transfer

Heat transfer between gas and solid occurs only when gas and solid are in contact with each other. Radiative effects may be incorporated in the overall heat transfer coefficient U [J K^{-1} m^{-2} s^{-1}]. In practice, the parameter U is often used as a fiddle factor to fit the simulation results as well as possible to the experimental data.

Assumption 11: Uniform internal pellet temperature

The heat conductivity of the solid is assumed to be so large that, given the processing conditions, the temperature differences inside the pellets are negligible during any transient of importance. In this case the pellets may have

any shape and size as long as the condition of uniform internal temperature is fulfilled. If one is dealing with a bed consisting of irregular particles, one must hope that this assumption is satisfied because otherwise modelling of the packed bed is impossible, but in the case considered here, the pellets are almost spherical. In Section 2.3 the justification and consequences of this assumption of uniform internal pellet temperatures will be discussed in more detail.

Assumption 12: Chemical reaction

In the induration zones an exothermal reaction takes place if the ore contains magnetite (Fe_3O_4), which then becomes

$$4\ Fe_3O_4 + O_2 \rightarrow 6\ Fe_2O_3 + (-\Delta H) \qquad (2.6)$$

where $(-\Delta H)$ is the heat of reaction [J mole^{-1}]. In certain cases the effect of this reaction was studied and then it was supposed to obey the equation

$$r(Cs,Ts) = Cs\ k = Cs\ k_0\ e^{-\frac{E}{R(Ts + 273)}} \qquad (2.7)$$

where

Cs = concentration of magnetite [mole m^{-3}]
E = activation energy [J mole^{-1}]
k = rate coefficient [s^{-1}]
k_0 = velocity constant [s^{-1}]
r = reaction rate [mole m^{-3} s^{-1}]
R = universal gas constant [J mole^{-1} K^{-1}]
Ts = solid temperature [^{o}C]

Assumption 13: Uniform and constant chemical composition of the gas

The chemical reaction (2.6) consumes oxygen from the gas. Due to the large gas throughput, only a few percent of the available oxygen is used for the reaction. Therefore, the change in chemical composition of the gas as function of time and position can be neglected.

Assumption 14: Uniform oxygen concentration inside the pellets

Because of the assumption of uniform internal pellet temperature (Assumption 11) and the uniform and constant chemical composition of the gas (Assumption 13), the magnetite concentration remains also uniformly distributed over the pellet, i.e. no radial concentration gradients originate due to chemical reaction if diffusion of oxygen through the pellet goes fast enough so that a uniform oxygen concentration inside the pellet is always maintained. Subject to this proviso, the oxygen concentration can be incorporated in the velocity constant k_0 of the reaction rate equation (2.7).

Assumption 15: Quasi-constant coefficients

The heat capacity of the pellets μs and the specific heat of the gas γg are known functions of temperature /54/. This dependence is so weak that, when working with locally constant coefficients, no errors of significance will be made. Hence, in each zone an average value has been used. The overall heat transfer coefficient U (see also Section 2.3) is a function of gas flow rate and temperature. For the flow dependence a simple square-root relation has been applied

$$U = U_0 \sqrt{Fg} \qquad (2.8)$$

with

U_0 = temperature-dependent coefficient [J K^{-1} $kg^{-\frac{1}{2}}$ m^{-1} $s^{-\frac{1}{2}}$]

Also here, the temperature dependence is relatively weak and use will be made of zone-averaged values for U_0. These values were determined experimentally by matching steady-state model results with experimental data. The coefficient values for the various zones are presented in Table 2.1.

Table 2.1 Parameter values of locally constant coefficients

quantity	1st firing zone	2nd firing zone	1st cooling zone	2nd cooling zone	dimension
μs	1650	2200	1900	1480	kJ K^{-1} m^{-3}
γg	1.13	1.16	1.13	1.08	kJ K^{-1} kg^{-1}
μ_{grate}	3580	4800	4130	3190	kJ K^{-1} m^{-3}
U_0	0.036	0.042	0.029	0.024	kJ $kg^{-\frac{1}{2}}K^{-1}m^{-1}s^{-\frac{1}{2}}$

Post scriptum: It is perhaps useful to point out that certain assumptions have not been made, for example are porosity, gas flow rate and gas inlet temperature changes possible as function of the horizontal position x.

2.3 *EFFECT OF INTERNAL PELLET TEMPERATURE GRADIENTS*

Lebelle et al. from Hoogovens /43/ constructed a static model of the pellet-indurating plant in which they took the radial heat conduction inside the pellets into account. They did not use our assumption of uniform internal pellet conditions, but introduced new assumptions to be able to derive their model equations, viz.

a. all pellets are spherical,

b. all pellets have the same size,

c. the pellets are equally contacted over the surface by the gas stream. From a photograph of a random sample of indurated pellets (Figure 2.1) it can be seen that the pellets are only roughly spherical (the wet pellets coming from the balling discs have different sizes and are deformed during transport on the conveyor belt because of their softness)/34/.

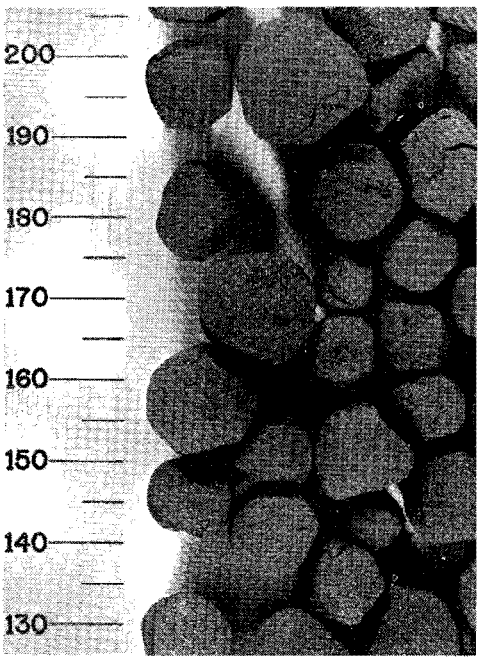

Figure 2.1

Photograph of some arbitrarily selected pellets on mm-scale

Owing to the packing of the pellets, the gas stream will not contact the surface uniformly.

Although the assumptions a, b and c are open to question, the simulation results of Lebelle et al. are in good agreement with corresponding results of our simplified model assuming uniform internal pellet conditions /69/, as well as with their own pot-test measurements /43/. Apparently, the heat conduction is indeed so large that temperature differences inside the pellets can be neglected.

It will now be demonstrated for spherical particles (an analytical treatment which takes internal pellet-temperature differences into account, is only feasible with such a simple geometry) that under pellet-bed conditions, heat transport inside the pellets by means of conduction is so fast compared with gas-pellet heat exchange that uniform internal pellet temperatures come about.

Consider a segment of the pellet bed and assume that all pellets are indeed spherical with the same radius and equally contacted over the surface by the gas stream. For a spherical particle of uniform and constant density ρs, specific heat γs and conductivity λs [J K^{-1} m^{-1} s^{-1}] the Fourier equation for heat conduction within a pellet at height z in the segment is

$$\frac{\partial Ts(r,z,\theta)}{\partial \theta} = \kappa s \left[\frac{\partial^2 Ts(r,z,\theta)}{\partial r^2} + \frac{2}{r} \frac{\partial Ts(r,z,\theta)}{\partial r} \right] \qquad (2.9)$$

where

$$\kappa s = \frac{\lambda s}{\rho s \ \gamma s} \qquad (2.10)$$

with

r = distance to the centre of the pellet [m]
Ts = temperature within the pellet [°C]
θ = residence time of the segment in the compartment [s]
κs = thermal diffusivity of the pellet material [m^2 s^{-1}]

The residence time θ tells us how far the segment has progressed through the plant, by means of the relation

$$x = \int_0^{\theta} Vs(\tau)\, d\tau \qquad (2.11)$$

where

Vs = grate velocity [m s^{-1}]

x = covered distance [m]

The boundary conditions for (2.9) are

$$\left.\frac{\partial Ts(r,z,\theta)}{\partial r}\right|_{r=0} = 0 \qquad (2.12)$$

$$\lambda s \left.\frac{\partial Ts(r,z,\theta)}{\partial r}\right|_{r=R} = h\,\{Tg(z,\theta) - Ts(r=R,z,\theta)\} \qquad (2.13)$$

and the initial condition is

$$Ts(r,z,\theta=0) = Ts_0 \qquad (2.14)$$

where

h = heat transfer coefficient [J m^{-2} K^{-1} s^{-1}]

R = radius of the pellet [m]

Tg = gas temperature [°C]

Neglecting, according to Assumption 7, the non-stationary accumulation term in the gas heat balance and assuming constant gas flow rate Fg and specific heat γg, this balance can be written as

$$\gamma g\, Fg \frac{\partial Tg(z,\theta)}{\partial z} = h\, A\, \{Ts(r=R,z,\theta) - Tg(z,\theta)\} \qquad (2.15)$$

with boundary condition

$$Tg(z=0,\theta) = Tg_{in}(\theta) \qquad (2.16)$$

where

A = heat transfer area between gas and pellets per unit volume of the pellet bed [m^{-1}]

Tg_{in} = inlet gas temperature of the segment [°C]

The equations (2.9) to (2.16) together describe the thermal behaviour of a pellet in the cooling zone. They can be solved

analytically after application of central differences with respect to the z direction. The accuracy of this segmentation will be discussed in Chapter 4. In this way Equation (2.15) goes over into

$$\gamma g\ Fg\ \{Tg_n(\theta) - Tg_{n-1}(\theta)\} = h\ A\ \frac{Z}{N}\ \{Ts_{a,n}(R,\theta) - Tg_{a,n}(\theta)\} \qquad (2.17)$$

The use of central differences can be visualised by division of the height Z of the segment into N Layers (see Figure 2.2) and introducing for each layer $n=1,2,\ldots,N$ the following approximations

$$\left.\frac{\partial Tg(\theta)}{\partial z}\right|_{n-\frac{1}{2}} = \frac{Tg_n(\theta) - Tg_{n-1}(\theta)}{Z/N} \qquad (2.18)$$

and

$$Tg_{a,n} = \frac{1}{2}\ (Tg_{n-1} + Tg_n) \qquad Ts_{a,n} = \frac{1}{2}\ (Ts_{n-1} + Ts_n) \qquad (2.19)$$

where Tg_{n-1} and Tg_n are the input and output gas temperatures of layer n, respectively. $Tg_{a,n}$ is the average gas temperature in layer n. $Ts_{a,n}$ is the average solid temperature in layer n.

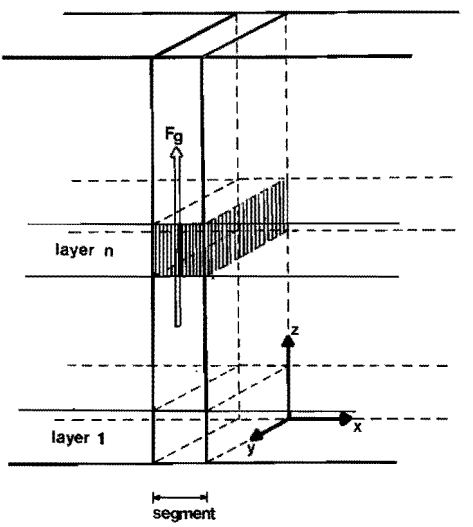

Figure 2.2 Division of a segment into layers

Substitution of a new variable

$$u_n(r,\theta) = r\, Ts_{a,n}(r,\theta) \tag{2.20}$$

into (2.9), (2.13) and (2.17) yields, for layer n

$$\frac{\partial u_n(r,\theta)}{\partial \theta} = \kappa s \frac{\partial^2 u_n(r,\theta)}{\partial r^2} \tag{2.21}$$

$$\frac{1}{R}\frac{\partial u_n(r,\theta)}{\partial r}\bigg|_{r=R} = -\frac{h}{\lambda s}\left[\frac{u_n(R,\theta)}{R} - Tg_{a,n}(\theta)\right] + \frac{u_n(R,\theta)}{R^2} \tag{2.22}$$

$$\gamma g\, Fg\, \{Tg_n(\theta) - Tg_{n-1}(\theta)\} = h\, A\, \frac{Z}{N}\left[\frac{u_n(R,\theta)}{R} - Tg_{a,n}(\theta)\right] \tag{2.23}$$

Laplace transformation of (2.21) with respect to time (introducing q as the Laplace variable) yields a second-order ordinary-differential equation in r which is easily solved with the boundary condition for $r = 0$ /57/, provided the initial temperature (see (2.14)) is independent of the radius.

$$\tilde{u}_n(r,q) = \frac{\sinh(r\sqrt{\frac{q}{\kappa s}})}{\sinh(R\sqrt{\frac{q}{\kappa s}})}\{\tilde{u}_n(R,q) - \frac{R\, Ts_0}{q}\} + \frac{r\, Ts_0}{q} \tag{2.24}$$

Now $\tilde{u}_n(R,q)$ can be found by differentiation of (2.24) with respect to r and substitution into the transform of boundary condition (2.22), which yields

$$\frac{\tilde{u}_n(R,q)}{R} = \frac{1}{G(q)}\tilde{Tg}_{a,n} + \frac{\lambda s}{h\, R}\left[R\sqrt{\frac{q}{\kappa s}}\coth(r\sqrt{\frac{q}{\kappa s}}) - 1\right]\frac{Ts_0}{q} \tag{2.25}$$

where

$$G(q) = 1 + \frac{\lambda s}{h\, R}\left[R\sqrt{\frac{q}{\kappa s}}\coth(R\sqrt{\frac{q}{\kappa s}}) - 1\right] \tag{2.26}$$

Suppose that 1 m^3 pellets contains P pellets. These pellets will have a total heat capacity

$$\mu s = \frac{4}{3}\pi R^3 P\, \rho s\, \gamma s \tag{2.27}$$

and a gas-pellet contact surface

$$A = 4 \pi R^2 P \tag{2.28}$$

Together with (2.10) we get the following expression for λs

$$\lambda s = \frac{3 \kappa s \mu s}{A R} \tag{2.29}$$

Substitution of (2.29) into (2.25) and the transformed version of (2.23) gives, if (2.23) and (2.25) are combined to eliminate $\tilde{u}_n(R,q)$,

$$\tilde{T}g_n(q) = \frac{1 + \tau_1 \frac{3\kappa s}{R^2} \{R\sqrt{\frac{q}{\kappa s}} \coth(R\sqrt{\frac{q}{\kappa s}}) - 1\}}{1 + \tau_2 \frac{3\kappa s}{R^2} \{R\sqrt{\frac{q}{\kappa s}} \coth(R\sqrt{\frac{q}{\kappa s}}) - 1\}} \left[\tilde{T}g_{n-1}(q) - \frac{Ts_0}{q}\right] + \frac{Ts_0}{q} \tag{2.30}$$

with

$$\tau_1 = \mu s \{\frac{1}{hA} - \frac{1}{2 \gamma g Fg N/Z}\} \tag{2.31}$$

$$\tau_2 = \mu s \{\frac{1}{hA} + \frac{1}{2 \gamma g Fg N/Z}\} \tag{2.32}$$

Choosing Ts_0 as the zero point of the temperature scale, the relation between the temperature of the gas leaving *any* layer n and the gas inlet temperature of a segment becomes

$$\frac{\tilde{T}g_n(q)}{\tilde{T}g_0(q)} = \left[\frac{1 + \tau_1 \frac{3\kappa s}{R^2} \left[R\sqrt{\frac{q}{\kappa s}} \coth(R\sqrt{\frac{q}{\kappa s}}) - 1\right]}{1 + \tau_2 \frac{3\kappa s}{R^2} \left[R\sqrt{\frac{q}{\kappa s}} \coth(R\sqrt{\frac{q}{\kappa s}}) - 1\right]}\right]^n \tag{2.33}$$

Obviously, the response of the gas *outlet* temperature of the segment is found by replacing n by N.

The amplitude ratio and phase shift of this transfer function for typical coefficient values of the cooling zone of the pellet-indurating plant are plotted in the Bode diagram in Figure 2.3. Curve a represents the situation with finite internal conductivity $\lambda s = 0.58$ J K^{-1} m^{-1} s^{-1} and

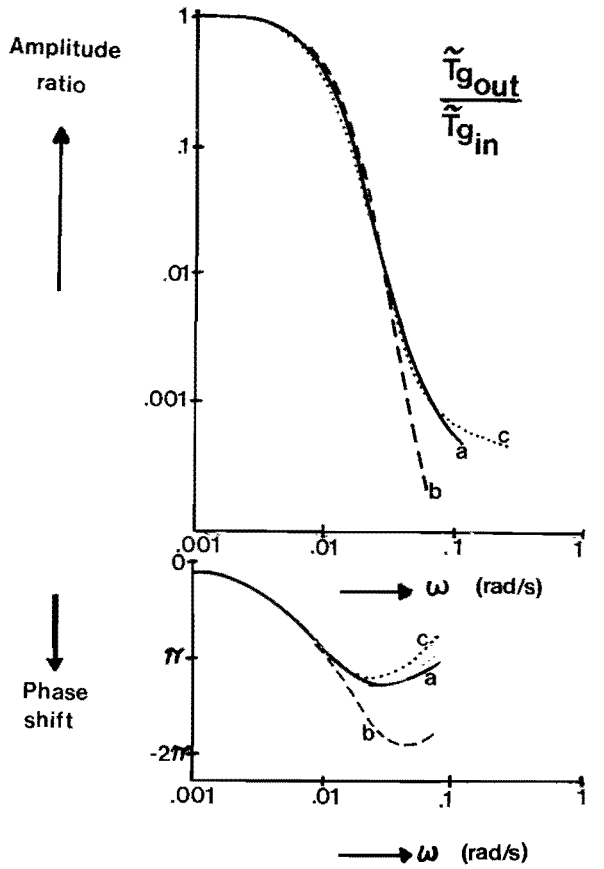

Figure 2.3 Frequency response of the outlet gas temperature of a segment after an inlet gas temperature disturbance
Curve a: situation with finite conductivity
Curve b: situation with infinite conductivity and unchanged heat transfer coefficient
Curve c: situation with infinite conductivity and adapted heat transfer coefficient

h = 210 J K^{-1} m^{-2} s^{-1}. If we make the assumption of uniform internal temperature, i.e. infinite thermal conductivity, the frequency response according to Curve b comes about, where $\lambda s = \infty$ and h = 210 J K^{-1} m^{-2} s^{-1}. As we shall explain below, the heat transfer coefficient h can be adapted so as to take the conductivity inside the pellet into account. A better approximation of Curve a is obtained for $\lambda s = \infty$ with h = 140,

as is shown by Curve c. Now, the approximate solution is satisfactory up to the frequency $\omega = 4 \times 10^{-2}$ rad s^{-1}, i.e. heat transfer phenomena with periods of two minutes will still be described satisfactorily in spite of the neglection of the internal pellet temperature gradients. Such an adapted value of h is called an "overall heat-transfer coefficient" and will be denoted by a separate symbol U.

Compared with the total processing time of the pellets on the moving grate, which is about 30 minutes, signal components in the frequency range above, say, $\omega = 0.1$ rad s^{-1} will not play any part of importance in the dynamic behaviour of the total plant. It will be shown in the subsequent simulation chapters that the main time constants of the process are at least an order of magnitude larger.

The inverse Laplace transformation of (2.33) is simple in a number of cases, for example if $n=1$ and the gas inlet temperature is constant

$$\hat{T}g_0(q) = \frac{Tg_0}{q} \tag{2.34}$$

Then, the solution is given by /57/

$$Tg_1(\theta) = Tg_0 - \sum_{l=1}^{\infty} C_l \, e^{-p_l^2 \, \kappa s \, \theta / R^2} \tag{2.35}$$

in which

$$C_l = \frac{2\,(1 - \tau_1/\tau_2)\left[\dfrac{sin(p_l)}{p_l} - cos(p_l)\right]}{1 - cos(p_l)\dfrac{sin(p_l)}{p_l}} \; \frac{sin(p_l)}{p_l} \tag{2.36}$$

where p_l represents the roots of

$$p_l \, coth(p_l) - 1 + \frac{R^2}{3 \, \kappa s \, \tau_2} = 0 \tag{2.37}$$

Equation (2.35) gives the output gas temperature response of

of a pellet layer if the input gas temperature is constant for residence time $\theta > 0$. Hence, it describes the temperature behaviour around the transport grate very accurately.

Differentiation of (2.35) with respect to θ yields the impulse response of one layer and by means of convolution integrals the behaviour of the complete segment could, in principle, be calculated. This calculation, however, is very cumbersome and unremunerative for practical purposes.

The effect in time domain of introducting an overall heat transfer coefficient U can be seen in Figure 2.4 /69/ where Curve a represents the output gas temperature of *one* pellet layer with initial temperature of 1200°C, cooled by a gas flow of 15°C found analytically according to the equations (2.9) to (2.16). Curve b represents the same case, but with uniform temperature ($\lambda s = \infty$) and the same heat transfer coefficient as in Curve a. Curve c is calculated with an adapted (smaller) value for h. It intersects Curve a twice, and apart from its values at very small values of θ, Curve c is a fairly good approximation of Curve a. The curves as presented in Figure 2.4 have been calculated for a few different set of parameters. It must be added that in the example of this figure, the diameter is about twice as large as the average pellet diameter. The reason is that with large diameters the effect can be better demonstrated. The differences between the three curves would have been about four times smaller with a more realistic pellet diameter of 0.01 m.

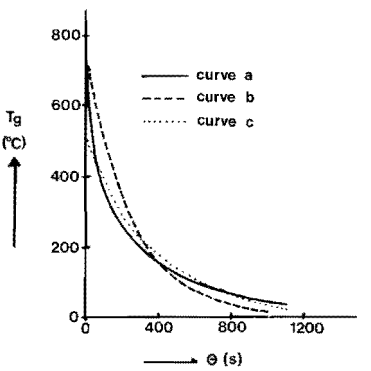

Figure 2.4 The effect of finite thermal conductivity in time domain

The procedure of taking an adapted value for the heat transfer coefficient to compensate for the approximation of infinite internal conduction can be visualised by considering an RC-network analog for the problem of heating or cooling a pellet. In Figure 2.5 the RC analog of heat transfer (resistance) and conduction (RC-ladder network) is shown. If the ladder network only consists of two interacting RC circuits, the transfer function is

$$\frac{\hat{T}s(r=0,q)}{\hat{T}g(q)} = \frac{1}{(R+R_1)C_1R_2C_2q^2 + \{(R+R_1)(C_1+C_2)+(R_2C_2)\}q + 1} \qquad (2.38)$$

If we neglect internal conduction without changing the heat transfer coefficient $h(\sim 1/R)$, the transfer function becomes

$$\frac{\hat{T}s(r=0,q)}{\hat{T}g(q)} = \frac{1}{R(C_1+C_2)q + 1} \qquad (2.39)$$

A better approximation of (2.38) will be obtained when we take instead of R in (2.39)

$$R^* = R + R_1 + R_2 \frac{C_2}{C_1 + C_2} \qquad (2.40)$$

which means a smaller value for the overall heat transfer coefficient $U = 1/R^*$ than for the convective heat transfer coefficient $h = 1/R$.

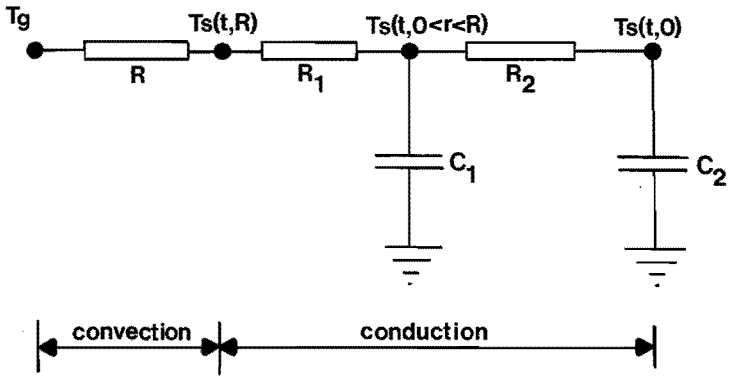

Figure 2.5 RC analog for heat transfer by convection and conduction

2.4 MOVING SEGMENT EQUATIONS

Starting from the equations (2.9) to (2.16) which describe the thermal behaviour of a segment of the pellet bed including internal pellet temperature differences, in this section the segment equations based on uniform internal pellet conditions will be derived.

Integration of (2.9) multiplied by $4\pi r^2$ with respect to r from the center of the pellet $r=0$ to the boundary $r=R$ yields

$$\int_0^R 4\pi r^2 \frac{\partial Ts(r,z,\theta)}{\partial \theta} dr = \int_0^R 4\pi r^2 \kappa s \{\frac{\partial^2 Ts(r,z,\theta)}{\partial r^2} + \frac{2}{r}\frac{\partial Ts(r,z,\theta)}{\partial r}\} dr \quad (2.41)$$

Defining a volumetric mean temperature by

$$Ts^*(z,\theta) = \frac{1}{\frac{4}{3}\pi R^3} \int_0^R Ts(r,z,\theta)\, 4\pi r^2 dr \quad (2.42)$$

and assuming mathematical properties of the function $Ts(r,z,\theta)$ such that integration with respect to r and differentiation with respect to θ may change order, (2.41) can be written as

$$\frac{4}{3}\pi R^3 \frac{\partial Ts^*(z,\theta)}{\partial \theta} = \int_0^R 4\pi r^2 \kappa s \left[\frac{\partial^2 Ts(r,z,\theta)}{\partial r^2} + \frac{2}{r}\frac{\partial Ts(r,z,\theta)}{\partial r}\right] dr \quad (2.43)$$

The right-hand side of (2.43) may be evaluated as follows

$$\int_0^R 4\pi r^2 \kappa s \{\frac{\partial^2 Ts}{\partial r^2} + \frac{2}{r}\frac{\partial Ts}{\partial r}\} dr = \int_0^R 4\pi r^2 \kappa s \frac{\partial^2 Ts}{\partial r^2} dr + \int_0^R 8\pi r\, \kappa s \frac{\partial Ts}{\partial r} dr = \quad (2.44)$$

$$= \int_0^R 4\pi r^2 \kappa s \frac{\partial^2 Ts}{\partial r^2} dr + 4\pi r^2 \kappa s \frac{\partial Ts}{\partial r}\Big|_0^R - \int_0^R 4\pi r^2 \kappa s \frac{\partial^2 Ts}{\partial r^2} dr$$

Hence, by means of (2.12)

$$\frac{4}{3}\pi R^3 \frac{\partial Ts^*(z,\theta)}{\partial \theta} = 4\pi R^2 \kappa s \frac{\partial Ts(r,z,\theta)}{\partial r}\Big|_{r=R} \quad (2.45)$$

Using (2.10) and (2.13) we find that

$$\frac{4}{3}\pi R^3 \rho s\ \gamma s\ \frac{\partial Ts^*(z,\theta)}{\partial \theta} = h\ 4\pi R^2\ \{Tg(z,\theta) - Ts(R,z,\theta)\} \qquad (2.46)$$

In the derivation up till now we did not assume infinite heat conductivity. However, in general, the pellet temperature at the surface of the pellet $Ts(R,z,\theta)$ will not be equal to the mean pellet temperature $Ts^*(z,\theta)$, when - because of finite heat conductivity - a temperature gradient exists inside the pellet.

If we approximate $Ts(R,z,\theta)$ by $Ts^*(z,\theta)$, the absolute value of the right-hand side of (2.46) increases causing the average pellet temperature to change too rapidly. This was compensated by replacing the gas-pellet heat transfer coefficient h by the smaller overall heat transfer coefficient U as shown in Section 2.3. In this way we find instead of (2.46) and (2.15)

$$\mu s\ \frac{\partial Ts^*(z,\theta)}{\partial \theta} = U\ A\ \{Tg(z,\theta) - Ts^*(z,\theta)\} \qquad (2.47)$$

$$\gamma g\ Fg\ \frac{\partial Tg(z,\theta)}{\partial z} = U\ A\ \{Ts^*(z,\theta) - Tg(z,\theta)\} \qquad (2.48)$$

with initial and boundary conditions

$$Ts^*(z,\theta=0) = Ts^*_0(z) \qquad (2.49)$$

$$Tg(z=0,\theta) = Tg_{in}(\theta) \qquad (2.50)$$

This set of equations describes the thermal behaviour of a segment moving along with the pellets through the plant.

2.5 TOTAL BED EQUATIONS

The equations (2.47) to (2.50) can be extended to the whole bed of particles by defining instead of the residence time θ the time t and the horizontal location in the bed x (see also (2.11)). Then the heat balances for an infinitesimal element of the pellet bed result in the following set of partial differential equations

$$\mu s \frac{\partial Ts(x,z,t)}{\partial t} + \mu s\ Vs(t) \frac{\partial Ts(x,z,t)}{\partial x} = U(Fg(x,t))\ A\ \{Tg(x,z,t) - Tg(x,z,t)\} \tag{2.51}$$

$$\gamma g\ Fg(x,t) \frac{\partial Tg(x,z,t)}{\partial z} = U(Fg(x,t))\ A\ \{Ts(x,z,t) - Tg(x,z,t)\} \tag{2.52}$$

The gas flow rate Fg, denoted as function of x and t, depends on ε, ΔP and Tg according to (2.4)

$$\frac{Fg^2}{2\varepsilon^2} ln \frac{\rho g_{in}}{\rho g_{out}} + \int_0^Z (A_1\ \eta g\ Fg + A_2\ Fg^2)dz = - \int_{P(0)}^{P(Z)} \rho g\ dP \tag{2.4}$$

The overall heat transfer coefficient is a function of Fg

$$U = U_0 \sqrt{Fg} \tag{2.8}$$

μs, γg and U_0 are locally constant (sse Table 2.1 on page 16). If the assumption of uniform internal pellet conditions also applies to a (small) magnetite concentration inside the pellet, the material balance gives

$$\frac{\partial Cs(x,z,t)}{\partial t} + Vs(t) \frac{\partial Cs(x,z,t)}{\partial x} = - k(Ts)\ Cs(x,z,t) \tag{2.53}$$

and to the right-hand side of (2.51) an extra term $(-\Delta H)\ k\ Cs$ must be added to represent the heat produced by the chemical reaction. The rate coefficient k depends on the pellet temperature according to (2.7)

$$k(Ts) = k_0\ e^{- \frac{E}{R(Ts+273)}} \tag{2.7}$$

The accompanying initial and boundary conditions are

$$Ts(x,z,t=0) = Ts_0(x,z) \tag{2.54}$$

$$Cs(x,z,t=0) = Cs_0(x,z) \tag{2.55}$$

$$Ts(x=0,z,t) = Ts_{in}(z,t) \tag{2.56}$$

$$Cs(x=0,z,t) = Cs_{in}(z,t) \tag{2.57}$$

$$Tg(x,z=0,t) = Tg_{in}(x,t). \tag{2.58}$$

For a simulation of the dynamic behaviour of the pellet-indurating plant the equations (2.51) to (2.53) together with the equations (2.4), (2.7) and (2.8) must be solved.

For a comparison of the effectiveness of different simulation methods the addition of Equation (2.53) does not fundamentally change the problem. Moreover, when pure hematite ores are processed in the indurating plant, no chemical reaction can be ignored and the pellet-bed equations are essentially the same for indurating and cooling zones.

Let us now take a closer look at the equations (2.51), (2.52), (2.4) and (2.8), for, after all, mathematical modelling not only serves to arrive at quantitative simulation results, but also to gain insight into the model's behaviour, by inspection of the equations as well as by (approximate) analytical solution. The equations (2.51) and (2.52) form a set of hyperbolic partial-differential equations with differential quotients with respect to three independent variables x, t and z. At first sight they have a simple structure with attractive features like one-way influences (see Figure 5.3).

For a set of hyperbolic partial-differential equations the solution at a certain point in space and time is completely determined by the initial and/or boundary conditions which are situated on the same characteristic as the point of which the solution is required. Physically speaking, this comes down to the solution by following a segment moving along with the bed. In this way, i.e. solving the partial differential equations along the characteristics, the total bed equations go over again into the moving segment equations (2.47) and (2.48). Under certain simplifying assumptions these equations can be solved analytically as is shown in Chapter 4.

However, the additional equation (2.8) and especially the

flow-pressure drop relation like (2.4) or any similar expression, complicate the solution of (2.51) and (2.52) enormously. For the gas flow rates $Fg(t,x)$ are significantly dependent on the pressure drop ΔP, the bed porosity ε and the gas temperatures $Tg(t,x,z)$ everywhere in the bed. Hence, due to variations in pellet and gas temperatures in the bed during transients, the gas flow distribution over the bed will also change. Therefore, inside a zone, all flows and temperatures are influenced by and have an effect on all other flows and temperatures. Moreover, since the total gas flow rate to a zone of the bed is coupled with the pressure difference over the bed by means of one or more appropriate fan characteristics, the total gas flow rate through a compartment can change, which will have an effect on other compartments of the plant where the same gas stream is flowing through. In this way, all temperatures and flows are coupled with all other temperatures and flows everywhere in the bed.

In order to avoid burdening the discussion that follows with the complications of taking the interactions between the indurating and the cooling zones into account, we shall subsequently limit the discussion to the cooling zones of the pelletising plant, but the results are equally applicable to the burning zones. In Chapter 9 we shall briefly reconsider the problem introduced by the coupling.

Due to these interactions, the solutions for the moving segment equations were found to be of little use for the dynamic simulation of the bed equations together with (2.4) and (2.8). Hence, the studies of the moving segment equations mainly served as a first guide to get insight in the problem and to find the necessary number of layers in a segment for an accurate simulation of the vertical temperature profiles, resulting in a so-called β-rule /57/.

However, although we do not transform the equations (2.51) and (2.52) to their characteristic form, this does not mean that we did not make advantage of the fact that the solution is determined on a characteristic path. As will be shown in Section 5.4, the numerical integration method used in the

digital calculation in the time domain takes such a ratio for the time and position intervals that the equations are in fact solved for points lying on the characteristic.

Chapter Three

TRANSFORMATION METHODS

3.1 INTRODUCTION

The difficulties in solving the dynamic bed equations are caused by the distributed character together with the nonlinearity of the equations. In case certain assumptions and/or approximations are permissible, feasible solutions can be obtained after transformation of the equations into a more manageable form. For the purpose of analog and hybrid simulation the equations are approximated by a set of difference-differential euqtaions and for digtal simulation by a set of difference equations.

In Section 3.2 the backward- and central-difference approximations, which will be used in the subsequent chapters, are applied to a single first-order differential equation and are shown to be mathematically sound.

The equations (2.51) and (2.52) have to be solved together with (2.5) and (2.8) which determine the values of Fg and $\dot{U}$. The non-linear character together with the coupling of these equations complicates the solution. A considerable saving of computations can be obtained by linearisation. In Section 3.3 the linearisation procedure is described and applied to the model equations.

Linear(ised) partial-differential equations can also be simplified to ordinary-differential equations or pure algebraic equations by means of integral-transform methods. In Section 3.4 some of them are surveyed and Laplace transformation is found to be preferable.

Linear partial-differential equations can be solved analytically without segmentation. In Chapter 4, however, it will be shown for a segment of the pellet bed that segmentation methods are superior.

By means of the transformation methods discussed in this

chapter the moving bed equations can be prepared for simulation on digital, hybrid or analog computers.

3.2 FINITE-DIFFERENCE METHODS

In literature about process dynamics /15,27/ the transformation of (partial-)differential equations to difference(-differential) equations is mostly performed as follows: the continuous space and/or time coordinates which occur in the differential operator(s) are divided into a number of segments within which the time- and/or space-dependent variables are assumed to be uniform. The values of these dependent variables in successive segments are obtained by defining input and output variables for a segment and equating each input of a segment to an output of a preceding segment, etc. By means of a simple relationship a value can be assigned to the variable in the segment: if a so-called backward-difference approximation is used, the outgoing value of the segment is taken equal to the value in the segment, and with a central-difference approximation the value in the segment is taken equal to the arithmetic mean of incoming and outgoing values.

We call this procedure to transform a differential equation into a set of difference equations *segmentation*. In the various dialects encountered in literature, many synonyms exist for segmentation, e.g. lumping, discretisation, taking finite differences.

The distributed character of the equations (2.51) and (2.52) is removed by segmentation of the space-dependent quantities, e.g. temperatures Ts and Tg, gas flow rate Fg, heat transfer coefficient U and specific heats μs and γg. We are forced to follow this procedure, since, except for some simple field problems /26/, no analog machines are available which simulate three-dimensional partial-differential equations. When using analog or hybrid simulators, one of the independent variables may remain continuous, while in digital calculations segmentation must be applied to all continuous independent variables.

The process of segmentation will be discussed in general in this section. As different finite-difference schemes will be used for various simulations, the actual transformations of (2.51) and (2.52) to their respective finite-difference approximations will be postponed to Sections 2 of Chapters 5 to 8. Here, only a short survey will be given of the applied difference schemes and of some of their mathematical properties.

The process equations that are obtained after segmentation and backward- or central-difference approximation of the original differential equations are equal to the equations that represent some linear multistep algorithms. Following the numerical analysis of Lambert /41/, we will show for a first-order differential equation that these algorithms - and hence the resulting backward- and central-difference approximations - are *consistent*, *stable* and *convergent*.

Consider the boundary value problem for a single first-order differential equation

$$\frac{df}{dx} = \phi(x,f) \tag{3.1}$$

with boundary condition

$$f(0) = f_0 \tag{3.2}$$

We seek a solution in the range $0 \leq x \leq X$ and we assume that the problem has a unique, continuously differentiable solution, which we shall indicate by $f(x)$. Consider the sequence of points $\{x_m\}$ defined by $x_m = m\ \Delta x$, $m=0,1,2,\ldots,M$. The parameter Δx is called the steplength. We seek an approximate solution on the discrete set $\{x_m | m=0,1,2,\ldots,M=X/\Delta x\}$. Let f_m be an approximation to the exact solution at x_m, that is, to $f(x_m)$, and let $\phi_m = \phi(x_m,f_m)$. If a computational method for determining the sequence $\{f_m\}$ takes the form of a linear relationship between f_{m+j}, ϕ_{m+j}, $j=0,1,\ldots,k$, we call it a linear k-step method. The general linear multistep method may thus be written as

$$\sum_{j=0}^{k} \alpha_j f_{m+j} = \Delta x \sum_{j=0}^{k} \beta_j \phi_{m+j} \tag{3.3}$$

where α_j and β_j are constants. We assume that $\alpha_k \neq 0$ and that not both α_0 and β_0 are zero. Since (3.3) can be multiplied on both sides by the same constant without altering the relationship, we assume that $\alpha_k = 1$.

The method (3.3) is explicit if $\beta_k = 0$, and implicit if $\beta_k \neq 0$. For an explicit method, equation (3.3) yields the current value f_{m+k} directly in terms of f_{m+j}, ϕ_{m+j}, $j=0,1,\ldots,k-1$, which at this stage of the computation, have already been calculated. An implicit method, however, will call for the solution, at each stage of the computation, of the equation

$$f_{m+k} = \Delta x\ \beta_k\ \phi(x_{m+k}, f_{m+k}) + \psi \tag{3.4}$$

where ψ is a known function of the previously calculated values f_{m+j}, ϕ_{m+j}, $j=0,1,\ldots,k-1$. When the original differential equation in (3.1) is linear, then (3.4) is also linear in f_{m+k}, and there is no problem in solving it.

To determine the coefficients α_j, β_j, we consider the Taylor-series expansion of $f(x_m+\Delta x)$ about x_m:

$$f(x_m+\Delta x) = f(x_m) + \Delta x \left.\frac{df}{dx}\right|_{x=x_m} + \frac{(\Delta x)^2}{2!} \left.\frac{d^2f}{dx^2}\right|_{x=x_m} + \ldots. \tag{3.5}$$

If we truncate this expansion after two terms and substitute for $\frac{df}{dx}$ the differential equation (3.1), we have

$$f(x_m+\Delta x) = f(x_m) + \Delta x\ \phi(x_m, f(x_m)) \tag{3.6}$$

a relation which is in error by

$$\frac{(\Delta x)^2}{2!} \left.\frac{d^2f}{dx^2}\right|_{x=x_m} + \frac{(\Delta x)^3}{3!} \left.\frac{d^3f}{dx^3}\right|_{x=x_m} + \ldots \tag{3.7}$$

Equation (3.6) expresses an *approximate* relation between *exact* values of the solution of (3.1). We can also interpret it as an *exact* relation between *approximate* values of the solution of (3.1) if we replace $f(x_m)$, $f(x_m+\Delta x)$ by f_m, f_{m+1}, respectively, yielding

$$f_{m+1} = f_m + \Delta x\ \phi_m \tag{3.8}$$

an explicit linear one-step method. It is, in fact, Euler's rule, the simplest of all linear multistep methods. This relation is also known as forward-difference approximation. The error associated with it is given by the expression (3.7).

In the same way Taylor-series expansion of $f(x_{m+1}-\Delta x)$ about x_{m+1} gives the backward-difference approximation

$$f_{m+1} = f_m + \Delta x\ \phi_{m+1} \tag{3.9}$$

which is the simplest implicit one-step method. This relation is in error by

$$\frac{(\Delta x)^2}{2!}\left.\frac{d^2 f}{dx^2}\right|_{x=x_{m+1}} - \frac{(\Delta x)^3}{3!}\left.\frac{d^3 f}{dx^3}\right|_{x=x_{m+1}} + - \ldots \tag{3.10}$$

Similar techniques can be used to derive any linear method of given specification. Thus if we wish to find the most accurate one-step implicit method

$$f_{m+1} + \alpha_0 f_m = \Delta x\ (\beta_1 \phi_{m+1} + \beta_0 \phi_m) \tag{3.11}$$

we write down the associated approximate relationship

$$f(x_m+\Delta x) + \alpha_0 f(x_m) = \Delta x\{\beta_1 \left.\frac{df}{dx}\right|_{x=x_m+\Delta x} + \beta_0 \left.\frac{df}{dx}\right|_{x=x_m}\} \tag{3.12}$$

and choose α_0, β_1, β_0 so as to make the approximation as accurate as possible. The following expansions are used

$$f(x_m+\Delta x) = f(x_m) + \Delta x \left.\frac{df}{dx}\right|_{x=x_m} + \frac{(\Delta x)^2}{2!}\left.\frac{d^2 f}{dx^2}\right|_{x=x_m} + \ldots \tag{3.13}$$

$$\left.\frac{df}{dx}\right|_{x=x_m+\Delta x} = \left.\frac{df}{dx}\right|_{x=x_m} + \Delta x \left.\frac{d^2 f}{dx^2}\right|_{x=x_m} + \frac{(\Delta x)^2}{2!}\left.\frac{d^3 f}{dx^3}\right|_{x=x_m} + \ldots \tag{3.14}$$

Substituting in (3.12) and collecting the terms on the left-hand side gives

$$C_0 f(x_m) + C_1 \Delta x \left.\frac{df}{dx}\right|_{x=x_m} + C_2 (\Delta x)^2 \left.\frac{d^2 f}{dx^2}\right|_{x=x_m} + C_3 (\Delta x)^3 \left.\frac{d^3 f}{dx^3}\right|_{x=x_m} + \ldots \simeq 0 \qquad (3.15)$$

where

$$C_0 = 1 + \alpha_0$$

$$C_1 = 1 - \beta_1 - \beta_0$$

$$C_2 = \frac{1}{2} - \beta_1$$

$$C_3 = \frac{1}{6} - \frac{1}{2}\beta_1$$

Thus, on order to make the approximation (3.12) second-order correct, we choose $\alpha_0 = -1$, $\beta_1 = \beta_0 = \frac{1}{2}$. C_3 then takes the value $-1/12$.

The linear second-order one-step method can now be described by

$$f_{m+1} = f_m + \frac{\Delta x}{2}(\phi_{m+1} + \phi_m) \qquad (3.16)$$

the trapezoidal rule or central-difference approximation. Its local truncation error is

$$-\frac{1}{12}(\Delta x)^3 \left.\frac{d^3 f}{dx^3}\right|_{x=x_m} + \ldots \qquad (3.17)$$

For the numerical simulation of (2.51) and (2.52) we use backward and central finite-difference methods. A basic property which we demand of the finite-difference methods is that the solution generated by the methods converges to the exact solution as the step length tends to zero. Before investigating whether our difference methods meet these requirements, some mathematical properties have to be defined.

By definition, the linear multistep method (3.3) is said to be *convergent*, if for all boundary value problems (3.1), (3.2)

$$\lim_{\substack{\Delta x \to 0 \\ m\Delta x = x_m}} f_m = f(x_m) \qquad (3.18)$$

holds for all $x \in [0,X]$, and for all solutions $\{f_m\}$ of the difference equation (3.3) satisfying boundary condition (3.2).

The linear multistep method (3.3) is defined to be of *order* p if in (3.15) $C_0 = C_1 = \ldots = C_p = 0, \quad C_{p+1} \neq 0$.

Also by definition, the linear multistep method (3.3) is said to be *consistent* if it has order $p \geq 1$.

The first characteristic polynomial of the linear multistep method (3.3) is defined as

$$\rho(\zeta) = \sum_{j=0}^{k} \alpha_j \zeta^j \tag{3.19}$$

By definition the linear multistep method (3.3) is said to be *stable*, if no root of the first characteristic polynomial (3.19) has a modulus greater than one, and if every root with modulus one is simple, a condition that is bound to appeal to any control engineer. The necessary and sufficient conditions for a linear multistep method to be convergent are that it be consistent and stable, as is shown in /41/.

Application of the definition of consistency and stability to (3.9) and (3.16) immediately shows the convergence property of the backward- and central-difference approximations for ordinary differential equations.

A more general definition of consistency is that the segmented equations reduce to the original (partial) differential equation in the limit of vanishing interval length. Stability is defined more generally as the condition that the solution of the differential equation problem remains finite in a finite time interval.

Multidimensional versions of backward- and central-difference approximations are derived in Chapter 5. They yield practical finite-difference schemes for the numerical solution of (2.51) and (2.52), which are known in mathematical literature as the first- and second-order correct, implicit difference formulae for hyperbolic partial differential equations /48/. By the method of Von Neumann /48/ it can be proven that both difference approximations are again consistent, stable and convergent.

3.3 LINEARISATION

When the solution of a non-linear *static* model requires a large number of time-consuming calculations (in the case of the pellet-indurating plant gas flow rates are determined for each segment as a function of pressure drop, and the void fraction and gas temperatures in all other segments, and the heat transfer coefficients are calculated as functions of the gas flows), the digital simulation of a *dynamic* model may become even more time consuming than a static simulation, unless, of course the latter comes down to the same. After segmentation of the time variable, a single computation step in the time direction might require as much time as a static solution. A possibility to speed up the calculation of the dynamic behaviour is to replace the time-consuming non-linear expressions by their linear approximations.

Starting from non-linear static equations, operating values for a typical process situation are calculated for each variable everywhere in the bed. These steady-state values are obtained from an Algol program based on a numerical simulation of the equations (2.51) to (2.53) without accumulation terms together with the equations (2.4) and (2.8) /69/. Some of the resulting steady-state pellet and gas temperature profiles are shown in Figures 3.1 and 3.2. The values given by this program are taken as the starting point in our dynamic model studies, after which all non-linear expressions are expanded into Taylor series to describe the effect of deviations from the stationary operating conditions. The linearised equations are obtained by neglecting all second and higher order terms, and retaining linear expressions only.

To make this linearisation procedure permissible, all deviations as well as the second- and higher-order derivatives must be small ('small' signals and 'smooth' non-linearities). An attractive feature of the linearisation approach is that it gives a first estimate of the dynamic response, for its results are true for the non-linear case as well, provided the disturbances are sufficiently small and Taylor series expansion is possible (no hysteresis for example). Therefore, it can be used for the design of regulators controlling non-

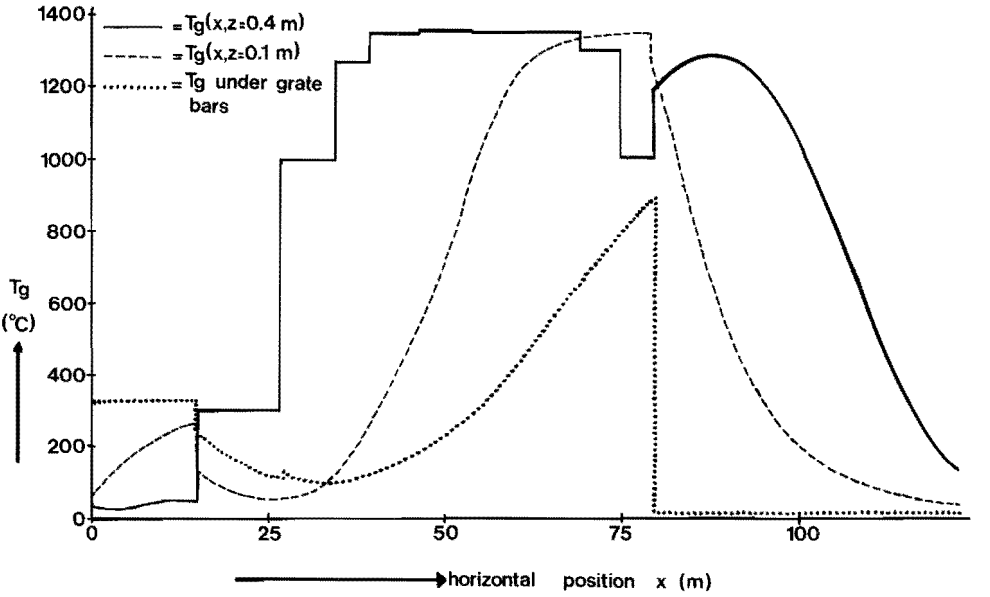

Figure 3.1 Steady-state gas temperature profiles of the pellet-indurating plant

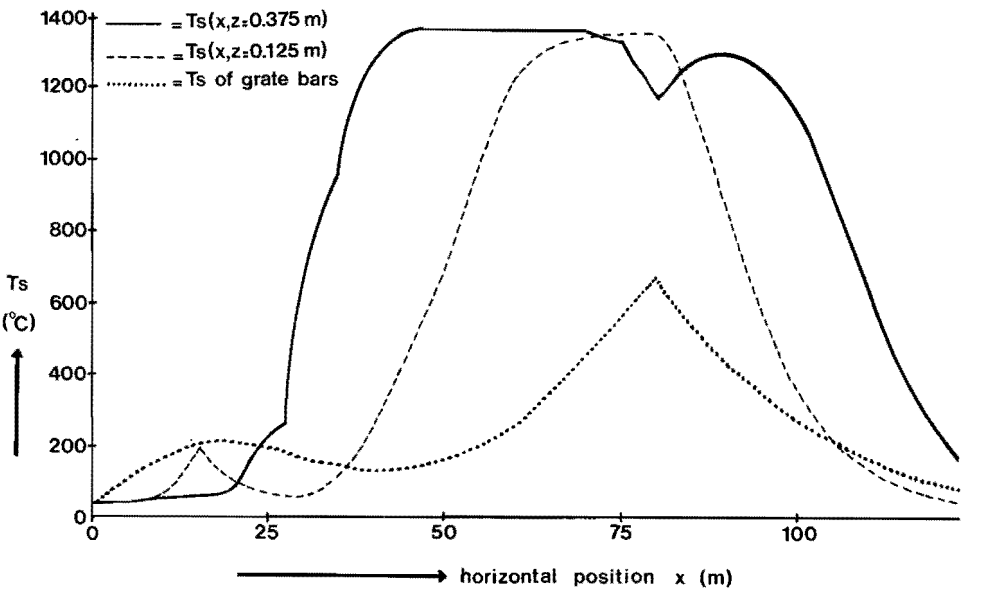

Figure 3.2 Steady-state pellet temperature profiles of the pellet-indurating plant

linear processes /56/. Of course, the linearisation approach is not necessarily applicable to start-up and shut-down procedures or feed-forward control problems.

The problem of establishing the range over which the linear approximation leads to satisfactory results has received little attention in the literature. For simple problems, Douglas developed a perturbation analysis to test the validity of the linearisation /20/. In more complicated situations, however, the dummy equations which are needed to test the linearity are more difficult to solve than the original non-linear equations. In those circumstances this aspect can be partly covered by a seperate approach based on static non-linear calculations. When each of the input variables (alone, and in combination with each other) are successively in the neighbourhood of and further away from the steady-state value around which the equations have been linearised, the degree of non-linearity of the non-linear static model can be investigated. In the case of the pellet-indurating plant, variations of the input variables with 1% and 10% with respect to their original steady-state values did not show any striking non-linear effects.

To calculate the dynamics of the cooling zones, equations (2.51) and (2.52), which are non-linear when gas flow and bed velocity disturbances are considered, are linearised around a steady state (denoted by overlined symbols)

$$\mu s\,\frac{\partial(\overline{Ts}+ts)}{\partial t} + \mu s\,(\overline{Vs}+vs)\,\frac{\partial(\overline{Ts}+ts)}{\partial x} = A(\overline{U} + \overline{\frac{\partial U}{\partial Fg}}\,fg)\{(\overline{Tg}+tg)-(\overline{Ts}+ts)\} \tag{3.20}$$

$$\gamma g\,(\overline{Fg}+fg)\,\frac{\partial(\overline{Tg}+tg)}{\partial z} = A(\overline{U} + \overline{\frac{\partial U}{\partial Fg}}\,fg)\,\{(\overline{Ts}+ts) - (\overline{Tg}+tg)\} \tag{3.21}$$

where small symbols denote deviations from the steady-state values. The linearised equations become after reaarangement and subtraction of the steady-state relations

$$\{\mu s\,\frac{\partial}{\partial t} + \mu s\,\overline{Vs}\,\frac{\partial}{\partial x} + \overline{U}\,A\}\,ts - \overline{U}\,A\,tg + \mu s\,\overline{\frac{\partial Ts}{\partial x}}\,vs +$$

$$+ \overline{\frac{\partial U}{\partial Fg}}\,A\,(\overline{Ts} - \overline{Tg})\,fg = 0 \tag{3.22}$$

$$\{\gamma g\ \overline{Fg}\ \frac{\partial}{\partial z} + \overline{U}\ A\}\ tg - \overline{U}\ A\ ts + \{\gamma g\ \overline{\frac{\partial Tg}{\partial z}} - \overline{\frac{\partial U}{\partial Fg}}\ A\ (\overline{Ts} - \overline{Tg})\}fg = 0 \tag{3.23}$$

Owing to the linearisation procedure the deviation of the gas flow rate from steady state, fg, which is used in (3.22) and (3.23) as an input variable, depends linearly on variations in pressure drop, void fraction, and the gas density which is determined by the temperature. Hence, instead of (2.5), we have

$$fg = \overline{\frac{\partial Fg}{\partial \Delta P}}\ \delta\Delta P + \overline{\frac{\partial Fg}{\partial \epsilon}} + \overline{\frac{\partial Fg}{\partial Tg}}\ tg \tag{3.24}$$

The last term on the right-hand side of (3.24) is small compared with the other ones and will at first instance be neglected. Lateron, it will be shown that its effects should also be incorporated. Likewise, the ε dependences of μs and A are small in comparison with the ε dependence of Fg and therefore they are omitted in (3.20) and (3.21).

3.4 INTEGRAL-TRANSFORM METHODS

The usefulness of an integral-transform method is determined by the types of operation performed on $f(x)$ which are transformed by the integral

$$F(q) = \int_a^b k(x,q)\ f(x)\ dx \tag{3.25}$$

into algebraic operations on $F(q)$. The kernel $k(x,s)$ determines the type of transformation. A summary of transform methods is given in /3/.

Best-known are the Laplace and Fourier transforms. Other transforms may be used to solve physical problems but most of them involve higher transcendental functions (like Bessel functions in Hankel transforms). A few are listed in Table 3.1. The emphasis in tabulation is on the operation which can be transformed most simply, since this is the key to the solution of the equations. From Table 3.1 it can be concluded that because of the type of the partial-differential equations (3.23) and (3.24) (all differential operators are of first order) for the solution of these equations other methods than

Table 3.1 SUMMARY OF INTEGRAL TRANSFORMS /3/

Operation	Transform	Transform of operation
$\frac{df(t)}{dt}$	One-sided Laplace transform $F(q) = \int_0^\infty e^{-qt} f(t)dt$	$q\,F(q) - f(0)$
	Two-sided Laplace transform $F(q) = \int_{-\infty}^\infty e^{-qt} f(t)dt$	$q\,F(q)$
	Fourier transform $F(\omega) = \int_{-\infty}^\infty e^{-j\omega t} f(t)dt$	$j\omega\,F(\omega)$
$t\,\frac{df(t)}{dt}$	Mellin transform $F_M(q) = \int_0^\infty f(t)\,t^{q-1}dt$	$-q\,F_M(q)$
$\frac{1}{t}\frac{d}{dt}(t\frac{df(t)}{dt}) - \frac{\nu^2}{t^2}f(t)$	Hankel transform $F(q) = \int_0^\infty f(t)tJ_\nu(qt)dt$	$-q^2\,F(q)$
$\frac{d^2f(t)}{dt^2} + \frac{b_0}{t}\frac{df(t)}{dt}$	Meijer transform $F_\nu(q) = \int_0^\infty f(t)t^{\nu+1}K_\nu(qt)dt$ (K_ν is a modified Bessel function)	$q^2F_\nu(q) - \frac{\Gamma(\nu+1)2^\nu}{q^\nu}f(0)$ $\nu = \frac{b_0 - 1}{2}$
$\frac{d}{dt}(1-t^2)\frac{df(t)}{dt}$	Legendre transform $F(n) = \int_{-1}^1 f(t)P_n(t)dt$ (P_n = a Legendre polynomial)	$-n(n+1)F(n)$

Laplace and Fourier transformation are less favourable.

Because of the fact that first-order differential equations are non-self-adjoint systems, only infinite integral transforms may be applied /61/.

Also, the application of other approximation methods is excluded by the first-order character of the differential equations. The modal analysis method /25/ and the functional approximation method /66/ are based on a functional approximation for the computer solution of initial-value partial-differential equation problems using eigenfunctions (modes). For application of these methods, the eigenvalue problem corresponding with a particular differential operator must have a discrete eigenvalue spectrum, since only in this case does the transformation of the differential operator make sense. Therefore, processes characterised by only first-order differential operators cannot use a modal simulation.

In conclusion, it can be said that for the set of partial-differential equations (3.23) and (3.24) semi-infinite Laplace and Fourier transform methods seem most promising. In Chapter 4, single and double Laplace transform methods will be applied to a segment moving along with the pellet bed, and compared with respect to accuracy and computer time. When the time-differential operator $\frac{d}{dt}$ is transformed to the frequency or the Laplace domain, use can be made of the control theory available in these domains and inverse transformation is often unnecessary. In Chapter 6 this method will be applied to the dynamic simulation of the cooling zone of the pellet-indurating plant.

Chapter Four

COMPARISON OF METHODS BASED ON LAPLACE TRANSFORMATION

4.1 INTRODUCTION

In this chapter we attempt to do two things, i.e. to arrive at the most efficient solution method of a segment moving along with the pellet bed by means of single or double, numerically or analytically inverted Laplace transformation, and to gain whatever insight may be gained by these kinds of exercises. After a presentation of the dimensionless partial-differential equations describing the dynamic thermal behaviour of a segment in a simplified case in Section 4.2, three types of solution are considered.

In Section 4.3 a double Laplace transform solution is presented. After double Laplace transformation of the segment equations and rearrangement of the resulting algebraic equations, the inverse transformation is found by a judicious series development of the transformed equations.

In Section 4.4 a single Laplace transform solution is derived. After single Laplace transformation of the segment equations, the resulting set of differential equations is further transformed into a set of difference equations by means of a central-difference approximation. Inverse Laplace transformation is applied after rearrangement of the equations.

In Section 4.5 a numerical inversion solution is given. After single Laplace transformation of the segment equations the resulting differential equations are solved with the Laplace variable as a parameter. The solution in the Laplace domain is numerically inverted.

In Section 4.6 the three methods are compared with respect to accuracy and computer time. The most efficient solution method, viz. the single Laplace transform solution, is used in a simulation study described in Chapter 6.

In Section 4.7 a general double Laplace transform solution

with non-uniform boundary conditions is derived.

Part of the results presented in this chapter have already been published in /11,12/.

4.2 SEGMENT EQUATIONS

In Section 2.4 the heat balances of solid and gas for a segment moving along with the pellet bed resulted in the following set of partial-differential equations

$$\mu s \frac{\partial Ts(z,\theta)}{\partial \theta} = U\,A\,\{Tg(z,\theta) - Ts(z,\theta)\} \tag{2.47}$$

$$\gamma g\, Fg \frac{\partial Tg(z,\theta)}{\partial z} = U\,A\,\{Ts(z,\theta) - Tg(z,\theta)\} \tag{2.48}$$

where we have written Ts instead of Ts^*, with initial and boundary conditions

$$Ts(z,\theta=0) = Ts_0(z) \tag{2.49}$$

$$Tg(z=0,\theta) = Tg_{in}(\theta) \tag{2.50}$$

If the inlet gas temperature $Tg_{in}(\theta)$ is constant and if the initial solid temperature $Ts_0(z)$ is independent of z, normalised dimensionless solid and gas temperatures can be defined by

$$S(z,\theta) = \frac{Ts(z,\theta) - Tg_{in}}{Ts_0 - Tg_{in}} \tag{4.1}$$

$$G(z,\theta) = \frac{Tg(z,\theta) - Tg_{in}}{Ts_0 - Tg_{in}} \tag{4.2}$$

provided that $Tg_{in} \neq Ts_0$. Restricting the problem further by assuming constant physical properties and constant gas flow rate, and introducing dimensionless residence time

$$\tau = \frac{U\,A}{\mu s}\,\theta \tag{4.3}$$

and dimensionless height

$$\zeta = \frac{U\ A}{\gamma g\ Fg}\ z \tag{4.4}$$

the moving segment equations (2.47) to (2.50) become

$$\frac{\partial S(\zeta,\tau)}{\partial \tau} = G(\zeta,\tau) - S(\zeta,\tau) \tag{4.5}$$

$$\frac{\partial G(\zeta,\tau)}{\partial \zeta} = S(\zeta,\tau) - G(\zeta,\tau) \tag{4.6}$$

with initial and boundary conditions

$$S(\zeta,\tau=0) = 1 \tag{4.7}$$

$$G(\zeta=0,\tau) = 0 \tag{4.8}$$

Other boundary conditions for this simplifyed model will be considered in Section 4.7.

4.3 DOUBLE LAPLACE TRANSFORM SOLUTION

A number of papers describing the thermal behaviour of a regenerator or a blast furnace stove were published between 1926 and 1931 /28,29,30,51,52,62/. A survey is given in the book by Jakob (1957) /35/. As this literature appeared before the advent of modern computers, many analytical solutions exist for the set of equations (4.5) to (4.8), but all of them are in infinite series form, so that for practical use the series must be truncated. The analytical solution obtained by Kohlmayr in equation (12) of /37/ (1968) was presented as being the most efficient of all. His solution will be derived here.

Let the double Laplace transform (DLT) of $G(\zeta,\tau)$ be defined by

$$\tilde{\tilde{G}}(p,q) = L\{G(\zeta,\tau);p,q\} = \int_0^\infty \int_0^\infty G(\zeta,\tau)\ e^{-p\zeta-q\tau} d\zeta d\tau \tag{4.9}$$

N.B. One-sided Laplace transformation with respect to ζ is permitted because the height of the segment of the pellet bed can be thought infinite without changing the model results at at any height z.

The DLT of $S(\zeta,\tau)$ is obtained analogously. The DLT formulation of (4.5) to (4.8) is then given by the following set of algebraic equations

$$-\tilde{\tilde{G}}(p,q) + (q+1)\,\tilde{\tilde{S}}(p,q) = \frac{1}{p} \tag{4.10}$$

$$(p+1)\,\tilde{\tilde{G}}(p,q) - \tilde{\tilde{S}}(p,q) = 0 \tag{4.11}$$

and the DLT of the normalised gas temperature response function $G(\zeta,\tau)$ is found as

$$\tilde{\tilde{G}}(p,q) = \frac{1}{p\{(p+1)(q+1) - 1\}} \tag{4.12}$$

Application of

$$\frac{1}{x-1} = \sum_{n=0}^{\infty} \frac{1}{x^{n+1}} \tag{4.13}$$

provided that $x^2>1$, converts (4.12) into

$$\tilde{\tilde{G}}(p,q) = \sum_{n=0}^{\infty} \frac{1}{p(p+1)^{n+1}(q+1)^{n+1}} \tag{4.14}$$

For the remaining task of inverting $\tilde{\tilde{G}}(p,q)$ the algebraic identity

$$\frac{1}{p(p+1)^{n+1}} = \frac{1}{p} - \sum_{m=0}^{n} \frac{1}{(p+1)^{m+1}} \tag{4.15}$$

can be substituted in (4.14)

$$\tilde{\tilde{G}}(p,q) = \sum_{n=0}^{\infty} \frac{1}{(q+1)^{n+1}} \left[\frac{1}{p} - \sum_{m=0}^{n} \frac{1}{(p+1)^{m+1}}\right] =$$

$$= \frac{1}{p\,q} - \sum_{n=0}^{\infty} \frac{1}{(q+1)^{n+1}} \sum_{m=0}^{n} \frac{1}{(p+1)^{m+1}} \tag{4.16}$$

This expression can be inverted because the elementary DLT pair

$$L\{ \frac{\zeta^m}{m!} e^{-a\zeta} \frac{\tau^n}{n!} e^{-b\tau} \; ; \; p,q \} = \frac{1}{(p+a)^{m+1}(q+b)^{n+1}} \tag{4.17}$$

is known. Thus the following representation of the gas temperature response function is found

$$G(\zeta,\tau) = 1 - e^{-\zeta-\tau} \sum_{n=0}^{\infty} \frac{\tau^n}{n!} \sum_{m=0}^{n} \frac{\zeta^m}{m!} \tag{4.18}$$

In computations, only a finite number of terms of this infinite series can be taken into account. The truncated solution is

$$G_{N,1}(\zeta,\tau) = 1 - e^{-\zeta-\tau} \sum_{n=0}^{N} \frac{\tau^n}{n!} \sum_{m=0}^{n} \frac{\zeta^m}{m!} \tag{4.19}$$

See Section 4.6 for an evaluation of this solution.

4.4 SINGLE LAPLACE TRANSFORM SOLUTION

According to the central-difference approximation (see Section 3.2) applied to the spatial variable, the following N differential and N algebraic equations result instead of the two original partial-differential equations (4.5) and (4.6) with boundary conditions (4.7) and (4.8)

$$\frac{dS_{a,n}(\tau)}{d\tau} = \frac{G_{n-1}(\tau) + G_n(\tau)}{2} - S_{a,n}(\tau) \tag{4.20}$$

$$\frac{G_n(\tau) - G_{n-1}(\tau)}{\zeta^*/N} = S_{a,n}(\tau) - \frac{G_{n-1}(\tau) + G_n(\tau)}{2} \tag{4.21}$$

for $n=1,2,\ldots,N$ with boundary conditions

$$S_{a,n}(\tau=0) = 1 \qquad \text{for } n=1,2,\ldots,N \tag{4.22}$$

$$G_0(\tau) = 0 \qquad \text{for } \tau>0 \tag{4.23}$$

where $S_{a,n}(\tau) = \frac{1}{2}\{S_{n-1}(\tau) + S_n(\tau)\}$. In Equations (4.5) to (4.8) ζ was an independent variable. Now, in the definition

of $S_{a,n}(\tau)$ and $G_n(\tau)$, n replaces ζ while the fixed height of the segment ζ^* acts as a parameter in the equations.

Applying Laplace transformation with respect to time and using the initial conditions, the following equations can be obtained

$$q\,\mathcal{S}_{a,n}(q) - 1 = \frac{1}{2}\{\mathcal{G}_{n-1}(q) + \mathcal{G}_n(q)\} - \mathcal{S}_{a,n}(q) \tag{4.24}$$

$$\frac{\mathcal{G}_n(q) - \mathcal{G}_{n-1}(q)}{\zeta^*/N} = \mathcal{S}_{a,n}(q) - \frac{1}{2}\{\mathcal{G}_{n-1}(q) + \mathcal{G}_n(q)\} \tag{4.25}$$

By elimination of $\mathcal{G}_n(q)$, $\mathcal{S}_{a,n}(q)$ can be expressed as a function of $\mathcal{G}_{n-1}(q)$ only. $\mathcal{G}_n(q)$ can be calculated afterwards according to (4.25). Together with the boundary condition (4.23) the following computation scheme results

$$\mathcal{G}_0(q) = 0 \tag{4.26}$$

$$\mathcal{S}_{a,n}(q) = \frac{\tau_+}{1 + \tau_+ q} + \frac{\mathcal{G}_{n-1}(q)}{1 + \tau_+ q} \quad \text{for } n=1,2,\ldots,N \tag{4.27}$$

$$\mathcal{G}_n(q) = \frac{\tau_-}{\tau_+}\mathcal{G}_{n-1}(q) + \frac{\tau_+ - \tau_-}{\tau_+}\mathcal{S}_{a,n}(q) \quad \text{for } n=1,2,\ldots,N \tag{4.28}$$

where

$$\tau_- = 1 - \frac{\zeta^*}{2N} \tag{4.29}$$

$$\tau_+ = 1 + \frac{\zeta^*}{2N} \tag{4.30}$$

Comparison of (2.31) and (2.32) with (4.29) and (4.30) shows that the dimensionless constants τ_- and τ_+ are similar to τ_1 and τ_2, respectively, when U is taken equal to h.

$$\tau_- = \frac{U\,A}{\mu s}\,\tau_1 \tag{4.31}$$

$$\tau_+ = \frac{U\,A}{\mu s}\,\tau_2 \tag{4.32}$$

Rearranging (4.26) to (4.28), the Laplace transform of the temperature of the outcoming gas can be written as

$$\mathcal{G}_N(q) = \frac{1}{q} - \frac{1}{q}\left[\frac{1 + \tau_- q}{1 + \tau_+ q}\right]^N \tag{4.33}$$

The gas temperature between the layers n and $n-1$ follows from this equation by replacing N by n (remember, however, that τ_+ and τ_- still depend on N).

The transfer function between the incoming and outgoing gas temperature of a segment can be derived in a similar way from (4.20) and (4.21), with boundary condition $S_{a,n}(\tau) = 0$ for $n=1,2,\ldots,N$ instead of (4.22), as

$$\frac{\mathcal{G}_N(q)}{\mathcal{G}_0(q)} = \left[\frac{1 + \tau_- q}{1 + \tau_+ q}\right]^N \tag{4.34}$$

It resembles the transfer function encountered in Chapter 2

$$\frac{\mathcal{T}g_N(q)}{\mathcal{T}g_0(q)} = \left[\frac{1 + \tau_1 q \frac{3\kappa s}{q R^2}\{R\sqrt{\frac{q}{\kappa s}}\coth(R\sqrt{\frac{q}{\kappa s}}) - 1\}}{1 + \tau_2 q \frac{3\kappa s}{q R^2}\{R\sqrt{\frac{q}{\kappa s}}\coth(R\sqrt{\frac{q}{\kappa s}}) - 1\}}\right]^N \tag{2.33}$$

Moreover, both transfer functions are identical when the thermal conductivity inside the pellets is infinite, as can be shown by application of the series development

$$\lim_{x\to 0}\{\frac{3}{x^2}(x\coth x - 1)\} = 1 \quad , \quad x = R\sqrt{\frac{q}{\kappa s}} \tag{4.35}$$

By means of the relation

$$\frac{1 + \tau_- q}{1 + \tau_+ q} = \frac{\tau_-}{\tau_+}\left[1 + \frac{1/\tau_- - 1/\tau_+}{q + 1/\tau_+}\right] \tag{4.36}$$

$\mathcal{G}_N(q)$ of (4.33) can also be written as

$$\mathcal{G}_N(q) = \frac{1}{q} - \frac{1}{q}\left[\frac{\tau_-}{\tau_+}\right]^N\left[1 + \frac{1/\tau_- - 1/\tau_+}{q + 1/\tau_+}\right]^N \tag{4.37}$$

Now, using the Laplace transform pair

$$L^{-1}\left[\frac{1}{q(q + 1/\tau_+)^r}\right] = \tau_+^r \left[1 - \sum_{m=0}^{r-1} \frac{\tau^m e^{-\tau/\tau_+}}{\tau_+^m m!}\right] \tag{4.38}$$

and the algebraic identity

$$1 + \sum_{r=1}^{N} \binom{N}{r} \left[\frac{\tau_+}{\tau_-} - 1\right]^r = \left[\frac{\tau_+}{\tau_-}\right]^N \tag{4.39}$$

the following representation of the gas temperature response function is found

$$G_{N,2}(\tau) = e^{-\tau/\tau_+} \left[\frac{\tau_-}{\tau_+}\right]^N \sum_{r=1}^{N} \binom{N}{r} \left[\frac{\tau_+ - \tau_-}{\tau_-}\right]^r \sum_{m=0}^{r-1} \frac{(\tau/\tau_+)^m}{m!} \tag{4.40}$$

The dependence of $G_{N,2}$ on the parameter ζ^* is hidden in the coefficients τ_+ and τ_-.

Another solution is obtained when the relation

$$\frac{1 + \tau_- q}{1 + \tau_+ q} = 1 + \frac{\tau_- - \tau_+}{\tau_+} \frac{q}{q + 1/\tau_+} \tag{4.41}$$

and, hence, by means of Newton's binomial formula

$$\left[\frac{1 + \tau_- q}{1 + \tau_+ q}\right]^N = 1 + \sum_{r=1}^{N} \binom{N}{r} \left[\frac{\tau_- - \tau_+}{\tau_+} \frac{q}{q + 1/\tau_+}\right]^r \tag{4.42}$$

is substituted into (4.33)

$$\tilde{G}_{N,3}(q) = -\frac{1}{q} \sum_{r=1}^{N} \binom{N}{r} \left[\frac{\tau_- - \tau_+}{\tau_+} \frac{q}{q + 1/\tau_+}\right]^r \tag{4.43}$$

Inverse Laplace transformation can be found in a similar way as for (4.37) resulting into

$$G_{N,3}(\tau) = -e^{-\tau/\tau_+} \sum_{r=1}^{N} \binom{N}{r} \left[\frac{\tau_- - \tau_+}{\tau_+}\right]^r \sum_{m=0}^{r-1} \binom{r-1}{m} \frac{(-\tau/\tau_+)^m}{m!} \qquad (4.44)$$

In spite of the similarity of (4.40) and (4.44) no simple way could be found to transform these formulae into each other.

From the formulae it looks - at first sight - difficult to recognise their accuracy when only a small number of terms are used. But in the derivation of (4.40) the principal part of the transfer function is split into a parallel circuit consisting of a proportional element and a first-order response function, and in the derivation of (4.44) into a parallel circuit consisting of a proportional element and a tame differentiator. Application of Newton's binomial formula shows that the N-th power of the right-hand side of (4.41) can be seen as a parallel circuit consisting of

- *1* proportional element
- *1* tame differentiator
- *2* tame differentiators in series

.

.

.

.

.

- N tame differentiators in series

The N-th power of the right-hand side of (4.36) can be seen as a parallel circuit consisting of

- *1* proportional element
- *1* first order
- *2* first orders in series

.

.

.

.

.

- N first orders in series

Hence, after n terms in the series development, (4.40) is more accurate for small values of τ and (4.44) is more accurate for

large values. Since the temperature responses at small and intermediate values of τ are more important than large values of τ (a segment is only a limited time in a zone and at longer residence times the outgoing gas temperature would approach the gas inlet temperature), only temperature response (4.40) will be evaluated in Section 4.6.

4.5 NUMERICAL-INVERSION SOLUTION

After Laplace transformation with respect to ζ, (4.5) to (4.8) give

$$\frac{d\hat{S}(p,\tau)}{d\tau} = \hat{G}(p,\tau) - \hat{S}(p,\tau) \tag{4.45}$$

$$p\,\hat{G}(p,\tau) = \hat{S}(p,\tau) - \hat{G}(p,\tau) \tag{4.46}$$

$$\hat{S}(p,\tau=0) = \frac{1}{p} \tag{4.47}$$

Elimination of $\hat{S}(p,\tau)$ and solution of the resulting differential equation gives the following expression for $\hat{G}(p,\tau)$

$$\hat{G}(p,\tau) = \frac{1}{p(p+1)}\, e^{-\frac{p}{p+1}\tau} \tag{4.48}$$

Introducing the definition of $\hat{G}(p,\tau)$, we obtain

$$\int_0^\infty G(\zeta,\tau)\, e^{-p\zeta}\, d\zeta = \frac{1}{p(p+1)}\, e^{-\frac{p}{p+1}\tau} \tag{4.49}$$

which, upon substitution of $x = e^{-\zeta}$, which amounts to the introduction of another vertical scale with finite bounds, becomes

$$\int_0^1 x^{p-1}\, G(-\ln(x),\tau)\, dx = \frac{1}{p(p+1)}\, e^{-\frac{p}{p+1}\tau} \tag{4.50}$$

The integral expression in the left-hand side of (4.50) can be approximated numerically by a finite sum of N terms consisting of the value of the integrand in a number of points x_n times a weighting factor w_n. The x_n and w_n have to be chosen so that

$\sum_{n=1}^{N} w_n x_n^{p-1} G(-\ln(x_n),\tau)$ approximates $\int_0^1 x^{p-1} G(-\ln(x),\tau)\,dx$.

Hence, we may write

$$\sum_{n=1}^{N} w_n x_n^{p-1} G(-\ln(x_n),\tau) = \frac{1}{p(p+1)} e^{-\frac{p}{p+1}\tau} \tag{4.51}$$

Let now p assume N different values $1,2,\ldots,N$. Then, (4.51) represents a set of N equations with N unknowns G. After matrix inversion, we can write instead of (4.51)

$$G_{N,4}(\zeta_n,\tau) = \sum_{p=1}^{N} A_{np} \frac{1}{p(p+1)} e^{-\frac{p}{p+1}\tau} \tag{4.52}$$

The index N refers to the fact that an $(N\times N)$-matrix has been inverted. The elements A_{np} of the $(N\times N)$-matrix $\underline{\underline{A}}$ have to be calculated only once from the x_n and w_n. Bellman et al. /7/ take for x_n the roots of the shifted Legendre polynomials of degree N with appropriate weighting factors w_n. For $N=3,4,\ldots,15$ the matrices $\underline{\underline{A}}$ resulting from this choice of x_n and w_n are given in appendix V of /7/.

The calculation procedure according to the numerical-inversion method can be summarised as follows: for N real values of p

$$\frac{1}{p(p+1)} e^{-\frac{p}{p+1}\tau}$$

is calculated. By multiplication with a known matrix $\underline{\underline{A}}$, N points of the response in the ζ domain are obtained. In the next section this method will be evaluated.

4.6 COMPARISON OF SOLUTION METHODS

The accuracy of the approximate solutions G_N from (4.19), (4.40) and (4.52) in the points (ζ_i,τ_j) where $i=1,2,\ldots,k$ and $j=1,2,\ldots,l$ can be expressed quantitatively by a quadratic error norm

$$I_q(N) = \left[\frac{1}{kl} \sum_{i=1}^{k} \sum_{j=1}^{l} \{G_{exact}(\zeta_i,\tau_j) - G_N(\zeta_i,\tau_j)\}^2 \right]^{\frac{1}{2}} \qquad (4.53)$$

As a second accuracy criterion the Chebyshev norm or maximum error norm is introduced

$$I_c(N) = \max_{\substack{i=1,2,\ldots,k \\ j=1,2,\ldots,l}} |G_{exact}(\zeta_i,\tau_j) - G_N(\zeta_i,\tau_j)| \qquad (4.54)$$

I_q penalises the deviation of G_N from G_{exact} in each point (ζ_i,τ_j) and therefore it is a measure of the quality with which one of the solutions fits the whole profile. I_c only accounts for the deviation in that point (ζ_i,τ_j), where the approximate solution G_N is worst, and therefore it only indicates the largest value of the difference $|G_{exact} - G_N|$ on a profile. If it is relatively small, then the first norm is bound to be relatively small too.

The exact solution $G_{exact}(\zeta_i,\tau_j)$ was approximated by calculating (4.19) for such a large value of N that

$$\left| \frac{G_N(\zeta_i,\tau_j) - G_{N+1}(\zeta_i,\tau_j)}{G_N(\zeta_i,\tau_j)} \right| < 10^{-10} \qquad (4.55)$$

and is plotted in Figure 4.1. In Figures 4.2 and 4.3 the two

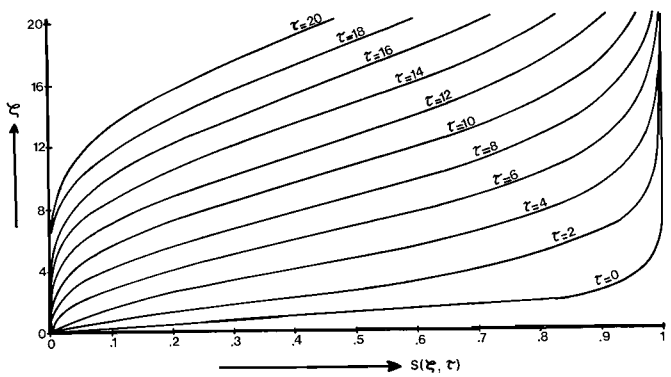

Figure 4.1 Gas temperature profiles at various times. Boundary and initial conditions: $G(\zeta=0,\tau) = 0$; $S(\zeta,\tau=0) = 1$

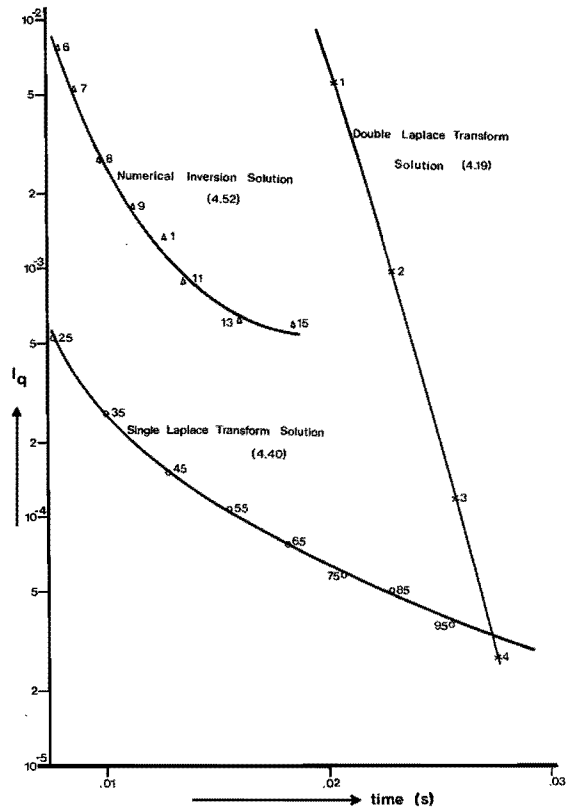

Figure 4.2 Accuracy of the three solution methods according to the quadratic error norm I_q versus time needed on the EL-X8. The number of terms N is indicated along the curves.

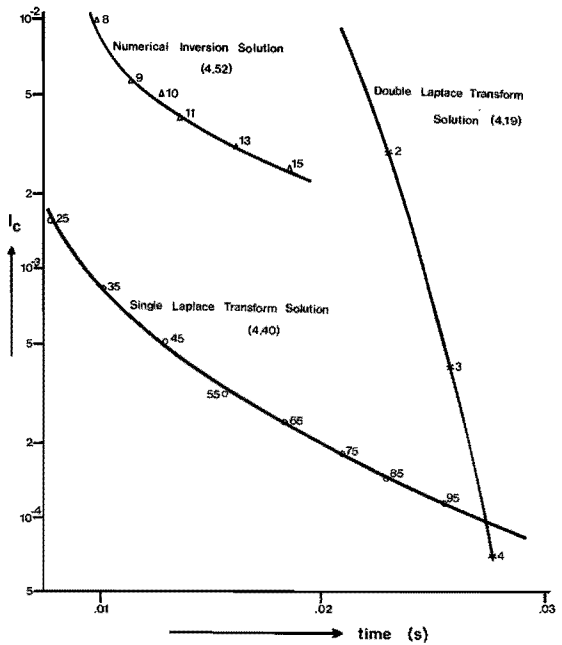

Figure 4.3 Accuracy of the three solution methods according to the Chebyshev norm I_c versus time needed on the EL-X8. The number of terms N is indicated along the curves.

error norms I_q and I_e with $k=l=10$ and $\tau_i=2,4,\ldots,20$, $\tau_j=2,4,\ldots,20$ are plotted for different values of N in (4.19), (4.40) and (4.52) versus the required computer time on the EL-X8 computer. The values of N used in the calculations are indicated along the curves. From these figures it can be seen that for none of the three solution methods are the results affected qualitatively by the choice between norm I_q or I_e. This means that the approximate solutions are smooth curves without the sudden appearance of large deviations.

According to Figure 4.2 the single Laplace transform solution (4.40) needs less computer time than the other methods if the accuracy norm I_q may be greater than 4×10^{-4}. If I_q must be smaller than 4×10^{-4} the double Laplace transform solution is the fastest method. This means that only for very accurate calculations the double Laplace transform solution is preferable. In view of the accuracy of the model equations, however, calculations with an accuracy better than 1% are unrealistic. Hence, for practical purposes, the single Laplace transform solution is the most efficient one.

For an accuracy of $I_q = 6 \times 10^{-4}$ the numerical-inversion solution needs 15 terms ($N=15$ in (4.52)) and the single Laplace transform solution 25 terms ($N=25$ in (4.19)), but nevertheless it is much faster. In building an analog model of the equations (4.40) and (4.52) the number of required integrators is of prime importance. This number equals the number N of terms needed in (4.40) and (4.52). Therefore, analog-simulation solutions using the numerical-inversion method may be more efficient than the usual finite-difference solutions. This results corresponds with the experience of others /2,31,61/ that in simulating distributed systems special integral-transform methods may offer special advantages, e.g. save analog computer hardware. However, this is only true for low values of N, since otherwise the numerical inversion method may yield very inaccurate results owing to the very large and opposite values of the coefficients of the $\underline{\underline{A}}$ matrix.

The three solution methods have only been compared for the equations of a segment (moving along with the bed) with uniform

initial condition. Non-uniform initial conditions complicate the double Laplace transform solution and the numerical-inversion solution, while the single Laplace transform solution can easily take it into account.

4.7 EXTENSION OF DOUBLE LAPLACE TRANSFORM SOLUTION FOR NON-UNIFORM INITIAL CONDITIONS

When the initial temperature profile of the segment can be expressed as a finite power series in ζ, the double Laplace transform solution is still possible, although it becomes more complicated. In this section we will derive the general double Laplace transform solution for a segment with a non-uniform initial condition and apply it to the cases of a linear and a parabolic initial solid temperature profile.

In addition to (4.5) and (4.6)

$$\frac{\partial S(\zeta,\tau)}{\partial \tau} = G(\zeta,\tau) - S(\zeta,\tau) \tag{4.56}$$

$$\frac{\partial G(\zeta,\tau)}{\partial \zeta} = S(\zeta,\tau) - G(\zeta,\tau) \tag{4.57}$$

we now have as initial condition

$$S(\zeta,\tau=0) = b_0 + b_1 \zeta + b_2 \zeta^2 + \ldots + b_n \zeta^n \tag{4.58}$$

and again as boundary condition

$$G(\zeta=0,\tau) = 0 \tag{4.59}$$

Applying the double Laplace transforms

$$\tilde{\tilde{G}}(p,q) = L\{G(\zeta,\tau);p,q\} = \int_0^\infty \int_0^\infty G(\zeta,\tau)\, e^{-p\zeta-q\tau}\, d\zeta d\tau \tag{4.60}$$

$$\tilde{\tilde{S}}(p,q) = L\{S(\zeta,\tau);p,q\} = \int_0^\infty \int_0^\infty S(\zeta,\tau)\, e^{-p\zeta-q\tau}\, d\zeta d\tau \tag{4.61}$$

and the single Laplace transforms

$$\tilde{S}(p,\tau=0) = L\{S(\zeta,\tau=0);p\} = \int_0^\infty S(\zeta,\tau=0)\, e^{-p\zeta}\, d\zeta \tag{4.62}$$

$$\tilde{G}(\zeta=0,q) = L\{G(\zeta=0,\tau);q\} = \int_0^\infty G(\zeta=0,\tau)\, e^{-q\tau}\, d\tau \tag{4.63}$$

to (4.56) to (4.59), the following set of coupled algebraic equations is obtained

$$q\,\tilde{\tilde{S}}(p,q) - \tilde{S}(p,\tau=0) = \tilde{\tilde{G}}(p,q) - \tilde{\tilde{S}}(p,q) \tag{4.64}$$

$$p\,\tilde{\tilde{G}}(p,q) - \tilde{G}(\zeta=0,q) = \tilde{\tilde{S}}(p,q) - \tilde{\tilde{G}}(p,q) \tag{4.65}$$

with initial and boundary conditions

$$\tilde{S}(p,\tau=0) = \frac{b_0}{p} + \frac{b_1}{p^2} + \frac{2b_2}{p^3} + \ldots + \frac{n!\,b_n}{p^{n+1}} \tag{4.66}$$

$$\tilde{G}(\zeta=0,q) = 0 \tag{4.67}$$

In this way the double Laplace transform of the normalised gas temperature is found as

$$\tilde{\tilde{G}}(p,q) = \frac{b_0}{p(pq+p+q)} + \frac{b_1}{p^2(pq+p+q)} + \frac{2\,b_2}{p^3(pq+p+q)} + \ldots + \frac{n!\,b_n}{p^{n+1}(pq+p+q)} \tag{4.68}$$

and the double Laplace transform of the solid temperature is given by

$$\tilde{\tilde{S}}(p,q) = \frac{b_0}{pq+p+q} + \frac{b_0+b_1}{p(pq+p+q)} + \frac{b_1+2b_2}{p^2(pq+p+q)} + \frac{2b_2+6b_3}{p^3(pq+p+q)} + \ldots +$$

$$+ \frac{i!\,b_i+(i+1)!\,b_{i+1}}{p^{i+1}(pq+p+q)} + \ldots + \frac{(n-1)!\,b_{n-1}+n!\,b_n}{p^n(pq+p+q)} + \frac{n!\,b_n}{p^{n+1}(pq+p+q)} \tag{4.69}$$

In order to obtain the inverse transform of (4.68) and (4.69), the inverse Laplace transformation of

$$\frac{1}{p^i(pq+p+q)} \qquad (i=0,1,2,\ldots,n+1)$$

must be known. Use is made of the two algebraic identities

$$\frac{1}{p^k(pq+p+q)} = \sum_{l=0}^{\infty} \frac{1}{p^k(p+1)^{l+1}(q+1)^{l+1}} \tag{4.70}$$

$$\frac{1}{p^k(p+1)^{l+1}} = \frac{1}{p^k} - \sum_{m=0}^{l} \frac{1}{p^{k-1}(p+1)^{m+1}} \tag{4.71}$$

In this way (4.68) and (4.69) can be described as the product of a number of series with terms of the form

$$\frac{1}{(p+c_1)^k(q+c_2)^l}$$

with inverse double Laplace transform

$$L^{-1}\left\{\frac{1}{(p+c_1)^k(q+c_2)^l}\,;\,\zeta,\tau\right\} = \frac{\zeta^{k-1}}{(k-1)!}e^{-c_1\zeta}\,\frac{\tau^{l-1}}{(l-1)!}e^{-c_2\tau} \tag{4.72}$$

Now the application of (4.70) and (4.71) yields

$$\frac{1}{p^i(pq+p+q)} = \sum_{j_0=0}^{\infty} \frac{1}{p^i(p+1)^{j_0+1}(q+1)^{j_0+1}}$$

$$\frac{1}{p^i(p+1)^{j_0+1}} = \frac{1}{p^i} - \sum_{j_1=0}^{j_0} \frac{1}{p^{i-1}(p+1)^{j_1+1}}$$

$$\frac{1}{p^{i-1}(p+1)^{j_1+1}} = \frac{1}{p^{i-1}} - \sum_{j_2=0}^{j_1} \frac{1}{p^{i-2}(p+1)^{j_2+1}}$$

$$\frac{1}{p^{i-2}(p+1)^{j_2+1}} = \frac{1}{p^{i-2}} - \sum_{j_3=0}^{j_2} \frac{1}{p^{i-3}(p+1)^{j_3+1}} \tag{4.73}$$

$$\vdots$$

$$\frac{1}{p(p+1)^{j_{i-1}+1}} = \frac{1}{p} - \sum_{j_i=0}^{j_{i-1}} \frac{1}{(p+1)^{j_i+1}}$$

$$\sum_{j_0=0}^{\infty} \frac{1}{(q+1)^{j_0+1}} = \frac{1}{q}$$

Subsequent substitution of these relations gives

$$\frac{1}{p^i(pq+p+q)} = \frac{1}{p^i q} - \sum_{j_0=0}^{\infty} \frac{1}{(q+1)^{j_0+1}} \sum_{j_1=0}^{j_0} \frac{1}{p^{i-1}} - \sum_{j_2=0}^{j_1} \frac{1}{p^{i-2}} - \sum_{j_3=0}^{j_2} \frac{1}{p^{i-3}} - \cdots - \sum_{j_{i-1}=0}^{j_{i-2}} \frac{1}{p} - \sum_{j_i=0}^{j_{i-1}} \frac{1}{(p+1)^{j_i+1}} \tag{4.74}$$

Rearrangement of terms gives

$$\begin{aligned}\frac{1}{p^i(pq+p+q)} = \frac{1}{p^i q} &- \sum_{j_0=0}^{\infty} \frac{j_0}{p^{i-1}(q+1)^{j_0+1}} + \sum_{j_0=0}^{\infty} \sum_{j_1=0}^{j_0} \frac{j_1}{p^{i-2}(q+1)^{j_0+1}} + \\ &- \sum_{j_0=0}^{\infty} \sum_{j_1=0}^{j_0} \sum_{j_2=0}^{j_1} \frac{j_2}{p^{i-3}(q+1)^{j_0+1}} + - \cdots + \\ &+ (-1)^{i-1} \sum_{j_0=0}^{\infty} \sum_{j_1=0}^{j_0} \sum_{j_2=0}^{j_1} \cdots \sum_{j_{i-1}=0}^{j_{i-2}} \frac{j_{i-1}}{p(q+1)^{j_0+1}} + \\ &+ (-1)^i \sum_{j_0=0}^{\infty} \sum_{j_1=0}^{j_0} \sum_{j_2=0}^{j_1} \cdots \sum_{j_{i-1}=0}^{j_{i-2}} \sum_{j_i=0}^{j_{i-1}} \frac{1}{(p+1)^{j_i+1}(q+1)^{j_0+1}}\end{aligned} \tag{4.75}$$

Now the double Laplace transform solution of (4.56) to (4.59) for any initial solid temperature profile of the form (4.58) can be obtained by substitution of (4.75) in (4.68) and (4.69) and using (4.72) in order to obtain the inverse double Laplace transform.

As an example, the double Laplace transform solution of (4.56) to (4.59) with the parabolic initial solid temperature profile

$$S(\zeta, \tau=0) = b_0 + b_1 \zeta + b_2 \zeta^2 \tag{4.76}$$

will be given. The Laplace transform of (4.76) is

$$\tilde{S}(p,\tau=0) = \frac{b_0}{p} + \frac{b_1}{p^2} + \frac{2b_2}{p^3} \tag{4.77}$$

Then the double Laplace transform of the normalised solid and gas temperatures are

$$\tilde{\tilde{S}}(p,q) = \frac{b_0}{pq+p+q} + \frac{b_0+b_1}{p(pq+p+q)} + \frac{b_1+2b_2}{p^2(pq+p+q)} + \frac{2b_2}{p^3(pq+p+q)} \tag{4.78}$$

$$\tilde{\tilde{G}}(p,q) = \frac{b_0}{p(pq+p+q)} + \frac{b_1}{p^2(pq+p+q)} + \frac{2b_2}{p^3(pq+p+q)} \tag{4.79}$$

With the help of (4.75) one finds

$$\begin{aligned}
\tilde{\tilde{S}}(p,q) = {} & \sum_{j_0=0}^{\infty} \frac{b_0}{(p+1)^{j_0+1}(q+1)^{j_0+1}} + \\
& + (b_0+b_1)\left(\frac{1}{pq} - \sum_{j_0=0}^{\infty}\sum_{j_1=0}^{j_0} \frac{1}{(p+1)^{j_1+1}(q+1)^{j_0+1}}\right) + \\
& + (b_1+2b_2)\left(\frac{1}{p^2q} - \sum_{j_0=0}^{\infty} \frac{j_0+1}{p(q+1)^{j_0+1}} + \right. \\
& \qquad \left. + \sum_{j_0=0}^{\infty}\sum_{j_1=0}^{j_0}\sum_{j_2=0}^{j_1} \frac{1}{(p+1)^{j_2+1}(q+1)^{j_0+1}}\right) \\
& + 2b_2\left(\frac{1}{p^3q} - \sum_{j_0=0}^{\infty} \frac{j_0+1}{p^2(q+1)^{j_0+1}} + \sum_{j_0=0}^{\infty}\sum_{j_1=0}^{j_0} \frac{j_1+1}{p(q+1)^{j_0+1}} + \right. \\
& \qquad \left. - \sum_{j_0=0}^{\infty}\sum_{j_1=0}^{j_0}\sum_{j_2=0}^{j_1}\sum_{j_3=0}^{j_2} \frac{1}{(p+1)^{j_3+1}(q+1)^{j_0+1}}\right)
\end{aligned} \tag{4.80}$$

and

$$\tilde{G}(p,q) = b_0\left(\frac{1}{pq} - \sum_{j_0=0}^{\infty}\sum_{j_1=0}^{j_0}\frac{1}{(p+1)^{j_1+1}(q+1)^{j_0+1}}\right)$$

$$+ b_1\left(\frac{1}{p^2q} - \sum_{j_0=0}^{\infty}\frac{j_0+1}{p(q+1)^{j_0+1}} + \sum_{j_0=0}^{\infty}\sum_{j_1=0}^{j_0}\sum_{j_2=0}^{j_1}\frac{1}{(p+1)^{j_2+1}(q+1)^{j_0+1}}\right)$$

$$+ 2b_2\left(\frac{1}{p^3q} - \sum_{j_0=0}^{\infty}\frac{j_0+1}{p^2(q+1)^{j_0+1}} + \sum_{j_0=0}^{\infty}\sum_{j_1=0}^{j_0}\frac{j_1+1}{p(q+1)^{j_0+1}} + \right. \tag{4.81}$$

$$\left. - \sum_{j_0=0}^{\infty}\sum_{j_1=0}^{j_0}\sum_{j_2=0}^{j_1}\sum_{j_3=0}^{j_2}\frac{1}{(p+1)^{j_3+1}(q+1)^{j_0+1}}\right)$$

Now using the inverse double Laplace transform (4.72), the normalised solid and gas temperatures as a function of ζ and τ become

$$S(\zeta,\tau) = b_0\left(e^{-\zeta-\tau}\sum_{j_0=0}^{\infty}\frac{\zeta^{j_0}\tau^{j_0}}{j_0!\,j_0!}\right) + (b_0+b_1)\left(1 - e^{-\zeta-\tau}\sum_{j_0=0}^{\infty}\sum_{j_1=0}^{j_0}\frac{\zeta^{j_0}\tau^{j_1}}{j_0!\,j_1!}\right) +$$

$$+ (b_1+2b_2)\left(\zeta - e^{-\tau}\sum_{j_0=0}^{\infty}\frac{(j_0+1)^{j_0}}{j_0!} + e^{-\zeta-\tau}\sum_{j_0=0}^{\infty}\sum_{j_1=0}^{j_0}\sum_{j_2=0}^{j_1}\frac{\zeta^{j_0}\tau^{j_2}}{j_0!\,j_2!}\right) +$$

$$+ 2b_2\left(\frac{\zeta^2}{2} - e^{-\tau}\sum_{j_0=0}^{\infty}\frac{(j_0+1)\zeta^{j_0}\tau}{j_0!} + e^{-\tau}\sum_{j_0=0}^{\infty}\sum_{j_1=0}^{j_0}\frac{(j_1+1)\tau^{j_0}}{j_0!} + \right.$$

$$\left. - e^{-\zeta-\tau}\sum_{j_0=0}^{\infty}\sum_{j_1=0}^{j_0}\sum_{j_2=0}^{j_1}\sum_{j_3=0}^{j_2}\frac{\zeta^{j_0}\tau^{j_3}}{j_0!\,j_3!}\right) \tag{4.82}$$

and

$$G(\zeta,\tau) = b_0\left(1 - e^{-\zeta-\tau}\sum_{j_0=0}^{\infty}\sum_{j_1=0}^{j_0}\frac{\tau^{j_0}\zeta^{j_1}}{j_0!j_1!}\right) +$$

$$+ b_1\left(\zeta - e^{-\tau}\sum_{j_0=0}^{\infty}\frac{(j_0+1)\tau^{j_0}}{j_0!} + e^{-\zeta-\tau}\sum_{j_0=0}^{\infty}\sum_{j_1=0}^{j_0}\sum_{j_2=0}^{j_1}\frac{\tau^{j_0}\zeta^{j_2}}{j_0!j_2!}\right) +$$

$$+ 2b_2\left(\frac{\zeta^2}{2} - e^{-\tau}\sum_{j_0=0}^{\infty}\frac{(j_0+1)\zeta\tau^{j_0}}{j_0!} + e^{-\tau}\sum_{j_0=0}^{\infty}\sum_{j_1=0}^{j_0}\frac{(j_1+1)\tau^{j_0}}{j_0!} +\right.$$

$$\left. - e^{-\zeta-\tau}\sum_{j_0=0}^{\infty}\sum_{j_1=0}^{j_0}\sum_{j_2=0}^{j_1}\sum_{j_3=0}^{j_2}\frac{\tau^{j_0}\zeta^{j_3}}{j_0!j_3!}\right) \qquad (4.83)$$

In Figures 4.4 to 4.6 the solid temperature profiles at various times are plotted for linear and parabolic initial conditions.

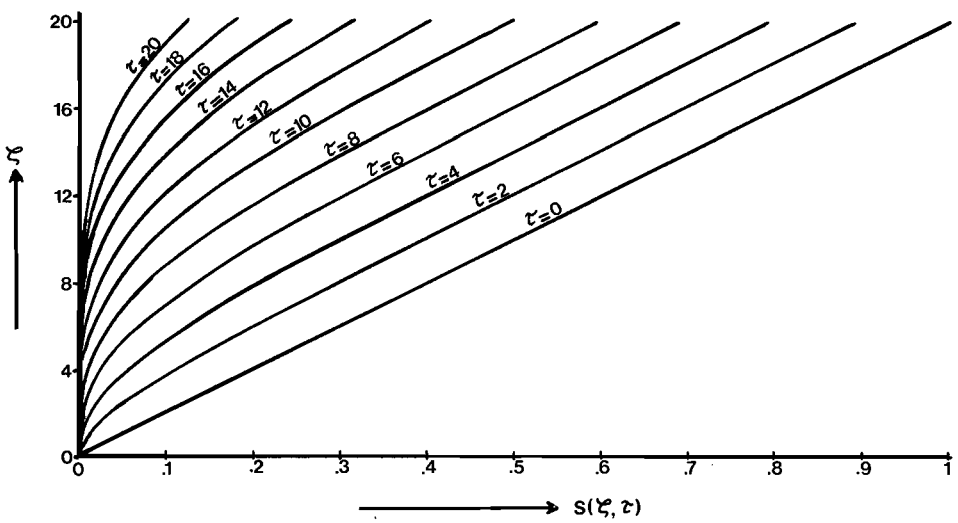

Figure 4.4 Solid temperature profiles at various times. Linearly raising initial profile: $S(\zeta,\tau=0) = 0.05 \times \zeta$; boundary condition: $G(\zeta=0,\tau) = 0$.

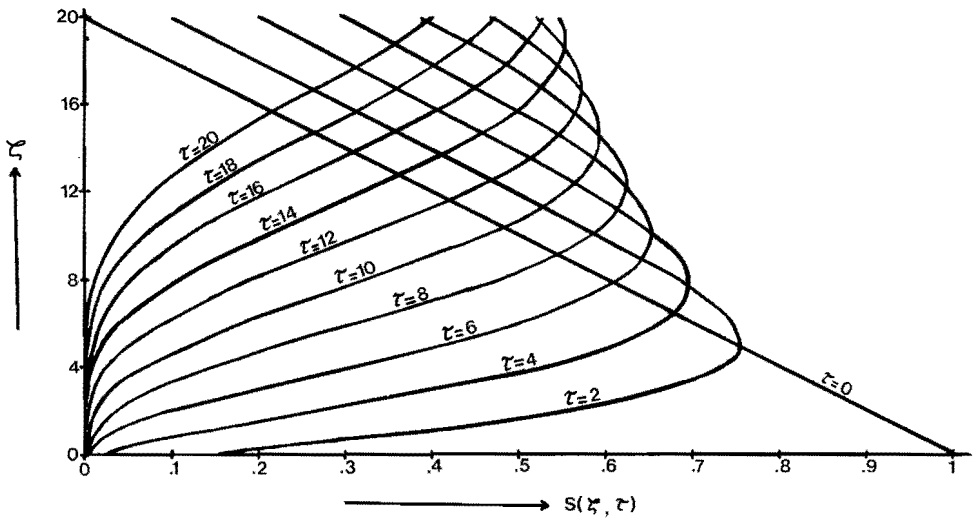

Figure 4.5 Solid temperature profiles at various times. Linearly descending initial profile: $S(\zeta,\tau=0) = 1 - 0.05 \times \zeta$; boundary condition: $G(\zeta=0,\tau) = 0$.

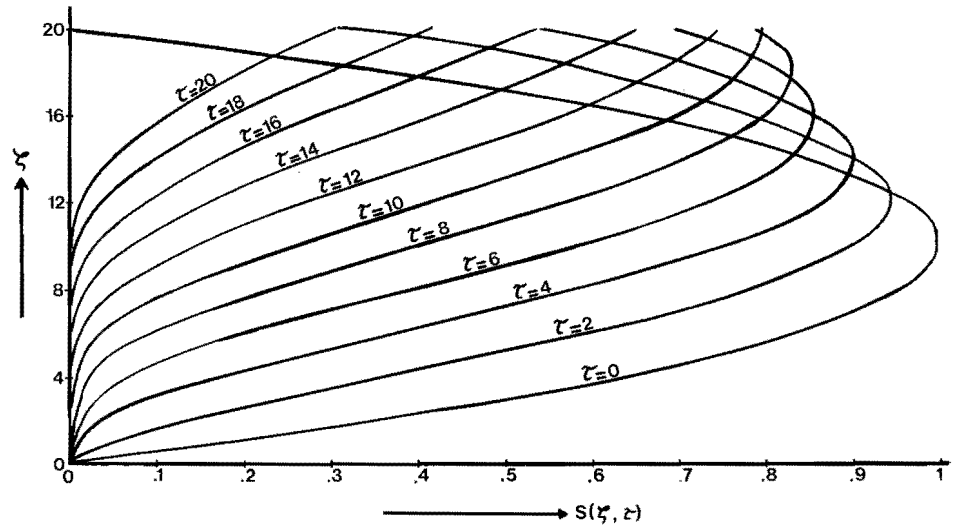

Figure 4.6 Solid temperature profiles at various times. Parabolic initial condition: $S(\zeta,\tau=0) = 0.2 \times \zeta - 0.01 \times \zeta^2$; boundary condition: $G(\zeta=0,\tau) = 0$.

Chapter Five

DIGITAL SIMULATION IN TIME DOMAIN

5.1 INTRODUCTION

Finite-difference approximation is necessary for the solution of partial-differential equations on a digital computer when analytical solutions do nor exist or are too tedious. The extension of backward- and central-difference approximations from ordinary differential equations to partial-differential equations is fairly straightforward. The derivation of finite-difference approximations for the linearised model equations describing the thermal behaviour of the pellet bed is given in Section 5.2. In the case of a backward-difference approximation simple equations result. With a central-difference approximation the large number of terms appearing in the resulting difference equations can be reduced by introduction of new variables, which considerably simplifies the calculations.

The static and dynamic accuracy of the methods is considered in Section 5.3. A further analysis of the central-difference approximation resulted in a calculation scheme that is even simpler than that of the backward-difference method and still more accurate.

After the conclusions in Section 5.4, the various calculation schemes are given explicitly in the appendix in Section 5.5.

5.2 FINITE-DIFFERENCE APPROXIMATIONS

When using finite differences, the three-dimensional TXZ-volume of interest in the txz-space is divided into a three-dimensional array of elementary volumes as shown in Figure 5.1. When the period of interest $[0,T]$ is divided into L intervals, the horizontal bed length X into M segments and the vertical

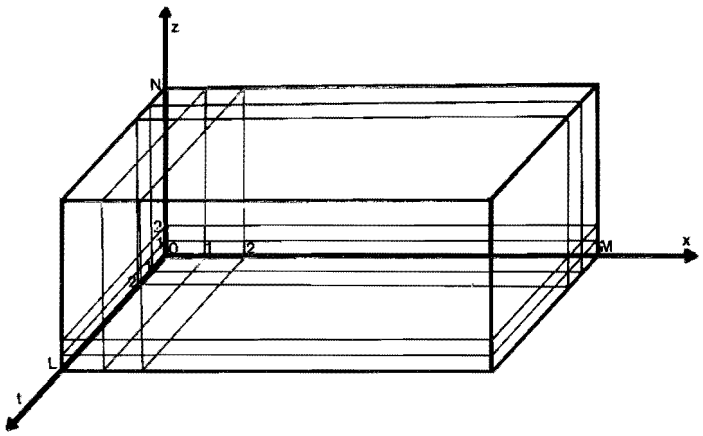

Figure 5.1 Division of the TXZ domain in elementary volumes

height Z into N layers, $L\times M\times N$ elementary volumes originate. The coordinates of the grid points are given by lT/L, mX/M and nZ/N where $l=0,1,2,\ldots,L$, $m=0,1,2,\ldots,M$ and $n=0,1,2,\ldots,N$. Depending on the finite-difference scheme used, various difference approximations of (3.22) and (3.23) can be made. We will apply a first- and second-order correct approximation using backward and central differences, respectively.

5.2.1 Backward differences

When backward differences are applied, the solid and gas temperatures *in* the elementary volume (l,m,n), which is defined as $\{t,x,z \mid t\varepsilon(l-1,l]\times T/L, x\varepsilon(m-1,m]\times X/M, z\varepsilon(n-1,n]\times Z/N\}$, are taken equal to their *output* values. The temperature derivatives in the elementary volume are according to a multidimensional version of (3.9) approximated as follows

$$\left.\frac{\partial ts}{\partial t}\right|_{l,m,n} \simeq \frac{L}{T}\{ts_{l,m,n} - ts_{l-1,m,n}\} \tag{5.1}$$

$$\left.\frac{\partial ts}{\partial x}\right|_{l,m,n} \simeq \frac{M}{X}\{ts_{l,m,n} - ts_{l,m-1,n}\} \tag{5.2}$$

$$\left.\frac{\partial tg}{\partial z}\right|_{l,m,n} \simeq \frac{N}{Z}\{tg_{l,m,n} - tg_{l,m,n-1}\} \tag{5.3}$$

With the help of these approximations the equations corresponding to (3.22) and (3.23) can be solved numerically. After elimination of undesired variables, the unknown gas and solid temperatures can be expressed as linear functions of the already known temperatures and the velocities.

For the backward-difference approximation the numerical solution can be expressed as follows

$$\begin{vmatrix} ts_{l,m,n} \\ tg_{l,m,n} \end{vmatrix} = \left\| \quad \underline{\underline{A}} \quad \right\| \cdot \begin{vmatrix} ts_{l-1,m,n} \\ ts_{l,m-1,n} \\ tg_{l,m,n-1} \\ vs_{l} \\ fg_{l,m} \end{vmatrix} \tag{5.4}$$

where $\underline{\underline{A}}$ is a (2×5)-matrix which, due to assumption 15 in Section 2.2, is only a function of m and n.

$$\underline{\underline{A}} = \left\| \begin{vmatrix} a_{11} & a_{12} & a_{13} & a_{14} & a_{15} \\ a_{21} & a_{22} & a_{23} & a_{24} & a_{25} \end{vmatrix} \right\| \tag{5.5}$$

The coefficients of $\underline{\underline{A}}$ are given in the appendix in Section 5.5.

If the initial and boundary conditions $ts_{0,m,n}$, $ts_{l,0,n}$ and $tg_{l,m,0}$ as well as vs_{l} and $fg_{l,m}$ are known, equation (5.4) can be applied to each elementary volume (l,m,n), starting from $(1,1,1)$ to (L,M,N).

5.2.2 Central differences

Consider one of the $L\times M\times N$ elementary volumes, e.g. the (l,m,n)-th in Figure 5.2. The center of this elementary volume is located at position $l-\frac{1}{2},m-\frac{1}{2},n-\frac{1}{2}$. Therefore, the physical properties of the whole of the (l,m,n)-th volume will be represented by the appropriate symbol having the index $l-\frac{1}{2},m-\frac{1}{2},n-\frac{1}{2}$.

When central differences are used, we take the solid and gas temperatures equal to the arithmetic mean of the temperatures at the eight grid points

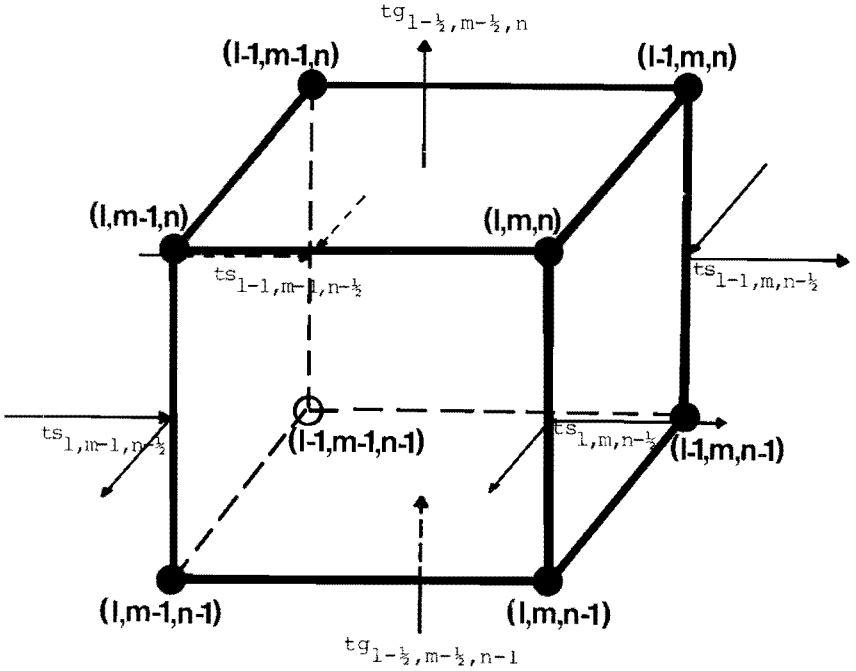

Figure 5.2 Definition of solid and gas temperatures of the elementary volume (l,m,n)

$$\overline{ts}_{l-\frac{1}{2},m-\frac{1}{2},n-\frac{1}{2}} = \frac{1}{8}\{(ts_{l,m,n}+ts_{l,m,n-1}) + (ts_{l-1,m,n}+ts_{l-1,m,n-1}) +$$

$$+ (ts_{l,m-1,n}+ts_{l,m-1,n-1}) + (ts_{l-1,m-1,n}+ts_{l-1,m-1,n-1})\} \quad (5.6)$$

$$\overline{tg}_{l-\frac{1}{2},m-\frac{1}{2},n-\frac{1}{2}} = \frac{1}{8}\{(tg_{l,m,n}+tg_{l-1,m,n}+tg_{l,m-1,n}+tg_{l-1,m-1,n}) +$$

$$+ (tg_{l,m,n-1}+tg_{l-1,m,n-1}+tg_{l,m-1,n-1}+tg_{l-1,m-1,n-1})\} \quad (5.7)$$

and the three differential quotients of equations (3.22) and (3.23) are according to (3.16) approximated as follows

$$\left.\frac{\partial ts}{\partial t}\right|_{l-\frac{1}{2},m-\frac{1}{2},n-\frac{1}{2}} \cong \frac{L}{4T}\{(ts_{l,m,n}+ts_{l,m,n-1}) + (ts_{l,m-1,n}+ts_{l,m-1,n-1}) +$$

$$- (ts_{l-1,m,n} + ts_{l-1,m,n-1}) - (ts_{l-1,m-1,n} + ts_{l-1,m-1,n-1})\} \qquad (5.8)$$

$$\left.\frac{\partial ts}{\partial x}\right|_{l-\frac{1}{2},m-\frac{1}{2},n-\frac{1}{2}} \simeq \frac{M}{4X}\{(ts_{l,m,n} + ts_{l,m,n-1}) + (ts_{l-1,m,n} + ts_{l-1,m,n-1}) +$$

$$- (ts_{l,m-1,n} + ts_{l,m-1,n-1}) - (ts_{l-1,m-1,n} + ts_{l-1,m-1,n-1})\} \qquad (5.9)$$

$$\left.\frac{\partial tg}{\partial z}\right|_{l-\frac{1}{2},m-\frac{1}{2},n-\frac{1}{2}} \simeq \frac{N}{4Z}\{(tg_{l,m,n} + tg_{l-1,m,n} + tg_{l,m-1,n} + tg_{l-1,m-1,n}) +$$

$$- (tg_{l,m,n-1} + tg_{l-1,m,n-1} + tg_{l,m-1,n-1} + tg_{l-1,m-1,n-1})\} \qquad (5.10)$$

A reduction of the number of temperatures needed for the numerical solution of (5.6) to (5.10) can be obtained by the introduction of new variables for some recurring groups of temperatures, viz. those which have been denoted in brackets *(...)* in (5.6) to (5.10). These new temperatures are averaged with respect to the t, x or z direction of the elementary volume. These averaged temperatures will be identified with index numbers halfway between the integer values and a bar over the symbols to indicate the averaging process. In this way the following new temperatures are introduced

$$\overline{ts}_{l,m,n-\frac{1}{2}} = \tfrac{1}{2}(ts_{l,m,n} + ts_{l,m,n-1}) \qquad (5.11)$$

$$\overline{ts}_{l-1,m,n-\frac{1}{2}} = \tfrac{1}{2}(ts_{l-1,m,n} + ts_{l-1,m,n-1}) \qquad (5.12)$$

$$\overline{ts}_{l,m-1,n-\frac{1}{2}} = \tfrac{1}{2}(ts_{l,m-1,n} + ts_{l,m-1,n-1}) \qquad (5.13)$$

$$\overline{ts}_{l-1,m-1,n-\frac{1}{2}} = \tfrac{1}{2}(ts_{l-1,m-1,n} + ts_{l-1,m-1,n-1}) \qquad (5.14)$$

$$\overline{tg}_{l-\frac{1}{2},m-\frac{1}{2},n} = \tfrac{1}{4}(tg_{l,m,n} + tg_{l-1,m,n} + tg_{l,m-1,n} + tg_{l-1,m-1,n}) \qquad (5.15)$$

$$\overline{tg}_{l-\frac{1}{2},m-\frac{1}{2},n-1} = \tfrac{1}{4}(tg_{l,m,n-1} + tg_{l-1,m,n-1} + tg_{l,m-1,n-1} + tg_{l-1,m-1,n-1}) \qquad (5.16)$$

and the equations (5.6) to (5.10) can be written as

$$\overline{\overline{ts}}_{l-\frac{1}{2},m-\frac{1}{2},n-\frac{1}{2}} = \tfrac{1}{4}\left(\overline{\overline{ts}}_{l,m,n-\frac{1}{2}} + \overline{\overline{ts}}_{l-1,m,n-\frac{1}{2}} + \overline{\overline{ts}}_{l,m-1,n-\frac{1}{2}} + \overline{\overline{ts}}_{l-1,m-1,n-\frac{1}{2}}\right) \tag{5.17}$$

$$\overline{\overline{tg}}_{l-\frac{1}{2},m-\frac{1}{2},n-\frac{1}{2}} = \tfrac{1}{2}\left(\overline{\overline{tg}}_{l-\frac{1}{2},m-\frac{1}{2},n} + \overline{\overline{tg}}_{l-\frac{1}{2},m-\frac{1}{2},n-1}\right) \tag{5.18}$$

$$\left.\frac{\partial ts}{\partial t}\right|_{l-\frac{1}{2},m-\frac{1}{2},n-\frac{1}{2}} \simeq \frac{L}{2T}\left(\overline{\overline{ts}}_{l,m,n-\frac{1}{2}} + \overline{\overline{ts}}_{l,m-1,n-\frac{1}{2}} + \right.$$

$$\left. - \overline{\overline{ts}}_{l-1,m,n-\frac{1}{2}} - \overline{\overline{ts}}_{l-1,m-1,n-\frac{1}{2}}\right) \tag{5.19}$$

$$\left.\frac{\partial ts}{\partial x}\right|_{l-\frac{1}{2},m-\frac{1}{2},n-\frac{1}{2}} \simeq \frac{M}{2X}\left(\overline{\overline{ts}}_{l,m,n-\frac{1}{2}} + \overline{\overline{ts}}_{l-1,m,n-\frac{1}{2}} + \right.$$

$$\left. - \overline{\overline{ts}}_{l,m-1,n-\frac{1}{2}} - \overline{\overline{ts}}_{l-1,m-1,n-\frac{1}{2}}\right) \tag{5.20}$$

$$\left.\frac{\partial tg}{\partial z}\right|_{l-\frac{1}{2},m-\frac{1}{2},n-\frac{1}{2}} \simeq \frac{N}{Z}\left(\overline{\overline{tg}}_{l-\frac{1}{2},m-\frac{1}{2},n} - \overline{\overline{tg}}_{l-\frac{1}{2},m-\frac{1}{2},n-1}\right) \tag{5.21}$$

In this way the equations corresponding to (3.22) and (3.23) can be solved numerically. After elimination of undesired variables the unknown gas and solid temperatures can be expressed as linear functions of the already known temperatures and the velocities. In matrix notation central-difference approximation gives the following relationship

$$\begin{vmatrix} \overline{\overline{ts}}_{l,m,n-\frac{1}{2}} \\ \overline{\overline{tg}}_{l-\frac{1}{2},m-\frac{1}{2},n} \end{vmatrix} = \left|\left| \underline{\underline{B}} \right|\right| \cdot \begin{vmatrix} \overline{\overline{ts}}_{l-1,m,n-\frac{1}{2}} \\ \overline{\overline{ts}}_{l,m-1,n-\frac{1}{2}} \\ \overline{\overline{ts}}_{l-1,m-1,n-\frac{1}{2}} \\ \overline{\overline{tg}}_{l-\frac{1}{2},m-\frac{1}{2},n-1} \\ \overline{\overline{vs}}_{l-\frac{1}{2}} \\ \overline{\overline{fg}}_{l-\frac{1}{2},m-\frac{1}{2}} \end{vmatrix} \tag{5.22}$$

where $\underline{\underline{B}}$ is a (2×6)-matrix, which, like $\underline{\underline{A}}$, is only a function of m and n.

$$\underline{\underline{B}} = \begin{vmatrix} b_{11} & b_{12} & b_{13} & b_{14} & b_{15} & b_{16} \\ b_{21} & b_{22} & b_{23} & b_{24} & b_{25} & b_{26} \end{vmatrix} \tag{5.23}$$

The coefficients of $\underline{\underline{B}}$ are given in the appendix in Section 5.5. The calculation procedure is the same as for the backward-difference approximation: when the initial and boundary conditions $\overline{ts}_{0,m,n-\frac{1}{2}}$, $\overline{ts}_{l,0,n-\frac{1}{2}}$ and $\overline{tg}_{l-\frac{1}{2},m-\frac{1}{2},0}$ as well as $\overline{vs}_{l-\frac{1}{2}}$ and $\overline{fg}_{l-\frac{1}{2},m-\frac{1}{2}}$ are known, equation (5.22) can be calculated for each elementary volume (l,m,n) starting from $(1,1,1)$ to (L,M,N). The "averaged" initial and boundary conditions $\overline{ts}_{0,m,n-\frac{1}{2}}$, $\overline{ts}_{l,0,n-\frac{1}{2}}$ and $\overline{tg}_{l-\frac{1}{2},m-\frac{1}{2},0}$ needed for starting the calculation procedure (5.22), are obtained by (5.11) and (5.15) from the 'real' initial and boundary conditions $ts_{0,m,n}$, $ts_{l,0,n}$ and $tg_{l,m,0}$.

5.3 ACCURACY OF THE SIMULATIONS

5.3.1 Determination of static accuracy

In the simulation studies of the cooling section of the pellet-indurating plant there are three place- and time-dependent input variables, viz. the solid inlet temperature $ts_{in}(t,z)$, the gas inlet temperature $tg_{in}(t,x)$ and the gas flow rate $fg(t,x)$, and one time-dependent variable, the velocity of the moving grate $vs(t)$. These four input variables determine the output variables: the solid and gas temperatures everywhere in the bed. A scheme of dependence is shown in Figure 5.3. In the simulations the responses after a step disturbance in one of the input variables will be investigated.

The accuracy of the static part of the response (the ultimate ultimate value which is reached after all transient phenomena have died out) will be studied first. This accuracy can be dealt with separately, for, when the dynamic part of the response is over, $\frac{\partial ts}{\partial t} = \frac{\partial tg}{\partial t} = 0$ in (3.22) and (3.23) and the

ultimate temperatures follow from the steady-state equations

$$\mu s\ \overline{Vs}\ \frac{\partial ts}{\partial x} + \mu s\ \overline{\frac{\partial Ts}{\partial x}}\ vs \;=\; \overline{U}\ A\ (tg - ts) + \overline{\frac{\partial U}{\partial Fg}}\ A\ (\overline{Tg} - \overline{Ts})\ fg \qquad (5.24)$$

$$\gamma g\ \overline{Fg}\ \frac{\partial tg}{\partial z} + \gamma g\ \overline{\frac{\partial Tg}{\partial z}}\ fg \;=\; \overline{U}\ A\ (ts - tg) + \overline{\frac{\partial U}{\partial Fg}}\ A\ (\overline{Ts} - \overline{Tg})\ fg \qquad (5.25)$$

A first requirement for a solution method of (3.22) and (3.23) is that at least (5.24) and (5.25) are solved satisfactorily. The simulation of the equations (5.24) and (5.25) by means of a backward- and a central-difference approximation will be compared with each other and also with the more accurate simulation of the non-linear static model.

The procedure used for an accuracy test can be illustrated by the following example: Let the bed velocity Vs undergo a positive step disturbance which amounts to e.g. 10% of its steady-state value $\overline{Vs}$. The solid and gas temperatures in the bed eventually become constant, reaching their new static values. The accuracy of the static temperature changes can be

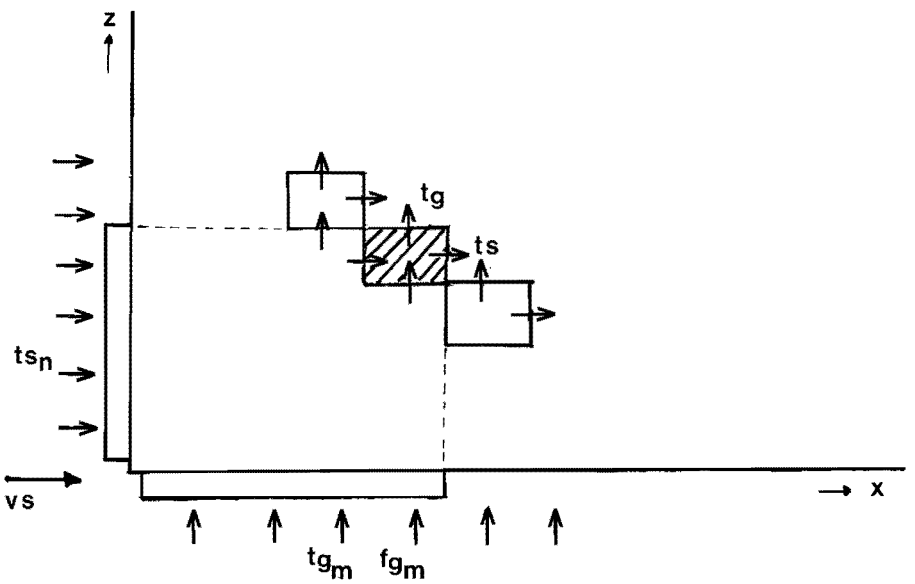

Figure 5.3 Scheme of dependence of input and output variables

determined by comparison with what we will call more accurate temperature changes. These are obtained by running the original non-linear model twice: once in the original working situation and once in the original situation with only the input velocity replaced by $1.1 \times \overline{Vs}$, and the differences in temperatures between these two static model runs we will call the more accurate static temperature changes. They are more accurate because they have been derived (1) by means of a more accurate numerical solution method, i.e. a fourth-order Runge-Kutta integration procedure /69/, and (2) from non-linear model equations. In the same way, the static accuracy after a gas flow rate change, and a solid or gas inlet temperature disturbance can be determined.

5.3.2 Static accuracy of the backward-difference model

In Figure 5.4 the static pellet temperature change above in the bed at $z=0.4$ m after a step disturbance of the incoming pellet temperature of 100 K is shown as function of the horizontal position x. The temperature scale has been chosen logarithmic since a priori, and in first approximation, an exponential decrease of $ts(t=\infty,x,z)$ as function of x is expected. However, as a result of the temperature dependence of the gas density ρg, the gas mass flow rate Fg increases with lower temperatures. Therefore, at the end of the cooling zone the pellets are better cooled than would correspond to an exponential decrease. This is shown by the convexity of the temperatures in Figure 5.4. Although finer segmentation results in a somewhat better correspondence, the inclination of the temperature profiles obtained by a backward-difference approximation is less steep

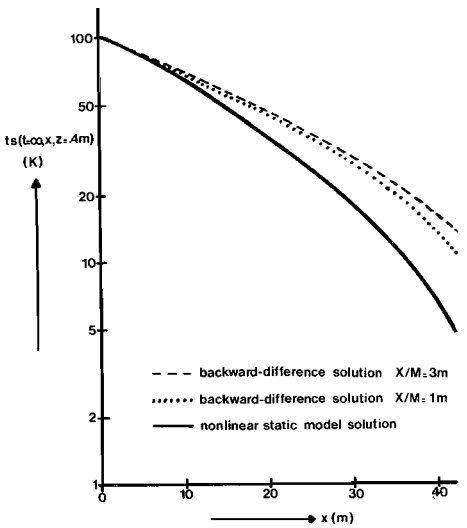

Figure 5.4 Static pellet temperature change at $z=0.4m$ after an inlet pellet temperature disturbance of 100 K.

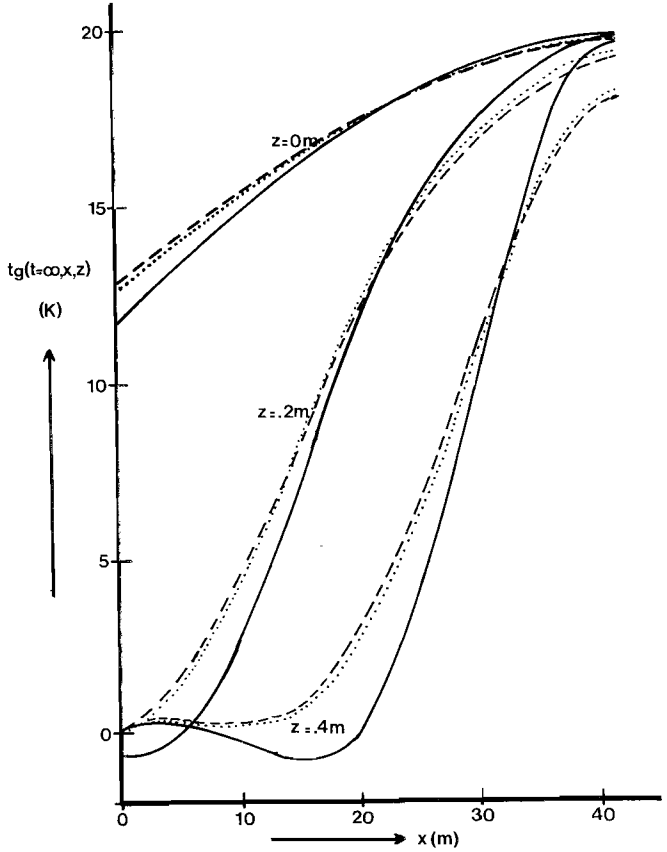

Figure 5.5 Static gas temperature change after a gas inlet temperature disturbance of 20 K according to the non-linear static model solution (———), and two backward-difference solutions *X/M=3m* (– – – –) and *X/M=1m* (·····)

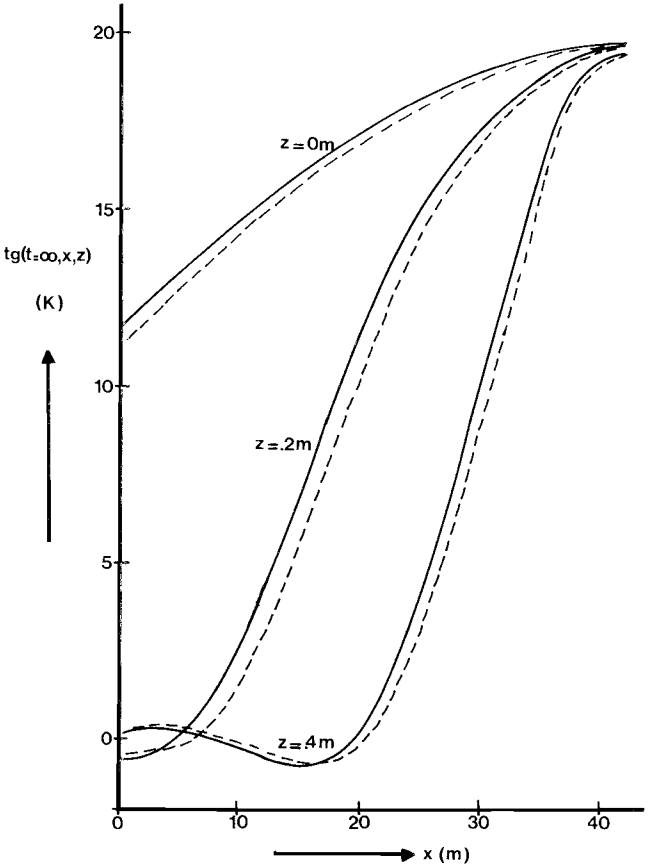

Figure 5.6 Static gas temperature change after a gas inlet temperature disturbance of 20 K with gas flow rate correction. according to the non-linear static model (————) and the backward-difference model with *X/M=3m* (– – – –)

than the corresponding more accurate solution. The remaining difference is mainly due to the changed gas flow distribution along the length of the bed owing to a different temperature profile, as will be illustrated below.

Figure 5.5 shows the static gas temperature changes at various heights in the bed ($z=0$, 0.2 and 0.4 m) after a step disturbance of the gas inlet temperature of 20 K, plotted against the horizontal position x. Also in these calculations the gas flow through the bed $Fg(x)$ was presumed to remain the same. From these temperature profiles it follows that a more refined segmentation with respect to the x direction does not improve the accuracy of the backward-difference approximation considerably. Particularly, the negative value of the static temperature change of the gas leaving the bed between $x=7$ and $x=21$ m is not reproduced in the backward-difference simulation. This reversal is remarkable, for it means that although the gas inlet temperature has been increased by 20 K, at some places the gas can leave the bed at a lower temperature than before. The reason herefore is formed by the temperature dependence of the gas flow rate. Because of the gas temperature disturbance the gas flow distribution over the length of the bed $Fg(x)$ changes. It becomes relatively smaller in the beginning of the cooling zone and larger at the end. The changed flow distribution together with the non-uniform pellet inlet temperature profile, will cause temperature profiles as produced by the non-linear static model. When the gas flow redistribution after a gas inlet temperature disturbance was appropriately taken into account by means of a corrective gas flow rate disturbance, a much better correspondence was obtained between our backward-difference simulation and the non-linear static model, as demonstrated by Figure 5.6. Obviously, this redistribution is more influential than the remaining non-linear effects (see also the results discussed in Section 7.3).

The static accuracy of the backward-difference model after a disturbance in the gas flow rate or the bed velocity is of the same order as for pellet and gas temperature disturbances.

5.3.3 Static accuracy of the central-difference model

With identical segmentation, the static accuracy of the central-difference model is better than the static accuracy of the backward-difference model. This result was found for each disturbance and for all responses. As an example, the gas temperature changes after a gas flow rate step disturbance are shown in Figure 5.7 for the backward- as well as the central-difference models together with the non-linear model temperature change as reference. In Figure 5.8, the differences between each approximation and the more accurate model results are sketched. The result is in agreement with the expectation that - with an equal number of segments - a second-order correct approximation gives better accuracy than a first-order correct one.

With the central-difference model a satisfactory static accuracy is obtained for all disturbances when the pellet

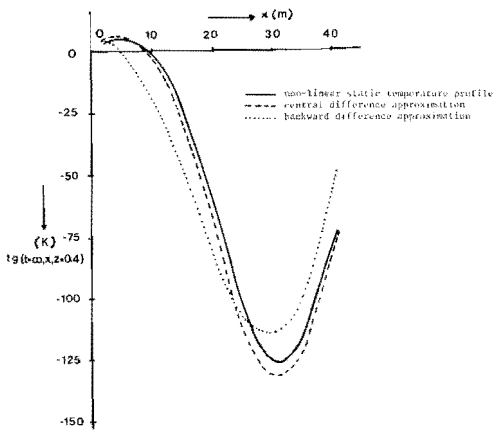

Figure 5.7 Static gas temperature change at $z=0.4m$ after a +10% gas flow rate change

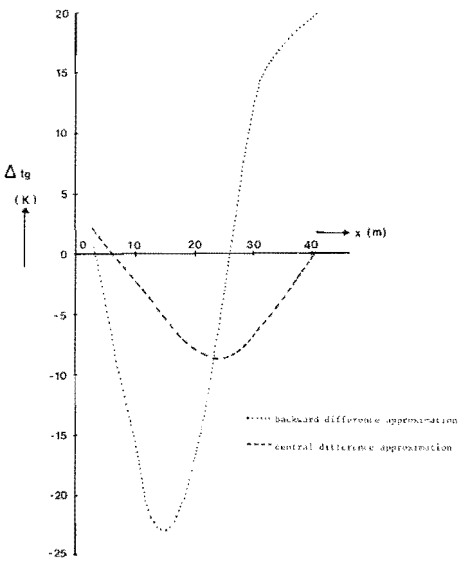

Figure 5.8 Difference between the backward- and central-difference models and the non-linear static model

bed is divided in horizontal segments of length $\Delta x = 3\ m$. The accuracy corresponding with this segmentation is even better than the static accuracy of the backward-difference model with segments of a length $\Delta x = 1\ m$.

5.3.4 Dynamic results

The problem of the determination of the accuracy of the dynamic part of a solution method for the cooling zone of the pellet bed is that - in contrast with the static situation where an accurate static simulation was available - there existed no exact dynamic solution as reference in the case considered here.

However, for a parallel-flow heat exchanger with constant physical properties the theoretically expected exact temperature responses after a step disturbance in inlet temperature or velocity are known to be either a pure delay function (with a gain factor) or a cut-off first-order response function or a cut-off ramp function /64/. Because of the resemblance between parallel-flow and cross-flow heat exchangers, similar dynamic behaviour will come about for the pellet bed. This means that after a step disturbance in (1) pellet inlet temperature, (2) gas inlet temperature, (3) bed velocity or (4) gas flow rate, the pellet temperature response will be about (1) a pure delay (with a gain factor), (2) a cut-off first-order response function or (3) (4) a cut-off ramp (see Figure 5.13).

Experience has taught us that in approximate solutions the difference between a cut-off first order, a normal first order and a cut-off ramp response function can not be distinguished very clearly. Therefore, the dynamic accuracy of the simulation method can be evaluated best by consideration of the response after a pellet inlet temperature disturbance.

In Figure 5.9 the backward-difference solution of the pellet temperature response function after a step disturbance in pellet inlet temperature of 100 K is shown together with the theoretically expected exact solution. The step character of the exact response function is approximated by an S-shaped curve, which becomes less steep further away from the beginning

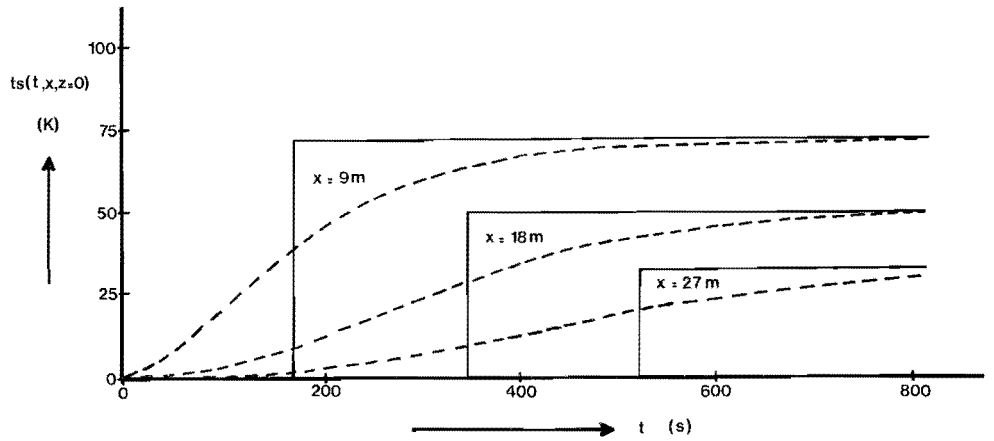

Figure 5.9 Pellet temperature responses at $z=0m$ and different horizontal position x in the bed after a pellet inlet temperature disturbance of 100 K according to the backward-difference approximation (------) compared with the theoretically expected responses (————).

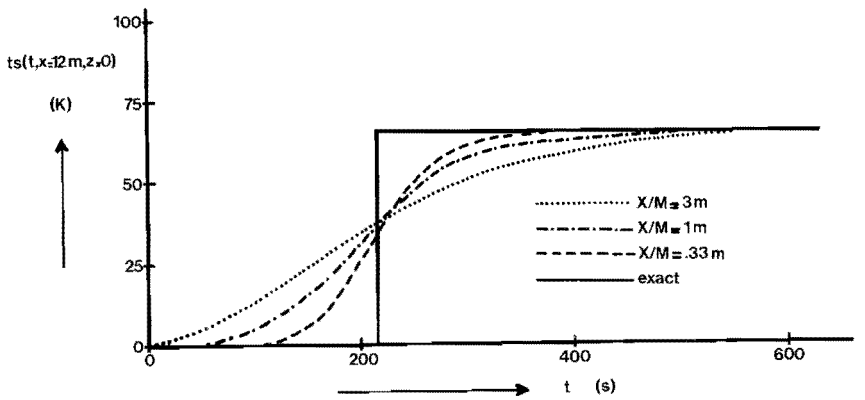

Figure 5.10 Pellet temperature responses at $x=12m$ and $z=0m$ to a pellet inlet temperature step disturbance of 100 K according to the backward-difference method with different segmentations, viz. $X/M=3m$, $X/M=1m$, $X/M=.33m$ compared with the theoretically expected response.

of the bed. Figure 5.10 demonstrates that a finer segmentation with respect to the x direction results in a better approximation of the step function by the S-shaped curve.

In Figure 5.11 the central-difference solution of the pellet temperature response function after a step disturbance in pellet inlet temperature is shown together with the exact solution. As can be seen from this figure, changing the ratio $\Delta x/\Delta t$ strongly influences the character of the response function. The ratio

$$\frac{\Delta x}{\Delta t} = \overline{Vs} \tag{5.26}$$

gives the best results, although even for this ratio the temperature responses show an oscillatory behaviour in the neighbourhood of the discontinuity. This oscillation causes no static error in the solution. It can be removed when for

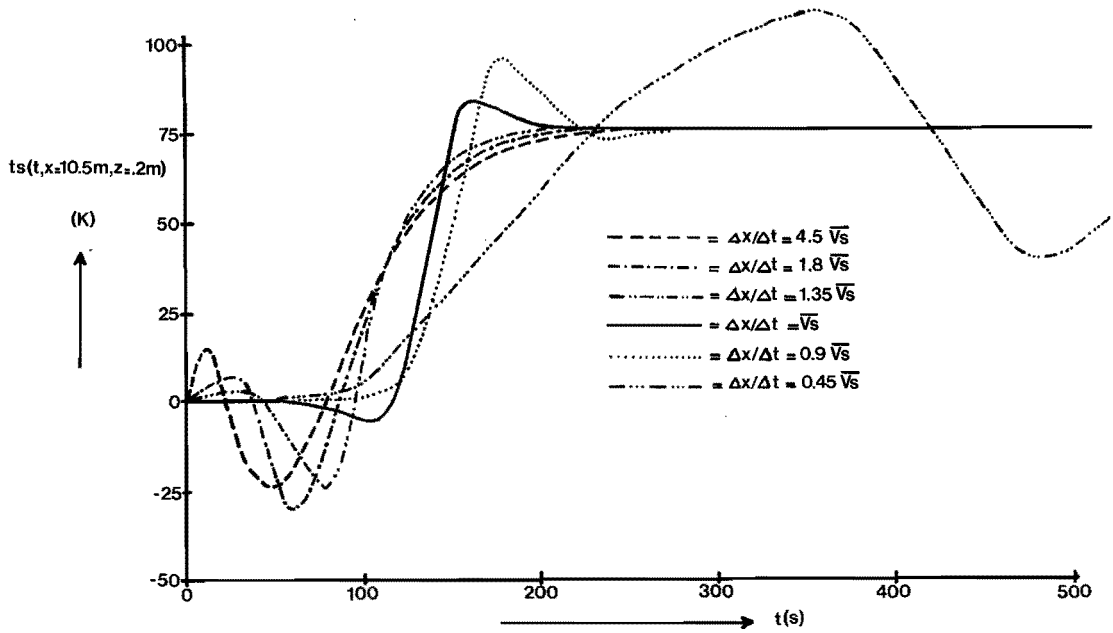

Figure 5.11 Pellet temperature responses at $x=10.5m$, $z=.2m$ to a pellet inlet temperature step disturbance of $100K$ according to the central-difference method (5.22) with $\Delta x=3m$ and different values for $\Delta x/\Delta t$.

the determination of the mean solid temperature only those pellet temperatures of the elementary volume are taken into account that are situated on or near the characteristic /48/

$$x = \overline{Vs}\, t \tag{5.27}$$

Then we have instead of (5.17)

$$\overline{ts}_{l-\frac{1}{2},m-\frac{1}{2},n-\frac{1}{2}} = \tfrac{1}{2}(\overline{ts}_{l,m,n-\frac{1}{2}} + \overline{ts}_{l-1,m-1,n-\frac{1}{2}}) \tag{5.28}$$

As a consequence, the elementary relationship between the unknown solid and gas temperatures and the already known temperatures and velocities becomes instead of (5.22)

$$\begin{vmatrix} \overline{ts}_{l,m,n-\frac{1}{2}} \\ \overline{tg}_{l-\frac{1}{2},m-\frac{1}{2},n} \end{vmatrix} = \left\| \quad \underline{\underline{C}} \quad \right\| \cdot \begin{vmatrix} \overline{ts}_{l-1,m,n-\frac{1}{2}} \\ \overline{ts}_{l,m-1,n-\frac{1}{2}} \\ \overline{ts}_{l-1,m-1,n-\frac{1}{2}} \\ \overline{tg}_{l-\frac{1}{2},m-\frac{1}{2},n-1} \\ \overline{vs}_{l-\frac{1}{2}} \\ \overline{fg}_{l-\frac{1}{2},m-\frac{1}{2}} \end{vmatrix} \tag{5.29}$$

where $\underline{\underline{C}}$, like $\underline{\underline{B}}$, is a (2×6)-matrix which is only a function of m and n.

$$\underline{\underline{C}} = \left\| \begin{matrix} c_{11} & c_{12} & c_{13} & c_{14} & c_{15} & c_{16} \\ c_{21} & c_{22} & c_{23} & c_{24} & c_{25} & c_{26} \end{matrix} \right\| \tag{5.30}$$

The coefficients of $\underline{\underline{C}}$ are given in the appendix in Section 5.5.

The result of the central-difference solution according to (5.29) is shown in Figure 5.12 for a pellet temperature response after an inlet pellet temperature step disturbance of 100 K. When again the ratio $\Delta x/\Delta t = \overline{Vs}$, the expected pure delay response is now simulated exactly. Values of $\Delta x/\Delta t$ that deviate from $\overline{Vs}$ cause oscillations in the neighbourhood of the discontinuity around the exact solution which are, however, still smaller than the oscillations corresponding with a solution according to (5.22).

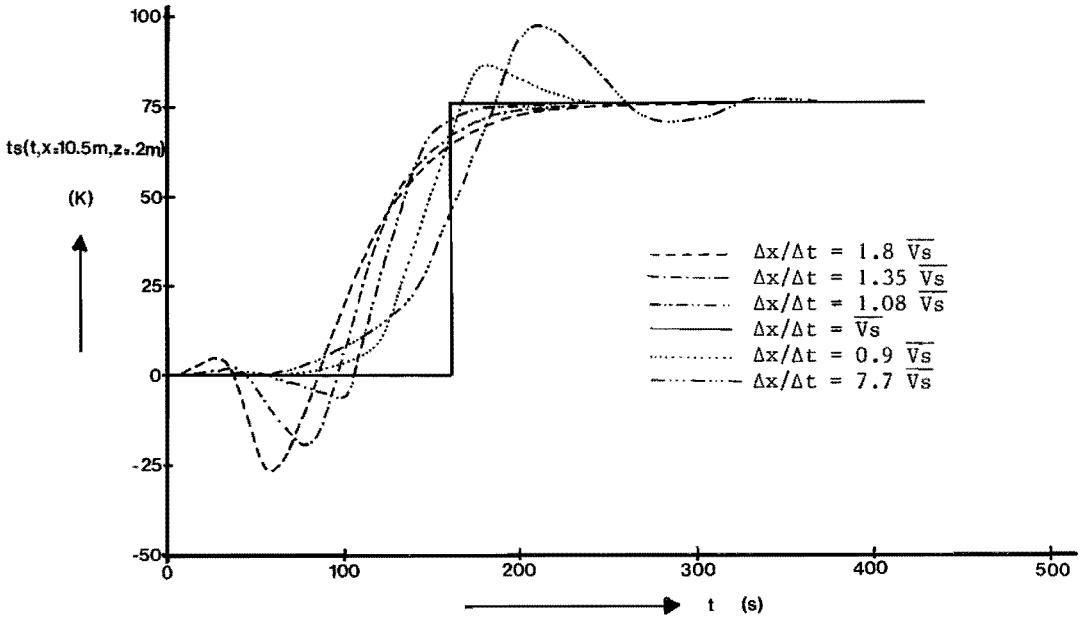

Figure 5.12 Pellet temperature responses at $x=10.5m$, $z=.2m$ to a pellet inlet temperature step disturbance of $100K$ according to the central-dofference method (5.29) with $\Delta x=3m$ and different values for $\Delta x/\Delta t$.

The explanation of the exact simulation of the pure delay function is that for $\Delta x/\Delta t = \overline{Vs}$ the coefficients c_{11}, c_{12}, c_{21} and c_{22} become zero (as can be seen immediately from the appendix) and, hence, $ts_{l,m,n-\frac{1}{2}}$ only depends on one solid temperature, viz. $ts_{l-1,m-1,n-\frac{1}{2}}$.

This also means that the central-difference approximation can be put in a calculation scheme consisting of a (2×4)-matrix, which is even smaller than the backward-difference calculation scheme. Hence, the statically and dynamically more accurate central-difference approximation can be put in such a form that it is even a faster solution method than the backward-difference approximation.

In Figure 5.13 the dynamic behaviour of the pellet bed after a step disturbance in each of the four input variables is shown according to both solution methods. From this picture it is seen that the central-difference solution produced the expected dynamic behaviour of a pure delay, a cut-off first order

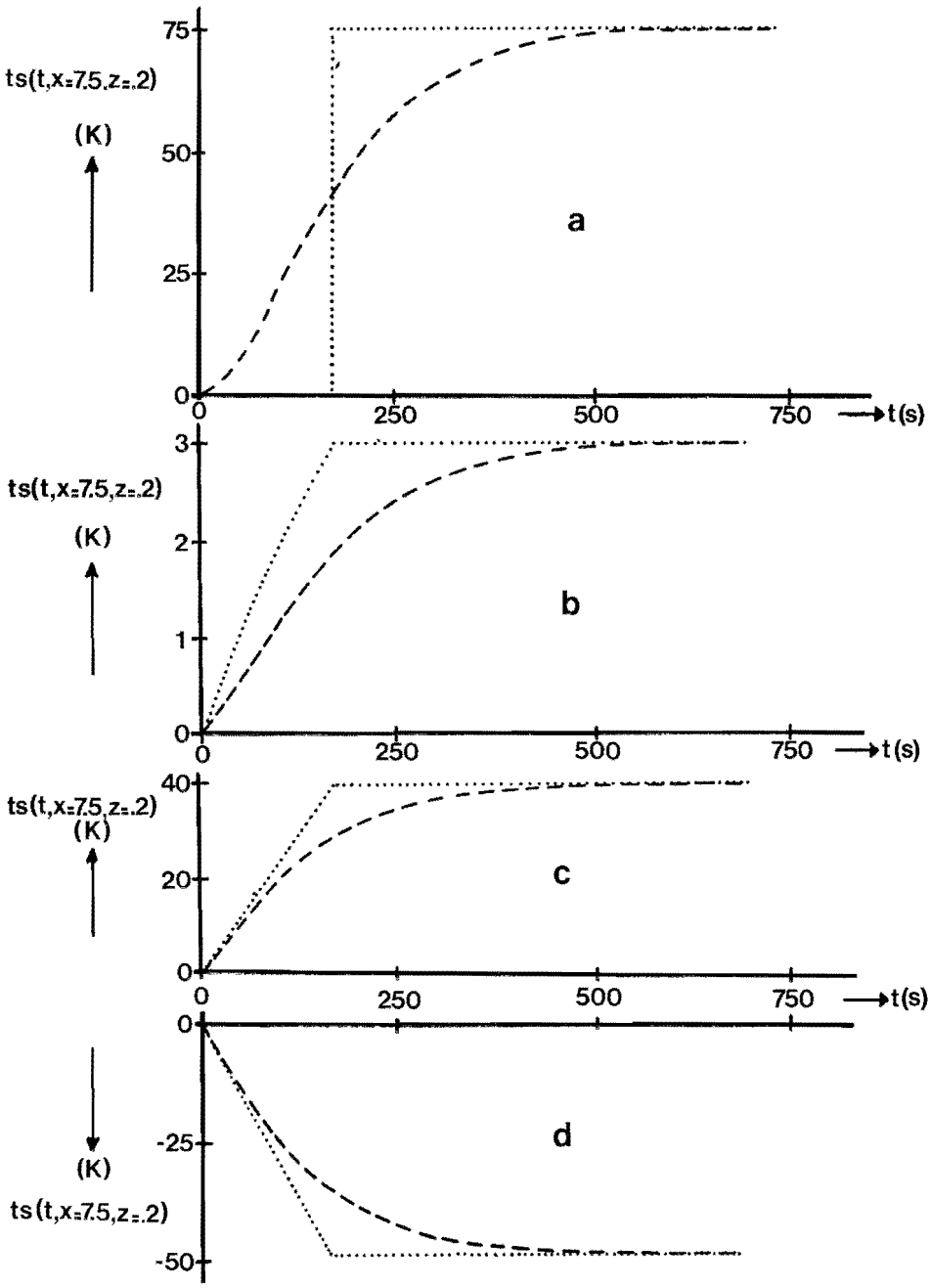

Figure 5.13 Pellet temperature responses at x=7.5 m, z=0.2 m after a step disturbance at t=0 in a/. pellet inlet temperature of 100 K, b/. gas inlet temperature of 20 K, c/. bed velocity of 10% $\overline{Vs}$, d/. gas flow rate of 10% $\overline{Fg}$, according to backward- (– – – –) and central-difference (·····) approximation. Δx=3 m, $\Delta x/\Delta t=\overline{Vs}$.

response and two cut-off ramp response functions, while the backward-difference solution shows after a pellet inlet temperature disturbance an S-shaped higher-order response function (instead of the pure delay) and after each of the other input disturbances a kind of first-order response function.

5.4 CONCLUSIONS

Two finite-difference models have been applied to simulate digitally the d namic behaviour of the cooling zone. The computing time for the simulation by means of the backward-difference approximation resulting in the calculation scheme (5.4) with a coarse horizontal segmentation ($\Delta x = 3m$) was about 2 minutes on the Philips EL-X8 computer. However, especially the dynamic accuracy was rather poor. Refinement of segmentation improved the accuracy but also raised the computation time. The accuracy of the dynamic part of the solution was not influenced appreciably by variations in the ratio $\Delta x/\Delta t$.

Better accuracy was obtained with the central-difference approximation resulting in the calculation scheme (5.22). Simulation with a coarse horizontal segmentation ($\Delta x = 3m$) produced static temperature profiles that are in close agreement with the exact ones and consumed about 4 minutes computer time on the EL-X8. The accuracy of the dynamic part of the solution is strongly influenced by the ratio $\Delta x/\Delta t$. The optimal value for this ratio is $\overline{Vs}$. The oscilatory behaviour of the temperature step responses which is encountered after a step disturbance when applying a central-difference approximation, could be removed by adaptation of the finite-difference scheme ((5.29) instead of (5.22)). In this way a calculation scheme was obtained that is even faster than the backward-difference approximation and still more accurate. It consumes about 1 minute computer time for the simulation of a dynamic response.

For studies involving feedback, e.g. from cooling to a burning zone, by means of digital simulation in the time

domain, many more time steps may have to be made and in that case the total computing time may still become fairly long.

5.5 APPENDIX: EXPRESSIONS FOR THE MATRIX ELEMENTS

The elements of the matrix $\underline{\underline{A}}$ are

$$a_{11} = \frac{\mu s\ L}{a_1\ T}$$

$$a_{12} = \frac{\mu s\ M\ \overline{Vs}}{a_1\ X}$$

$$a_{13} = \frac{A\ \overline{U}\ \gamma g\ \overline{Fg}}{a_1(\gamma g\ \overline{Fg} + A\ \overline{U}\ Z/N)}$$

$$a_{14} = -\frac{1}{a_1}\ \mu s\ \overline{\frac{\partial Ts}{\partial x}}$$

$$a_{15} = \frac{1}{a_1}\left\{A\ \overline{\frac{\partial U}{\partial Fg}}\ (\overline{Ts}-\overline{Tg}) + \frac{\overline{U}\ A\ Z/N}{\gamma g\ \overline{Fg} + A\ \overline{U}\ Z/N}\left[\overline{\frac{\partial U}{\partial Fg}}\ A(Ts-Tg) - \gamma g\ \overline{\frac{\partial Tg}{\partial z}}\right]\right\}$$

$$a_{21} = \frac{A\ \overline{U}\ \mu s\ L/T}{a_2(\mu s\ L/T + \mu s\ \overline{Vs}\ M/X + A\ \overline{U})}$$

$$a_{22} = \frac{A\ \overline{U}\ \mu s\ \overline{Vs}\ M/X}{a_2(\mu s\ L/T + \mu s\ \overline{Vs}\ X/M + A\ \overline{U})}$$

$$a_{23} = \frac{\gamma g\ \overline{Fg}\ N}{a_2\ Z}$$

$$a_{24} = -\frac{A\ \overline{U}\ \mu s\ \overline{\frac{\partial Ts}{\partial x}}}{a_2(\mu s\ L/T + \mu s\ \overline{Vs}\ M/X + A\ \overline{U})}$$

$$a_{25} = \frac{1}{a_2}\left[-\gamma g\ \overline{\frac{\partial Tg}{\partial z}} + \overline{\frac{\partial U}{\partial Fg}}\ A(\overline{Ts}-\overline{Tg}) + \frac{\overline{U}\ A}{\mu s\ L/T + \mu s\ \overline{Vs}\ M/X + \overline{U}\ A}\ \overline{\frac{\partial U}{\partial Fg}}\ A(\overline{Tg}-\overline{Ts})\right]$$

where

$$a_1 = \mu s\ L/T + \mu s\ \overline{Vs}\ M/X + A\ \overline{U} - \frac{(A\ \overline{U})^2}{\gamma g\ \overline{Fg}\ N/Z + A\ \overline{U}}$$

$$a_2 = \gamma g\ \overline{Fg}\ N/Z + A\ \overline{U} - \frac{(A\ \overline{U})^2}{\mu s\ L/T + \mu s\ \overline{Vs}\ M/X + A\ \overline{U}}$$

The matrix elements depend on m and n as the following quantities are a function of them: $\mu s_{m,n}$, $\overline{U}_{m,n}$, $\overline{Fg}_m$, $\gamma g_{m,n}$, $\left.\overline{\frac{\partial Ts}{\partial x}}\right|_{m,n}$, $\left.\overline{\frac{\partial U}{\partial Fg}}\right|_{m,n}$, $\overline{Ts}_{m,n}$, $\overline{Tg}_{m,n}$.

The elements of $\underline{\underline{B}}$ are

$$b_{11} = \frac{1}{b_1}\left[\mu s\ L/T - \mu s\ \overline{Vs}\ M/X - \tfrac{1}{2}\ \overline{U}\ A + \frac{\tfrac{1}{4}(\overline{U}\ A)^2}{(\gamma g\ \overline{Fg}\ N/Z + \tfrac{1}{2}\ \overline{U}\ A)}\right]$$

$$b_{12} = \frac{1}{b_1}\left[-\mu s\ L/T + \mu s\ \overline{Vs}\ M/X - \tfrac{1}{2}\ \overline{U}\ A + \frac{\tfrac{1}{4}(\overline{U}\ A)^2}{(\gamma g\ \overline{Fg}\ N/Z + \tfrac{1}{2}\ \overline{U}\ A)}\right]$$

$$b_{13} = \frac{1}{b_1}\left[\mu s\ L/T + \mu s\ \overline{Vs}\ M/X - \tfrac{1}{2}\ \overline{U}\ A + \frac{\tfrac{1}{4}(\overline{U}\ A)^2}{(\gamma g\ \overline{Fg}\ N/Z + \tfrac{1}{2}\ \overline{U}\ A)}\right]$$

$$b_{14} = \frac{1}{b_1}\{\overline{U}\ A\ (1 + \frac{\gamma g\ \overline{Fg}\ N/Z - \tfrac{1}{2}\ \overline{U}\ A}{\gamma g\ \overline{Fg}\ N/Z + \tfrac{1}{2}\ \overline{U}\ A})\}$$

$$b_{15} = -\frac{2\ \mu s}{b_1}\ \frac{\overline{\partial Ts}}{\partial x}$$

$$b_{16} = \frac{1}{b_1}\left[\frac{\overline{\partial U}}{\partial Fg}\ A(\overline{Tg}-\overline{Ts}) + \frac{\overline{\frac{\partial U}{\partial Fg}}\ A(\overline{Ts}-\overline{Tg}) - \gamma g\ \overline{\frac{\partial Tg}{\partial z}}}{\gamma g\ \overline{Fg}\ N/Z + \tfrac{1}{2}\ \overline{U}\ A}\right]$$

where

$$b_1 = \mu s\ L/T + \mu s\ \overline{Vs}\ M/X + \tfrac{1}{2}\ \overline{U}\ A - \frac{\tfrac{1}{4}\ (\overline{U}\ A)^2}{\gamma g\ \overline{Fg}\ N/Z + \tfrac{1}{2}\ U\ A}$$

and

$$b_{21} = \frac{\overline{U}\ A}{4\ b_2}\left[\frac{\mu s\ L/T - \mu s\ \overline{Vs}\ M/X - \tfrac{1}{2}\ \overline{U}\ A}{\mu s\ L/T + \mu s\ \overline{Vs}\ M/X + \tfrac{1}{2}\ \overline{U}\ A}\right]$$

$$b_{22} = \frac{\overline{U}\ A}{4\ b_2}\left[\frac{-\mu s\ L/T + \mu s\ \overline{Vs}\ M/X - \tfrac{1}{2}\ \overline{U}\ A}{+\mu s\ L/T + \mu s\ \overline{Vs}\ M/X + \tfrac{1}{2}\ \overline{U}\ A}\right]$$

$$b_{23} = \frac{\overline{U}\ A}{4\ b_2}\left[\frac{\mu s\ L/T + \mu s\ \overline{Vs}\ M/X - \tfrac{1}{2}\ \overline{U}\ A}{\mu s\ L/T + \mu s\ \overline{Vs}\ M/X + \tfrac{1}{2}\ \overline{U}\ A}\right]$$

$$b_{24} = \frac{1}{b_2}\{\gamma g\ \overline{Fg}\ N/Z - \tfrac{1}{2}\ \overline{U}\ A + \frac{\tfrac{1}{4}\ (\overline{U}\ A)^2}{\mu s\ L/T + \mu s\ \overline{Vs}\ M/X + \tfrac{1}{2}\ \overline{U}\ A}\}$$

$$b_{25} = -\frac{s}{b_2}\{\frac{\tfrac{1}{2}\ \overline{U}\ A}{\mu s\ L/T + \mu s\ \overline{Vs}\ M/X + \tfrac{1}{2}\ \overline{U}\ A}\}\ \frac{\overline{\partial Ts}}{\partial x}$$

$$b_{26} = \frac{1}{b_2}\{-\gamma g\ \overline{\frac{\partial Tg}{\partial z}} + \overline{\frac{\partial U}{\partial Fg}}\ A(\overline{Ts}-\overline{Tg}) + \frac{\tfrac{1}{2}\ \overline{U}\ A}{\mu s\ L/T + \mu s\ \overline{Vs}\ M/X + \tfrac{1}{2}\ \overline{U}\ A}\ \overline{\frac{\partial U}{\partial Fg}}\ A(\overline{Tg}-\overline{Ts})\}$$

where

$$b_2 = \gamma g\ \overline{Fg}\ N/Z + \tfrac{1}{2}\ \overline{U}\ A - \frac{\tfrac{1}{4}\ (\overline{U}\ A)^2}{\mu s\ L/T + \mu s\ \overline{Vs}\ M/X + \tfrac{1}{2}\ \overline{U}\ A}$$

Here also, the matrix elements depend on m and n as the following quantities are a function of them: $\mu s_{m,n}$, $\overline{U}_{m,n}$, $\overline{Fg}_m$, $\gamma g_{m,n}$, $\left.\overline{\frac{\partial Ts}{\partial x}}\right|_{m,n}$, $\left.\overline{\frac{\partial U}{\partial Fg}}\right|_{m,n}$, $\overline{Ts}_{m,n}$, $\overline{Tg}_{m,n}$.

The elements of $\underline{\underline{C}}$ are

$$c_{11} = \frac{1}{c_1}\{\mu s\ L/T - \mu s\ \overline{Vs}\ M/X\}$$

$$c_{12} = \frac{1}{c_1}\{-\mu s\ L/T + \mu s\ \overline{Vs}\ M/X\}$$

$$c_{13} = \frac{1}{c_1}\{\mu s\ L/T + \mu s\ \overline{Vs}\ M/X - \overline{U}\ A + \frac{\frac{1}{2}(\overline{U}\ A)^2}{\gamma g\ \overline{Fg}\ N/Z + \frac{1}{2}\overline{U}\ A}\}$$

$$c_{14} = \frac{b_1}{c_1} b_{14}$$

$$c_{15} = \frac{b_1}{c_1} b_{15}$$

$$c_{16} = \frac{b_1}{c_1} b_{16}$$

where

$$c_1 = \mu s\ L/T + \mu s\ \overline{Vs}\ M/X + \overline{U}\ A - \frac{\frac{1}{2}(\overline{U}\ A)^2}{\gamma g\ \overline{Fg}\ N/Z + \frac{1}{2}\overline{U}\ A}$$

and

$$c_{21} = \frac{\overline{U}\ A}{2c_2}\left[\frac{\mu s\ L/T - \mu s\ \overline{Vs}\ M/X}{\mu s\ L/T + \mu s\ \overline{Vs}\ M/X + \overline{U}\ A}\right]$$

$$c_{22} = \frac{\overline{U}\ A}{2c_2}\left[\frac{-\mu s\ L/T + \mu s\ \overline{Vs}\ M/X}{\mu s\ L/T + \mu s\ \overline{Vs}\ M/X + \overline{U}\ A}\right]$$

$$c_{23} = \frac{\overline{U}\ A}{2c_2}\left[\frac{\mu s\ L/T + \mu s\ \overline{Vs}\ M/X}{\mu s\ L/T + \mu s\ \overline{Vs}\ M/X + \overline{U}\ A}\right]$$

$$c_{24} = \frac{1}{c_2}\{\gamma g\ \overline{Fg}\ N/Z - \frac{1}{2}\overline{U}\ A + \frac{\frac{1}{2}(\overline{U}\ A)^2}{\mu s\ L/T + \mu s\ \overline{Vs}\ M/X + \overline{U}\ A}\}$$

$$c_{25} = -\frac{\mu s}{c_2}\left[\frac{\overline{U}\ A}{\mu s\ L/T + \mu s\ \overline{Vs}\ M/X + \overline{U}\ A}\right]\frac{\overline{\partial Ts}}{\partial x}$$

$$c_{26} = \frac{1}{c_2}\left[-\gamma g\ \frac{\overline{\partial Tg}}{\partial z} + \frac{\overline{\partial U}}{\partial Fg} A(\overline{Ts}-\overline{Tg}) + \frac{\overline{U}\ A}{\mu s\ L/T + \mu s\ \overline{Vs}\ M/X + \overline{U}\ A}\frac{\overline{\partial U}}{\partial Fg} A(\overline{Tg}-\overline{Te})\right]$$

where

$$c_2 = \gamma g\ \overline{Fg}\ N/Z + \frac{1}{2}\overline{U}\ A - \frac{\frac{1}{2}(\overline{U}\ A)^2}{\mu s\ L/T + \mu s\ \overline{Vs}\ M/X + \overline{U}\ A}$$

Chapter Six

DIGITAL SIMULATION IN THE FREQUENCY DOMAIN

6.1 INTRODUCTION

Instead of a digital simulation in the time domain, a simulation method using an integral-transform method can be applied. In Chapter 4 we found that single Laplace transformation provides the most efficient solution method using integral-transform theory for a segment of the pellet bed. Moreover, when working in the frequency domain inverse transformation to the time domain often is not necessary. The inverse transformation may be omitted when all results can be interpreted in terms of e.g. Bode and/or Nyquist diagrams. Especially for control studies extensive theory is available in frequency-domain terms.

In addition, the results of a simulation in the frequency domain can easily be incorporated in a larger model. Also, feedback control actions or the heat feedback by means of the gas streams between firing and cooling zones can easily be dealt with in the frequency domain. These advantages are due to the fact that convolutions on the time domain reduce to multiplications in the frequency domain.

After a presentation of the model equations in the frequency domain and a discription of the calculation procedure in Section 6.2, the static and dynamic accuracies of the method are considered in Section 6.3. The simulation results are discussed on the basis of Bode diagrams in Section 6.4. After the conclusions in Section 6.5, the expressions for the matrix elements are presented in the appendix in Section 6.6.

Part of this subject has been published in /*13*/.

6.2 SEGMENTATION AND FOURIER TRANSFORMATION

If we again apply central differences to the spatial coordinates but retain the derivatives with respect to time, we may obtain equations like

$$\left(\frac{\mu s}{2}\frac{\partial}{\partial t} + \frac{\mu s\ \overline{Vs}}{X/M} + \frac{\overline{U}\ A}{2}\right)\overline{ts}_{m,n-\frac{1}{2}} + \left(\frac{\mu s}{2}\frac{\partial}{\partial t} - \frac{\mu s\ \overline{Vs}}{X/M} + \frac{\overline{U}\ A}{2}\right)\overline{ts}_{m-1,n-\frac{1}{2}} + \tag{6.1}$$

$$- \frac{\overline{U}\ A}{2}\overline{tg}_{m-\frac{1}{2},n} - \frac{\overline{U}\ A}{2}\overline{tg}_{m-\frac{1}{2},n-1} + \left\{\frac{\overline{\partial U}}{\partial \overline{Fg}}\ A\ (\overline{Ts}-\overline{Tg})\right\}\overline{fg}_{m-\frac{1}{2}} + \mu s\ \frac{\overline{\partial Ts}}{\partial x}\ vs$$

$m=1,2,\ldots,M;\ n=1,2,\ldots,N.$

$$\left(\frac{\gamma g\ \overline{Fg}}{Z/N} + \frac{\overline{U}\ A}{2}\right)\overline{tg}_{m-\frac{1}{2},n} + \left(-\frac{\gamma g\ \overline{Fg}}{Z/N} + \frac{\overline{U}\ A}{2}\right)\overline{tg}_{m-\frac{1}{2},n-1} - \frac{\overline{U}\ A}{2}\overline{ts}_{m,n-\frac{1}{2}} +$$

$$- \frac{\overline{U}\ A}{2}\overline{ts}_{m-1,n-\frac{1}{2}} + \left\{\frac{\overline{\partial U}}{\partial \overline{Fg}}\ A\ (\overline{Tg}-\overline{Ts}) - \gamma g\ \frac{\overline{\partial Tg}}{\partial z}\right\}\overline{fg}_{m-\frac{1}{2}} \tag{6.2}$$

$m=1,2,\ldots,M;\ n=1,2,\ldots,N.$

The corresponding frequency-response representation may be written as

$$\begin{vmatrix} \tilde{\overline{ts}}_{m,n-\frac{1}{2}} \\ \tilde{\overline{tg}}_{m-\frac{1}{2},n} \end{vmatrix} = \left\| \underline{\underline{D}} \right\| \cdot \begin{vmatrix} \tilde{\overline{ts}}_{m-1,n-\frac{1}{2}} \\ \tilde{\overline{tg}}_{m-\frac{1}{2},n-1} \\ \tilde{vs} \\ \tilde{\overline{fg}}_{m-\frac{1}{2}} \end{vmatrix} \tag{6.3}$$

where $\underline{\underline{D}}$ is a (2x4)-matrix which is a function of m and n as well as $j\omega$, whose elements are given in the appendix in Section 6.6. These elements are complex functions of the angular frequency ω and can be written in the general form

$$d(\omega) = \frac{d_1 + d_3\ j\omega}{d_2 + j\omega} \tag{6.4}$$

Using relation (6.3) between the inlet and outlet variables of an element, the calculation of the dynamic behaviour of

the pellet bed is reduced to simple multiplication of matrices containing complex elements.

6.3 ACCURACY OF THE METHOD

The static accuracy will be the same for the digital frequency-domain simulation as for the digital time-domain simulation using central differences described in Section 5.3.3, since in both simulations the space-dependent part of the model (as described by the equations (5.24) and (5.25)) is the same.

To check the dynamic accuracy of the method, simulations with different numbers of segments M and layers N have been compared. The necessary number of layers for a satisfying simulation of the gas and pellet temperatures of the bed in vertical direction was found to be eight or more as in the static case /69/. The fact that an equal number of layers gives the same accuracy in the static case as in the dynamic case is explained by the absence of an accumulation term (dynamics) in the heat balance of the gas (3.23).

The dynamic accuracy is strongly influenced by the segmentation in the horizontal x direction. An exact analytical solution is possible for the somewhat simpler case of a gas-solid cross-flow heat exchanger with constant coefficients using threefold Laplace transformation /5/. However, this solution, which is a three-dimensional version of the solution derived in Section 4.3, takes an enormous amount of computer time /6/.

A more convenient approach to test the dynamic accuracy is to see how fast the solution (6.3) converges for increasing m. Moreover, the exact solution of the pellet temperature response function after a pellet inlet temperature disturbance is characterised by a pure time delay and a gain factor as can be deduced directly from (3.22) and (3.23), and as we also know already from the simulation results in Chapter 5. In the frequency domain the corresponding Bode diagram should show a constant amplitude ratio for all

frequencies and an exponential phase behaviour because of the logarithmic frequency scale.

Hence, the accuracy of the dynamic simulations of the space-lumped equations can be tested by comparing the Bode diagrams of a transfer function of the solid temperature at the end of a compartment of the bed after a disturbance in inlet pellet temperature with the exact ones. Figure 6.2 shows that for the first cooling zone segmentation of the horizontal length in $M=33$ segments gives satisfactory simulation results up to a frequency $\omega = 0.03\ s^{-1}$. At that frequency the error in amplitude ratio is less than 5% and the phase error is only 25^{o} while the phase shift is already -360^{o}.

Use of finer horizontal segmentation, which would give an accurate simulation also for higher frequencies, is not meaningful, since for frequencies above $\omega=0.04\ s^{-1}$ the assumption of uniform internal pellet properties is not valid any more (see Section 2.3). For accurate simulation results at higher frequencies a different model must be used. However, as has been said in Section 2.3, phenomena of such high frequencies do not influence the process.

6.4 DYNAMIC CHARACTERISTICS

In Figures 6.1 to 6.8 some transfer functions are shown for gas and solid temperature responses after disturbances in inlet solid and gas temperature, bed velocity or gas flow rate, which illustrate the dynamic behaviour of the cooling section of the pellet-indurating plant. In these Bode diagrams a resonance effect occurs, which is well known from parallel-flow heat exchangers /15,20,27/. Here, too, the first minimum resonance peak is at frequency

$$\omega = \frac{2\ \pi\ \overline{Vs}}{X} \qquad (6.5)$$

From Figures 6.3 and 6.4 it may be seen that the transfer functions $\hat{\vartheta}s/\hat{f}g$ and $\hat{\vartheta}s/\hat{v}s$ are almost identical except for a phase shift of π radians and a proportionality constant. This means that the dynamic effect of a velocity disturbance is

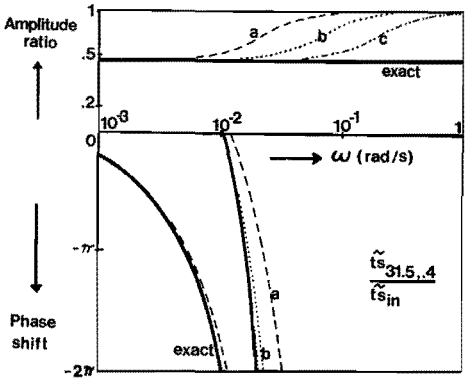

Figure 6.1 Frequency response of the pellet temperature $\tilde{ts}$ at $x=31.5m$, $z=0.4m$ to disturbances in solid inlet temperature $\tilde{ts}_0$. Curve a: $X/M=3m$; curve b: $X/M=1m$; curve c: $X/M=.33m$.

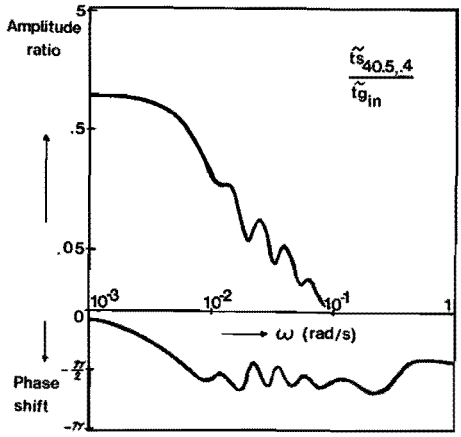

Figure 6.2 Frequency response of the pellet temperature $\tilde{ts}$ at $x=40.5m$, $z=0.4m$ to disturbances in gas inlet temperature $\tilde{tg}_0$. $X/M=3m$.

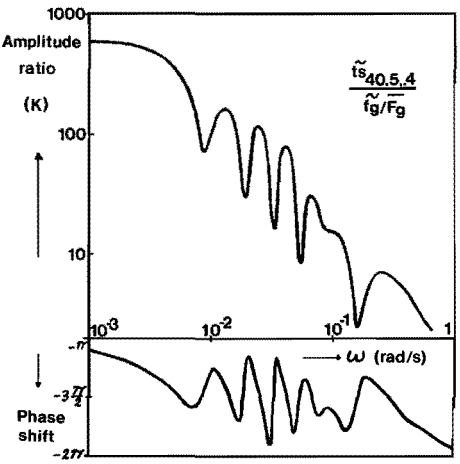

Figure 6.3 Frequency response of the pellet temperature $\tilde{ts}$ at $x=40.5m$, $z=0.4m$ to disturbances in gas flow rate $\tilde{fg}/Fg$. $X/M=3m$.

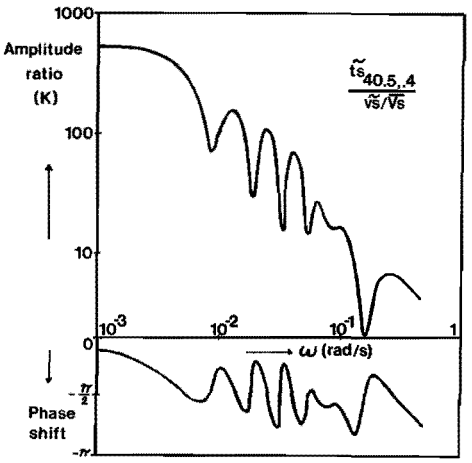

Figure 6.4 Frequency response of the pellet temperature $\tilde{ts}$ at $x=40.5m$, $z=0.4m$ to disturbances in bed velocity $\tilde{vs}/Vs$. $X/M=3m$.

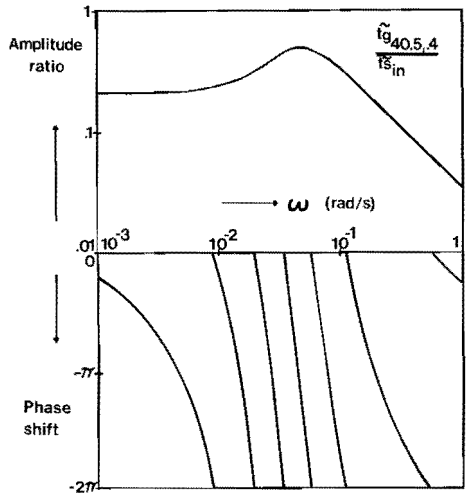

Figure 6.5 Frequency response of the gas temperature $\tilde{tg}$ at $x=40.5m$, $z=0.4m$ to disturbances in pellet inlet temperature $\tilde{ts}_0$. $X/M=3m$.

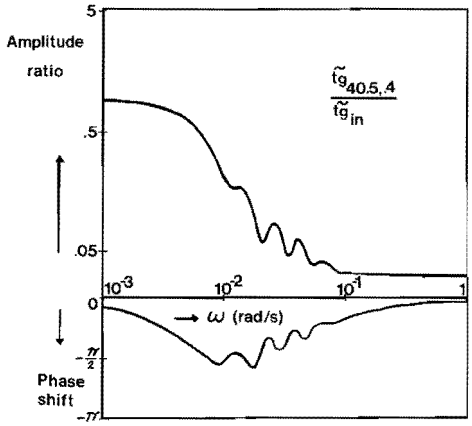

Figure 6.6 Frequency response of the gas temperature $\tilde{tg}$ at $x=40.5m$, $z=0.4m$ to disturbances in gas inlet temperature $\tilde{tg}_0$. $X/M=3m$.

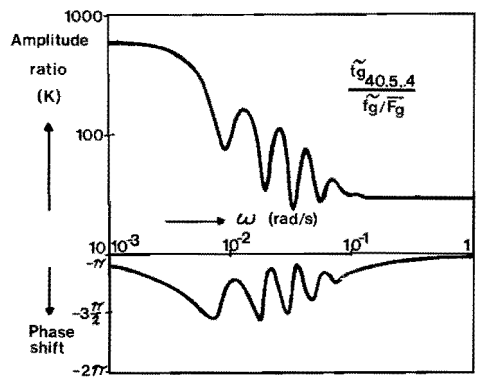

Figure 6.7 Frequency response of the gas temperature $\tilde{tg}$ at $x=40.5m$, $z=0.4m$ to disturbances in gas flow rate $\tilde{fg}/\overline{Fg}$. $X/M=3m$.

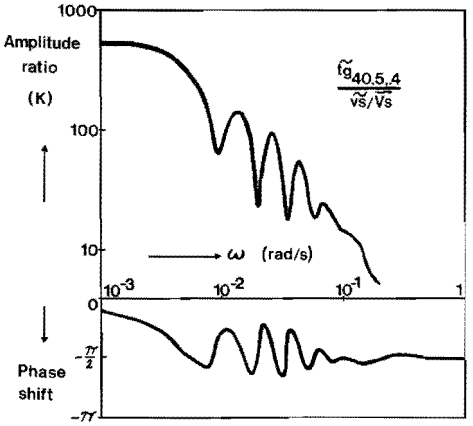

Figure 6.8 Frequency response of the gas temperature $\tilde{tg}$ at $x=40.5m$, $z=0.4m$ to disturbances in bed velocity $\tilde{vs}/\overline{Vs}$. $X/M=3m$.

opposite to that of a gas flow rate disturbance. This result indicates the usefulness of proportional feedforward compensation of the effect of the measurable bed velocity disturbances by means of gas flow rate adjustments.

Comparison of Figure 6.2 with Figures 6.3 and 6.4 shows that the resonance effect is less pronounced after a gas temperature disturbance than after a bed velocity or gas flow rate disturbance. Similar phenomena are found in the frequency-domain simulation of a steam-water parallel-flow heat exchanger /64/.

Application of the initial value theorem in the case of a step response gives

$$\lim_{t \to 0} \{f(t)\} = \lim_{|q| \to \infty} \{q \frac{\mathcal{F}(q)}{q}\} \qquad (6.6)$$

where $\mathcal{F}(q)$ is the transfer function and, hence, $\mathcal{F}(q)/q$ the Laplace transform of the step response. Therefore, from the Bode diagrams of $\mathcal{T}_g/\mathcal{T}_{g_{in}}$ and $\mathcal{T}_g/\mathcal{F}_g$ - where, as can be seen from Figures 6.6 and 6.7, for high frequencies the amplitude ratio's converge to a non-zero value and the phses to zero - it can be concluded that after a step disturbance of the inlet gas temperature or the gas flow rate, the responses in the time domain of the gas temperatures in the bed start with a non-zero value at $t=0$. This result, which is caused by the neglection of the accumulation term in the heat balance of the gas, is in accordance with what has been found in the other simulations (see Figures 7.9 and 8.10).

In Figure 6.9 transfer functions of the outlet water temperature of a steam-water parallel-flow heat exchanger to disturbances in steam temperature and water velocity are shown, together with the corresponding time-domain responses after a step disturbance. A cut-off first order response results after a temperature disturbance and a cut-off ramp after a velocity disturbance. The difference between both responses is difficult to recognise. In the Bode diagram the difference is more pronounced: zero values for the

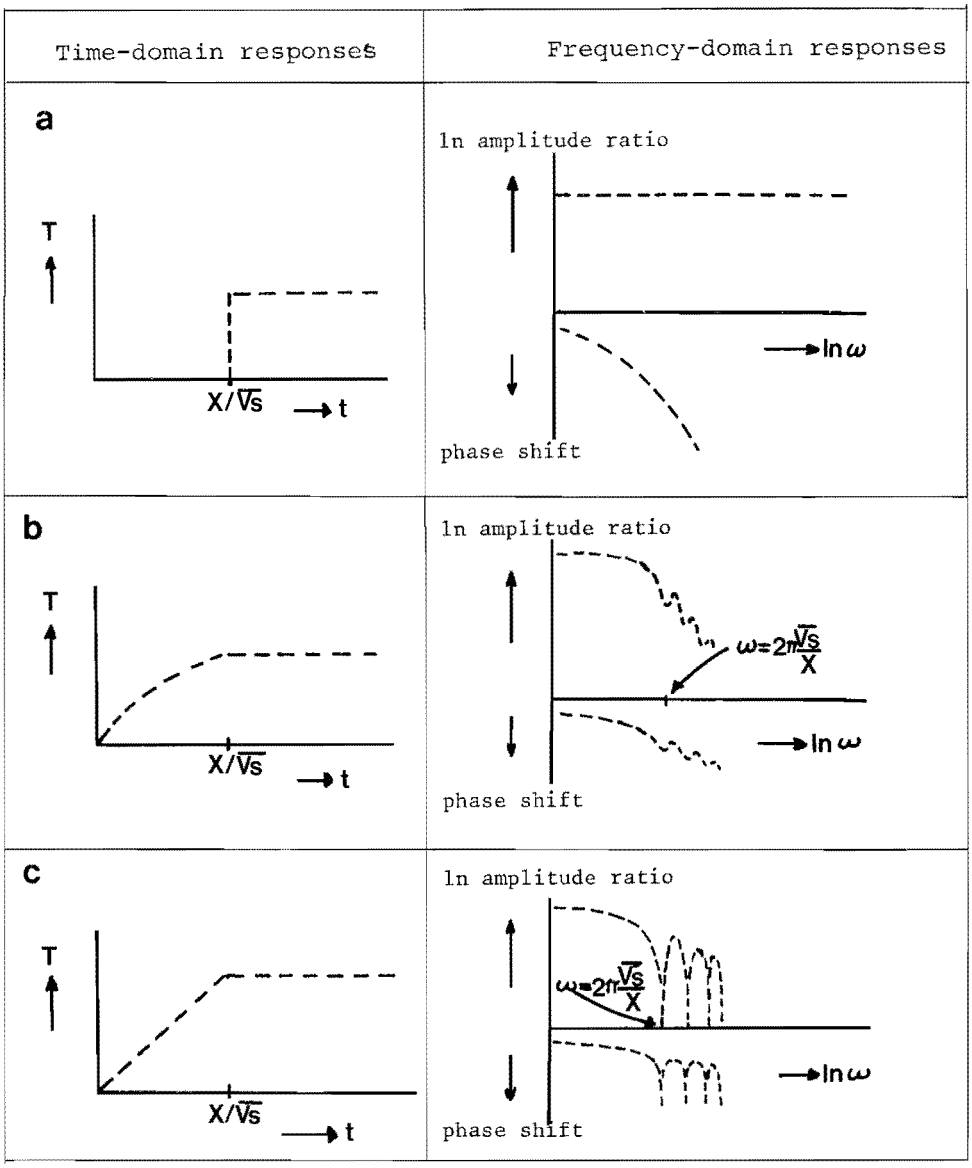

Figure 6.9 Time-domain and frequency-domain responses of the outlet water temperature of a parallel-flow heat exchanger /64/:
a. pure dead-time response function
b. cut-off first order response function
c. cut-off ramp response function

amplitude ratio in the Bode diagram after velocity disturbances at frequencies

$$\omega_k = 2 \pi k \frac{\overline{Vs}}{X} \qquad k=1,2,... \tag{6.7}$$

and a much weaker resonance effect after disturbances in water inlet temperature.

6.5 CONCLUSIONS

Computation time of the complete frequency response of the cooling section of the pellet-indurating plant is about 4 minutes on the ELX8 digital machine. Hence, the amount of computer time is somewhat larger than for the time-domain simulation of Chapter 5. However, after one calculation all transfer functions are known and for an investigation of the effect of different modes of control and various locations of sensor elements, repeated calculation of the cooling section is not necessary, since the closed-loop frequency response of a control system can be readily obtained from the open loop frequency response.

The similar dynamic behaviour of the pellet bed after gas flow rate and bed velocity disturbances as well as the different dynamic behaviour after gas inlet temperature disturbances compared with the behaviour after gas flow rate and bed velocity disturbances, was clearly demonstrated by their frequency responses. In time-domain simulations these differences can hardly be recognised.

By means of the frequency-domain simulation some properties of the dynamic behaviour are explained from a different point of view. In this way more insight in the process is obtained.

6.6 APPENDIX: EXPRESSIONS FOR THE MATRIX ELEMENTS

$$d_{11} = \frac{1}{d_1} \left[\left(\frac{2 \mu s \overline{Vs}}{X/M} - \mu s j\omega - \overline{U} A \right) \left(\frac{2 \gamma g \overline{Fg}}{Z/N} + \overline{U} A \right) + (\overline{U} A)^2 \right]$$

$$d_{12} = \frac{1}{d_1} \left[2 \overline{U} A \frac{2 \gamma g \overline{Fg}}{Z/N} \right]$$

$$d_{13} = -\frac{2}{d_1}\left(\frac{2\,\gamma g\,\overline{Fg}}{Z/N} + \overline{U}\,A\right)\left(\mu s\,\overline{\frac{\partial Ts}{\partial x}}\right)$$

$$d_{14} = \frac{2}{d_1}\left[\overline{U}\,A\,\{-\gamma g\,\overline{\frac{\partial Tg}{\partial z}} + \overline{\frac{\partial U}{\partial Fg}}\,A\,(\overline{Ts}-\overline{Tg})\} + \left(\frac{2\,\gamma g\,\overline{Fg}}{Z/N} + \overline{U}\,A\right)\overline{\frac{\partial U}{\partial Fg}}\,A\,(\overline{Tg}-\overline{Ts})\right]$$

$$d_{21} = \frac{1}{d_2}\left(\frac{4\,\mu s\,\overline{Vs}}{X/M}\,\overline{U}\,A\right)$$

$$d_{22} = \frac{1}{d_2}\left[\left(\frac{2\,\mu s\,\overline{Vs}}{X/M} + \mu s\,j\omega + \overline{U}\,A\right)\left(\frac{2\,\gamma g\,\overline{Fg}}{Z/N} - \overline{U}\,A\right) + (\overline{U}\,A)^2\right]$$

$$d_{23} = -\frac{2}{d_2}\left(\overline{U}\,A\,\mu s\,\overline{\frac{\partial Ts}{\partial x}}\right)$$

$$d_{24} = \frac{2}{d_2}\left[\{\overline{\frac{\partial U}{\partial Fg}}\,A\,(\overline{Ts}-\overline{Tg}) - \gamma g\,\overline{\frac{\partial Tg}{\partial z}}\}\{\frac{2\,\mu s\,\overline{Vs}}{X/M} + \mu s\,j\omega + \overline{U}\,A\} + \overline{U}\,A^2\,\overline{\frac{\partial U}{\partial Fg}}\,(\overline{Tg}-\overline{Ts})\right]$$

$$d_1 = d_2 = \left(\frac{2\,\mu s\,\overline{Vs}}{X/M} + \mu s\,j\omega + \overline{U}\,A\right)\left(\frac{2\,\gamma g\,\overline{Fg}}{Z/N} + \overline{U}\,A\right) - (\overline{U}\,A)^2$$

Chapter Seven

HYBRID SIMULATION

7.1 INTRODUCTION

When the digital simulation of partial-differential equations is prohibitively long and expensive, hybrid computers have been shown to have the potential to be several hundred times faster and cheaper (per solution) than are digital computers /67/. In /17/ comparative results are reported for a dynamic parameter optimisation problem concerning a chemical reactor. Digital results from an IBM360/65 were compared with calculations run on a hybrid computer AD4/IBM1800. While the differences between digital and hybrid results were less than 1%, the digital computing time proved to be roughly 500 times the hybrid computing time. However, as an extrapolation of the current trend would lead one to expect a five to fiftyfold increase in digital computing speed in the coming ten years /38/, the future may show a switch-over to on-line all-digital simulation.

In order to get an idea about the usefulness of a general-purpose hybrid computer for the calculation of the transient behaviour of the pellet-indurating plant, a simulation has been set up on the AD4/IBM1800 computer of the Delft University of Technology in 1972/73.

Part of this chapter has been presented at the 7th AICA conference on hybrid computation at Prague in August 1973 /*10*/.

7.2 IMPLEMENTATION

To solve partial-differential equations on a hybrid computer, they must be reduced to a set of ordinary-differential equations with only one continuous variable. For the process equations (3.22) and (3.23) one may conceive methods in which the continuous variable is the time t (called CTDXDZ method: continuous t, discrete x, discrete z) or the

length x (DTCXDZ method), or the height z (DTDXCZ method). A combination of time and one or two space variables is also possible, but because of its expected complexity this case will not be considered further.

A choice can be made between the above mentioned possibilities by reconsideration of the equations (3.22) and (3.23) which will be rewritten here unmodified

$$\{\mu s \frac{\partial}{\partial t} + \mu s \overline{Vs} \frac{\partial}{\partial x} + \overline{U} A\} ts - \overline{U} A tg + \mu s \frac{\overline{\partial Ts}}{\partial x} vs + \\ + \frac{\overline{\partial U}}{\partial Fg} A (\overline{Ts} - \overline{Tg}) fg = 0 \qquad (7.1)$$

$$\{\gamma g \overline{Fg} \frac{\partial}{\partial z} + \overline{U} A\} tg - \overline{U} A ts + \{\gamma g \frac{\overline{\partial Tg}}{\partial z} - \frac{\overline{\partial U}}{\partial Fg} A (\overline{Ts} - \overline{Tg})\} fg = 0 \qquad (7.2)$$

The steady-state values (denoted by overlined symbols) are obtained from the static model and are space-dependent, viz. $\overline{Tg}(x,z)$, $\overline{Ts}(x,z)$, $\overline{Fg}(x)$, $\overline{U}(x)$, $\frac{\overline{\partial U}}{\partial Fg}(x)$, $\frac{\overline{\partial Ts}}{\partial x}(x,z)$, $\frac{\overline{\partial Tg}}{\partial z}(x,z)$. The coefficients μs and γg are weakly temperature dependent and, therefore, they are taken locally constant. Hence, in (7.1) and (7.2) all coefficients are functions of x and/or z, but not of time t. Therefore, only the use of the continuous time method would not need function generators to provide x- or z-dependent coefficients and steady-state values, which would complicate the solution considerably. This problem does not exist when the CTDXDZ method is used. The x and z dependence of the coefficients is then accounted for by means of constant coefficients for a $\Delta x \Delta z$ element. The complete time behaviour of such an element can be calculated with constant coefficients. In our case we simulate a whole segment. The x and z dependence is effected by changing the coefficient values when proceeding from one segment to the next.

When in the literature about hybrid computation a choice must be made between CTDS (continuous time, discrete space) and DTCS methods, almost always the DTCS method is chosen. The motivation herefore is not always equally convincing.

Many authors, such as in /4,8,33/, confuse the problem by putting the following false dilemma: when using CTDS methods, reference is made to analog computation and when working with DTCS methods to hybrid computation, while for a just appraisal the comparison of CTDS and DTCS methods ought to be considered on the same machine.

In general it can be said that for hybrid simulation of a linearised model CTDS methods are preferable because of the space-dependent coefficients resulting from the linearisation procedure.

After application of the central-difference approximation for the differential quotients with respect to x and z, use of the CTDXDZ method implies that the original partial-differential equations (7.1) and (7.2) can be replaced by the following set of ordinary-differential equations

$$\frac{dts_{m,n-\frac{1}{2}}}{dt} = e_1 \frac{dts_{m-1,n-\frac{1}{2}}}{dt} + e_2\, ts_{m-1,n-\frac{1}{2}} + e_3\, ts_{m,n-\frac{1}{2}} + e_4\, tg_{m-\frac{1}{2},n-1} + \\ + e_5\, tg_{m-\frac{1}{2},n} + e_6\, vs + e_7\, fg_{m-\frac{1}{2}} \tag{7.3}$$

$$tg_{m-\frac{1}{2},n} = e_8\, ts_{m-1,n-\frac{1}{2}} + e_9\, ts_{m,n-\frac{1}{2}} + e_{10}\, tg_{m-\frac{1}{2},n-1} + e_{11}\, fg_{m-\frac{1}{2}} \tag{7.4}$$

where $m=1,2,\ldots,M;\ n=1,2,\ldots,N$.
The coefficient values are given in the appendix in Section 7.5.

The analog scheme of (7.3) and (7.4) for element (m,n) is shown in Figure 7.1. Analog implementation of the whole cooling section would require $M \times N$ analog circuits.

For multidimensional problems a significant reduction of computing hardware (over straightforward analog continuous-time simulation) is obtained by implementation of only one "line" on the analog computer. A "line" is defined as a set of solution points with one index constant, e.g. a set of solution points having the same x coordinate (a segment) or the same z coordinate (a layer).

In the fairly accurate digital solution of (3.22) and (3.23)

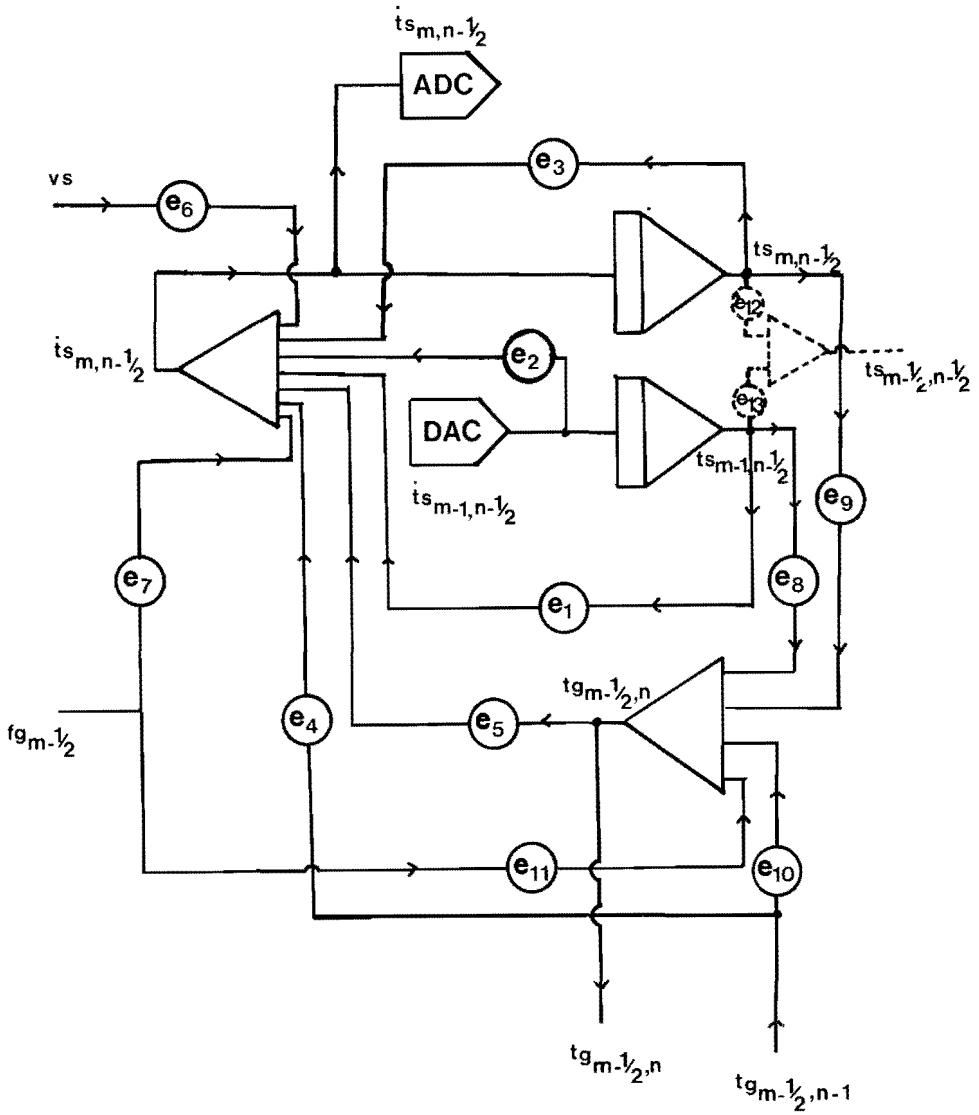

Figure 7.1 Analog scheme of the (m,n)-th element of the pellet bed. The dashed components must be added in order to circumvent the "see-saw" effect.

obtained in Chapter 5 using a central-difference model, the height Z was divided into $N=9$ layers and the length of the cooling zone into $M=13$ or 39 segments. On the AD4, the analog part of the hybrid computer, these nine layers, needed for an accurate simulation of one segment, could just be implemented. Therefore, the hybrid simulation was set up according to a line-multiplexing method /67/ with a segment as a "line". Thus, nine elements like Figure 7.1 were patched on the AD4, the outgoing gas temperature of element (m,n) being connected to the inlet one of element $(m,n+1)$. This computation procedure is visualised schematically in Figure 7.2.

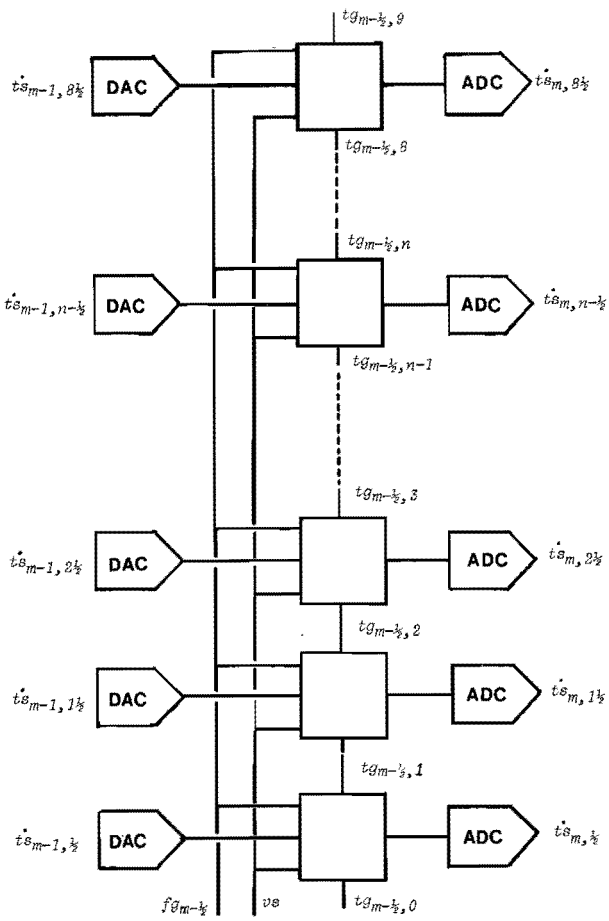

Figure 7.2 Schematic representation of hybrid simulation using the line-multiplexing principle

The coupling between segments (in the horizontal direction) was provided by the digital computer. The time behaviour of the outputs of the segment under consideration was stored in the digital computer by means of track-store units and A/D converters. After all interesting responses had been stored, the DCU's (digital coefficient units) of the analog part were provided with new values according to the steady-state values of the next segment. Afterwards, the stored output temperature responses of the last segment, i.e. the inputs to the new segment, were played back via D/A converters.

The procedure of storage and play-back of the *derivative* of the solid temperature was chosen. The value of the solid temperature itself in the next segment is obtained by integration (see Figure 7.1). The reason why this method was followed is the following: Since $ts_{m-1,n-\frac{1}{2}}$ as well as $\frac{dts}{dt}_{m-1,n-\frac{1}{2}}$ must be known, 18 time functions would have to be stored and played back for each segment. If we want to transport only half of this number of functions, we have to perform an integration or differentiation afterwards. If the solid temperature values are stored and played back, the differentiation of these values introduces large errors. The method known as θ-interpolation in the literature /67/ (use of central differences results in $\theta=\frac{1}{2}$) avoids this problem by storing in the digital machine just that combination of calculated values that will be needed as an input to the next segment, viz.

$$e_1 \frac{dts_{m,n-\frac{1}{2}}}{dt} + e_2 \, ts_{m,n-\frac{1}{2}} \qquad (7.5)$$

where the values of e_1 and e_2 of the next element must be used. However, this approach only satisfies single or uncoupled partial-differential equation problems and cannot be applied in our case. For, as can be seen from (7.3) and (7.4), apart from the combination (7.5) which is needed in (7.3), the temperature $ts_{m-1,n-\frac{1}{2}}$ itself is needed in (7.4). Therefore, the procedure of storage and play-back of the derivative of the pellet temperature was chosen.

The hybrid set-up may be summarised as follows: the analog

part provides high-speed integration with respect to time for all (discrete) values of z. Integration with respect to the x-direction was performed by storage and play-back of the derivatives of the pellet-temperature responses of a segment. Analog patching of a whole segment ($N=9$ elements) eliminated the problem of storage and play-back with respect to the z direction. The derivatives with respect to the x and z directions were taken into account by means of a central-difference approximation, exactly as has been done for all independent variables in Chapter 5.

However, application of the central-difference approximation with respect to the x dependence while integration of time is performed continuously, results in the so-called "see-saw" effect /60/. This effect causes the model to exhibit unrealistic reversals in outlet temperature responses (see Figure 7.3). The "see-saw" effect does not influence the ultimate static value of the temperature response, but the transient behaviour of the response is largely in error. Refined segmentation with respect to the x direction does not remove the effect. In Chapter 5 it was found that, when using central differences, the dynamic behaviour could be simulated accurately by taking the ratio of the steps in the x and t directions equal to $\overline{Vs}$:

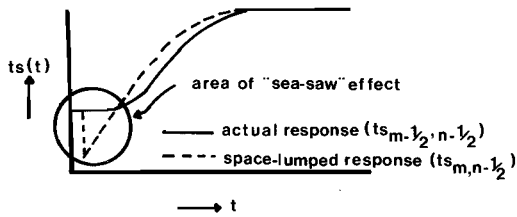

Figure 7.3 "See-saw" effect for step increase in inlet temperature

$$\frac{\Delta x}{\Delta t} = \overline{Vs} \tag{7.6}$$

If $\Delta x/\Delta t < \overline{Vs}$, oscillations originate at the end of the response. With $\Delta x/\Delta t > \overline{Vs}$, the response function starts with oscillations (see Figure 5.11). In the hybrid model where time is taken continuous, the limit case $\Delta t \to 0$ exists. Therefore, response functions as shown in Figure 7.3 arise.

To overcome the "see-saw" effect. Schidt and Clarke /60/

propose the method of "time-lumping" instead of space-lumping, by which they mean that the observation point is now becoming an arbitrary mass of the moving bed itself. In fact, they transform a partial-differential equation with respect to t and x, like (7.1), into an ordinary-differential equation with respect to the residence time

$$\theta = t - \frac{x}{\overline{Vs}} \tag{7.7}$$

This method of simulation of the pellet bed by considering "moving segments" suffers from three drawbacks:

1. Because of the linearisation procedure the method is complicated, since the variation of the coefficients and steady-state values as functions of θ must be implemented by function generators.

2. Although in this way the unrealistic reversals after a pellet inlet temperature disturbance have been eliminated, the time-lumped model tends to delay unrealistically responses to gas-side disturbances /60/.

3. With the use of the residence time θ being a combination of real time and horizontal distance, an additional complication arises, because finally results in real time and distance are required. Therefore, at the end of the simulation process an inverse transformation has to occur.

We found that the process of the "see-saw" effect can be avoided in the following way: In the central-difference approximation the pellet temperature in an element of length $\Delta x = X/M$ was replaced by the mean of the incoming and outgoing solid temperatures (as was done in deriving (7.3) from (7.1))

$$ts_{m-\frac{1}{2},n-\frac{1}{2}} = \frac{1}{2}\left(ts_{m-1,n-\frac{1}{2}} + ts_{m,n-\frac{1}{2}}\right) \tag{7.8}$$

and the derivative with respect to x by

$$\left.\frac{\partial ts}{\partial x}\right|_{m-\frac{1}{2},n-\frac{1}{2}} = \frac{ts_{m,n-\frac{1}{2}} - ts_{m-1,n-\frac{1}{2}}}{X/M} \tag{7.9}$$

Hence, these variables do not actually appear in the formulae. Instead use is made of what we might call "auxiliary variables",

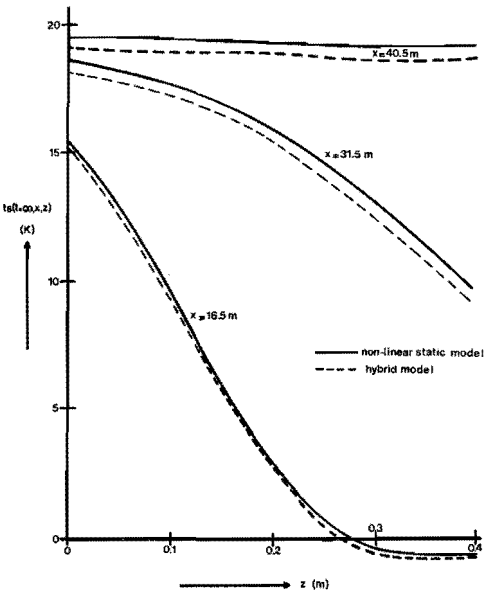

Figure 7.4 Static pellet temperature change after a gas temperature step disturbance of 20 K

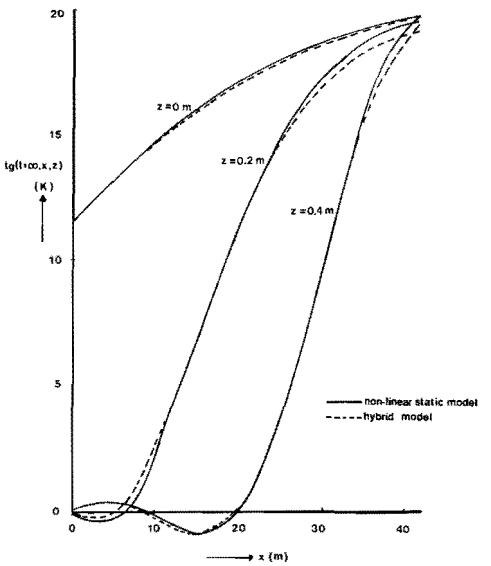

Figure 7.5 Static gas temperature change after a gas temperature step disturbance of 20 K

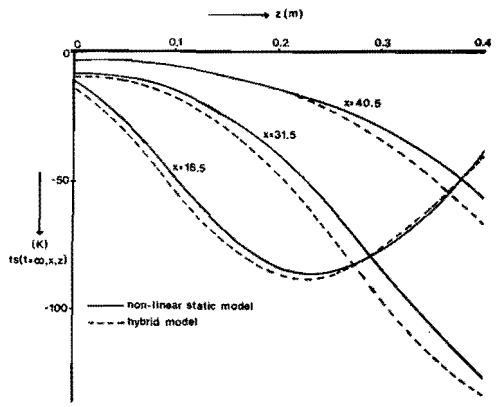

Figure 7.6 Static pellet temperature change after a gas flow step disturbance of 10% $\overline{Fg}$

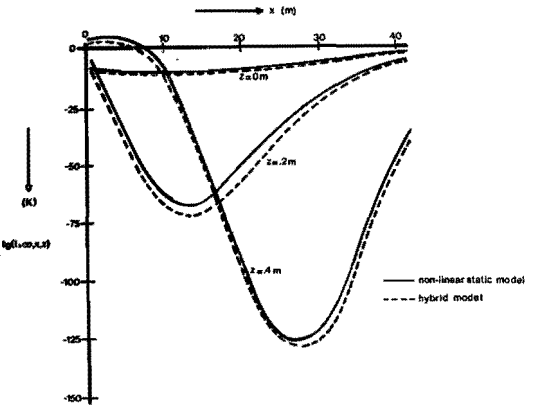

Figure 7.7 Static gas temperature change after a gas flow step disturbance of 10% $\overline{Fg}$

viz. $ts_{m-1,n-\frac{1}{2}}$ and $ts_{m,n-\frac{1}{2}}$, while the real temperature of element (m,n) is $ts_{m-\frac{1}{2},n-\frac{1}{2}}$. The see-saw effect arises when the auxiliary temperatures instead of the real temperatures are plotted and it can be avoided by also calculating the real temperatures according to (7.8)

$$ts_{m-\frac{1}{2},n-\frac{1}{2}} = e_{12}\, ts_{m,n-\frac{1}{2}} + e_{13}\, ts_{m-1,n-\frac{1}{2}} \qquad e_{12}=e_{13}=\frac{1}{2} \qquad (7.10)$$

This is implemented by patching the elements sketched in dotted lines in Figure 7.1 on the analog part of the hybrid machine. In all further hybrid simulations reported in this chapter use has been made of this implementation.

7.3 STATIC AND DYNAMIC RESULTS

The ultimate steady-state values after a step disturbance in one of the input variables are in good agreement with those calculated by means of the static non-linear digital model. This illustrated in Figures 7.4 to 7.7, which show profiles of static pellet and gas temperature changes after an inlet gas temperature disturbance of 20 K and a gas flow disturbance of 10% of the normal steady-state value $\overline{Fg}$. From these pictures it can be concluded that the dynamic hybrid simulation is at least statically satisfactory.

Most dynamic responses are in good agreement with the theoretically expected ones (see Figure 5.13). In Figure 7.8 are shown the pellet temperature step responses after a 10% gas flow rate disturbance. Similar dynamic responses are found after a 10% bed velocity disturbance, but then the signs of the responses are opposite.

An interesting effect observed in Figure 7.9, where some gas temperature responses after a disturbance of the gas inlet temperature of 20 K are presented for various heights in the bed. At the bottom of the bed the response is the sum of a step function (a constant part) and a first-order function. Higher up in the bed the gas response function loses its constant part (the step) and tends to be a higher-order response function.

From the simulation point of view, the explanation of this effect is as follows: going opwards in a segment, the outgoing gas temperature $tg_{m-\frac{1}{2},n}$ of element (m,n) is according to (7.4) the sum of a fraction of the incoming gas temperature $e_{10}\ tg_{m-\frac{1}{2},n-1}$ and the solid temperatures of the element with appropriate coefficients $e_8\ ts_{m-1,n-\frac{1}{2}} + e_9\ ts_{m,n-\frac{1}{2}}$. If only a gas inlet temperature disturbance is present , these solid temperatures are related by integration to the gas temperatures (see Figure 7.1). Roughly speaking, the outgoing gas temperature response of element (m,n) is partly proportional to the incoming gas temperature and further related to it by

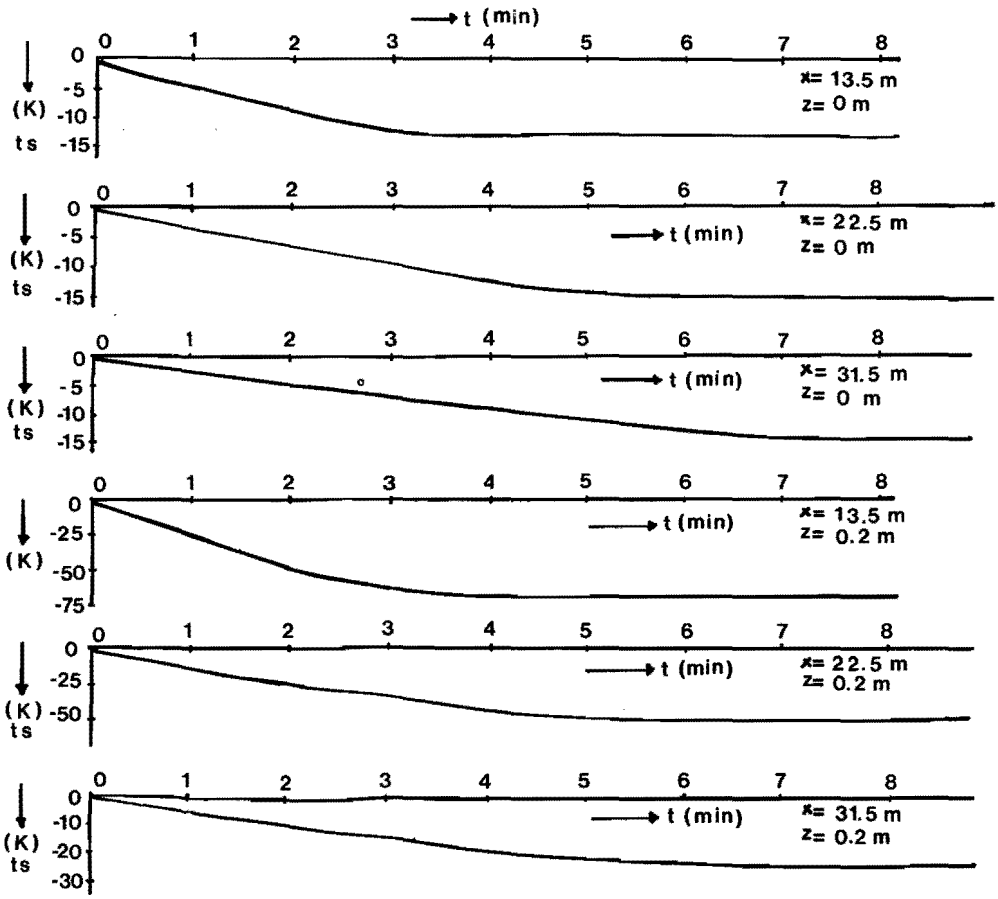

Figure 7.8 Pellet temperature step responses for $z=0$ and $0.2m$ and different positions of x after a gas flow rate disturbance of 10% $\overline{Fg}$.

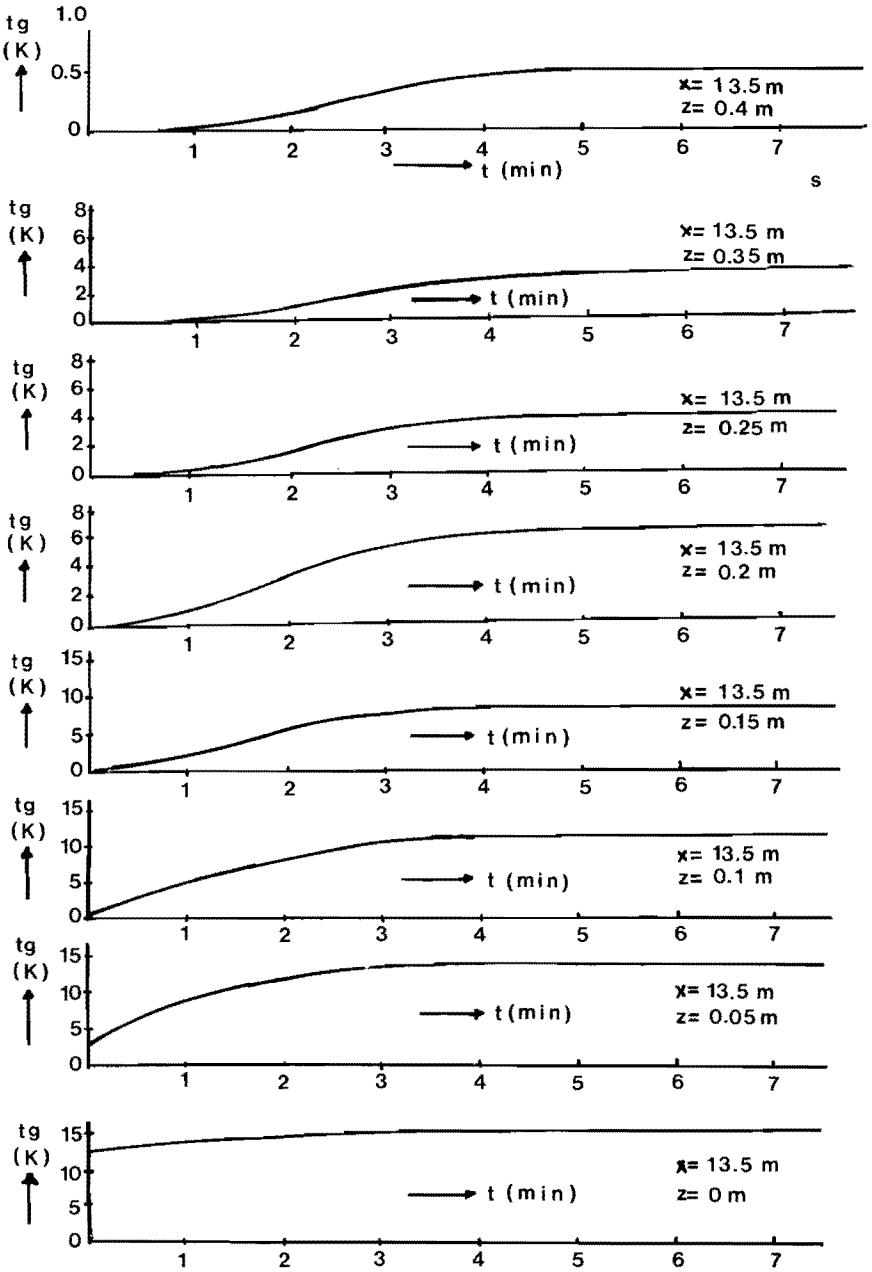

Figure 7.9 Gas temperature step responses for $x=13.5m$ and at various heights z after a gas inlet temperature disturbance of 20 K

an additional first-order response of this incoming gas temperature.

Physically, the following interpretation can be given: if a segment is considered to be a packed-bed heat exchanger, it is known from the literature that the heat and gas flow move at different velocities because the exchange of heat between the gas and the solid (pellets) slows the thermal wave with respect to the fluid wave /63/. The same effect is observed in Figure 7.9. Although the gas velocity is very high and variations in the gas flow rate therefore are almost immediately perceptible, it takes some time before the inlet gas temperature disturbance is sensed above in the bed.

In Figure 7.10 pellet temperature responses after a step disturbance in the pellet inlet temperature are shown for different places in the bed. The oscillations can be reduced by using a finer horizontal segmentation as is shown in

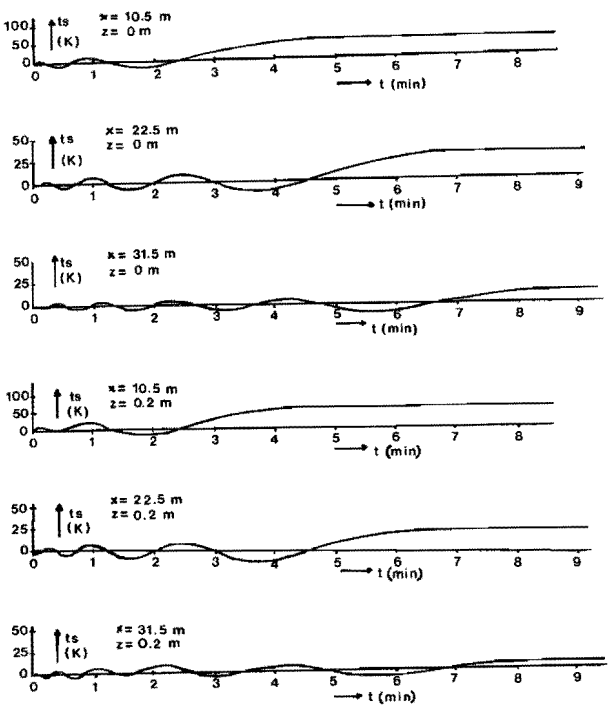

Figure 7.10 Pellet temperature step responses for different values of x and $z=0.2m$ after a disturbance of the pellet inlet temperature of 100 K.

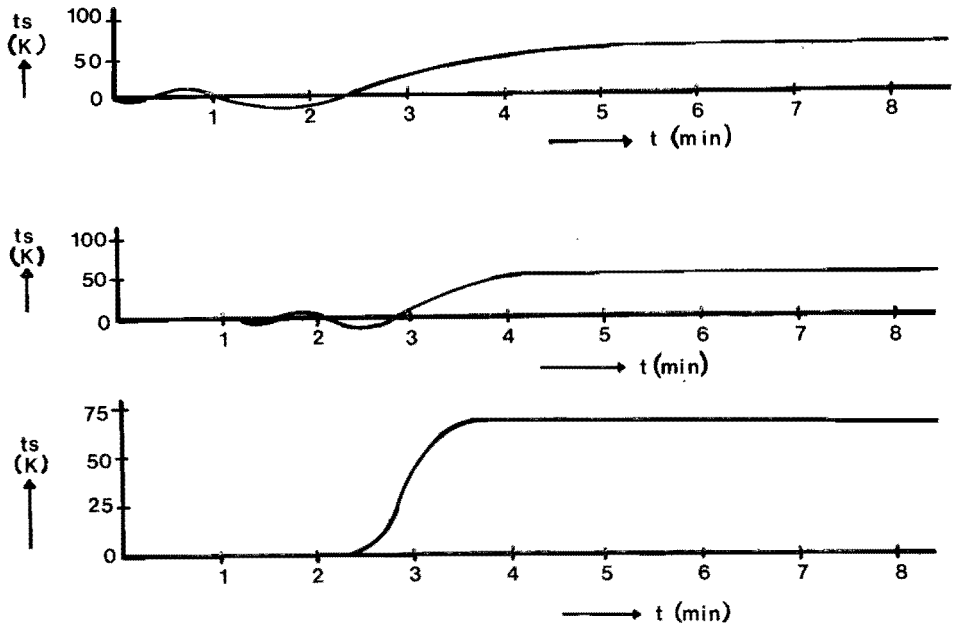

Figure 7.11 Pellet temperature step responses at $x=10.5m$, $z=0m$ after a disturbance of the pellet inlet temperature of 100 K with different segmentation in the x direction: a/ $\Delta x=3m$, b/ $\Delta x=1m$, c/ $\Delta x=.33m$.

Figure 7.11, whereas it should be noted that the oscillations in Figure 7.3 (the "see-saw" effect) cannot be reduced by refined segmentation.

When $\Delta x = X/M$ is taken smaller, the slope of the response curve becomes steeper and therefore the response function approximates better the theoretically expected gain factor plus pure time delay (see Figure 5.13).

7.4 CONCLUSIONS

A hybrid simulation was set up because of the fact that hybrid computers are known to be much faster than digital ones. A CTDS line-multiplexing method was shown to be a favourable hybrid implementation, given the linearised process equations.

The limiting factor in the speed of the hybrid simulation was the hybrid interface used for the function storage and play-back feature. The main part of the total computing time neede for the calculation of the cooling zones was the sample-

sample-loop time T_{sample} multiplied by the number of samples S taken from a signal, the number of signals (= the number of layers N) and the number of segments M.

Because of the large number of samples used for each signal much memory space was needed by the sampling procedure. Insufficient core memory necessitated the use of disc memory also for storing local subroutines and coefficient values. The total computing time therefore increased by a considerable amount of organisation time T_{org}

$$T_{tot} = M \times (N \times S \times T_{sample} + T_{org}) \qquad (7.11)$$

In the existing configuration the lower limit of the sample-loop time T_{sample} was about $1\ ms$ and the organisation time T_{org} about $0.5\ s$. With $M=13$, $N=9$ and $S=400$ the total computing time became about one minute. Hence, the speed advantage of hybrid over digital computation was reduced by the large number of disc transfers.

All static and dynamic results proved to be in good agreement with the theoretically expected ones.

7.5 APPENDIX: COEFFICIENT VALUES

$$e_1 = -1$$

$$e_2 = \frac{2\,\overline{Vs}}{X/M} - \frac{\overline{U}\,A}{\mu s}$$

$$e_3 = -\frac{2\,\overline{Vs}}{X/M} - \frac{\overline{U}\,A}{\mu s}$$

$$e_4 = e_5 = \frac{\overline{U}\,A}{\mu s}$$

$$e_6 = \frac{2\,M}{X}\,(\overline{Ts}_{m-1,n-\frac{1}{2}} - \overline{Ts}_{m,n-\frac{1}{2}})$$

$$e_7 = \frac{A}{\mu s}\,\overline{\frac{\partial U}{\partial Fg}}\,\{(\overline{Tg}_{m-\frac{1}{2},n-1} + \overline{Tg}_{m-\frac{1}{2},n}) - (\overline{Ts}_{m-1,n-\frac{1}{2}} + \overline{Ts}_{m,n-\frac{1}{2}})\}$$

$$e_8 = e_9 = \frac{\overline{U}\,A}{\overline{U}\,A + \frac{2\,\gamma g\,\overline{Fg}}{Z/N}}$$

$$e_{10} = \frac{\frac{2\ \gamma g\ \overline{Fg}}{Z/N} - \overline{U}\ A}{\frac{2\ \gamma g\ \overline{Fg}}{Z/N} + \overline{U}\ A}$$

$$e_{11} = \frac{A\ \frac{\overline{\partial U}}{\partial Fg}\ \{(\overline{T\varepsilon}_{m-1,n-\frac{1}{2}} + \overline{T\varepsilon}_{m,n-\frac{1}{2}}) - (\overline{Tg}_{m-\frac{1}{2},n-1} + \overline{Tg}_{m-\frac{1}{2},n})\}}{\frac{2\ \gamma g\ \overline{Fg}}{Z/N} + \overline{U}\ A} +$$

$$+ \frac{\frac{2\ \gamma g\ \overline{Fg}}{Z/N}\ (\overline{Tg}_{m-\frac{1}{2},n-1} - \overline{Tg}_{m-\frac{1}{2},n})}{\frac{2\ \gamma g\ \overline{Fg}}{Z/N} + \overline{U}\ A}$$

Chapter Eight

RC-NETWORK SIMULATION

8.1 INTRODUCTION

Conventional analog simulation of the whole cooling section requires far more analog components (viz. integrators and coefficients for at least 120 analog circuits as in Figure 7.1) than are available on a general-purpose analog computer such as the EAI680 with, typically, 30 integrators.

A similar situation exists for the simulation of parallel-flow heat exchangers. It was recognised in the literature that for these systems special-purpose analog machines (mainly consisting of resistors, capacitors and buffer amplifiers) would be preferable. However, the usefulness of the results of the first RC networks published in the literature is rather doubtful. The analog RC circuit of Mozley /49/ even ignores the use of buffer amplifiers needed for the simulation of the transport equation. Like Mozley, Ford /24/, Kourim /39/ and Mirsepassi /47/ give only results for the dynamic behaviour of a heat exchanger after inlet temperature disturbances of one of the fluids. However, the effect of variations in fluid flow is very important because the flow is mostly used as a correcting variable in a control system. But, if independent current sources are used for the RC-circuit simulation of flow disturbances, realisation is bound to be complicated and expensive.

In /36/, Jørgensen and Kümmel present results from special-purpose simulation of a transportation lag and a double-pipe heat exchanger with counter-current flows. Introducing variable resistances, realised by transistor-switch hardware, they were able to simulate flow disturbances without the use of independent current sources. This feature makes their method fairly attractive. A drawback of the method is that the RC circuit is complicated by the transistor-switch part.

In this chapter the simulation of the cooling section by means of a special-purpose RC network is described. The electric network derived consists only of passive elements (resistors and capacitors) and (buffer) amplifiers. No integrators are used contrary to hybrid simulation. In order to simulate flow disturbances, the buffer amplifiers are given a gain factor higher than 1. In this way the use of complicated transistor-switch hardware was circumvented. The proposed method can also take into account the linearised flow dependence of the heat transfer coefficient, a feature that is not present when variable resistors are used (Section 8.2).

In order to reduce the number of buffer amplifiers, use has been made of a backward-difference approximation of (3.22) and (3.23). The resulting set of equations for an elementary volume can easily be simulated on a flip-chip module. The static accuracy can be improved when the steady-state values are taken in a central-difference way, as is described in Section 8.3.

As regards the dynamic accuracy, it is shown in Section 8.4 that for continuous-time simulation the backward-difference approximation is second-order correct if a small "spurious" diffusion in the direction of x is assumed. Some extra model characteristics that can easily be taken into account when working with RC networks are also described here.

In Section 8.5 some typical simulation results are shown.

In conclusion (Section 8.6), some remarks on simulation speed, flexibility and costs of this rather uncommon simulation technique are discussed.

8.2 A SEMI-PASSIVE ELECTRIC ANALOG

For the same reason as mentioned in Section 7.2, also in the RC-network simulation time is chosen as the continuous variable. Application of a backward-difference approximation of (3.22) and (3.23) gives

$$\mu s \frac{dts_{m,n}}{dt} + \frac{\mu s \overline{Vs}}{X/M} (ts_{m,n} - ts_{m-1,n}) + \overline{U}_m A (ts_{m,n} - tg_{m,n}) +$$

$$+ \frac{\mu s}{X/M} \left(\overline{Ts}_{m,n} - \overline{Ts}_{m-1,n}\right) vs + \left.\frac{\overline{\partial U}}{\partial \overline{Fg}}\right|_m A \left(\overline{Ts}_{m,n} - \overline{Tg}_{m,n}\right) fg_m = 0 \quad (8.1)$$

$$\frac{\gamma g \, \overline{Fg}_m}{Z/N} \left(tg_{m,n} - tg_{m,n-1}\right) + \overline{U}_m A \left(tg_{m,n} - ts_{m,n}\right) + \quad (8.2)$$

$$+ \left[\frac{\gamma g}{Z/N} \left(\overline{Tg}_{m,n} - \overline{Tg}_{m,n-1}\right) + \left.\frac{\overline{\partial U}}{\partial \overline{Fg}}\right|_m A \left(\overline{Tg}_{m,n} - \overline{Ts}_{m,n}\right)\right] fg_m = 0$$

A backward-difference approximation has been taken because it can be implemented much more easily by means of RC elements than the more accurate central-difference approximation. The influence of the former approximation on the accuracy is discussed in Sections 8.3 and 8.4.

Physically speaking, all terms in (8.1) and (8.2) represent heat currents (dimension: J s^{-1}). When these heat currents are simulated by analog electric currents and the temperatures by voltages, equation (8.1) can be represented by the RC network of Figure 8.1 and equation (8.2) by the network of Figure 8.2. Both inter-coupled equations are simulated by

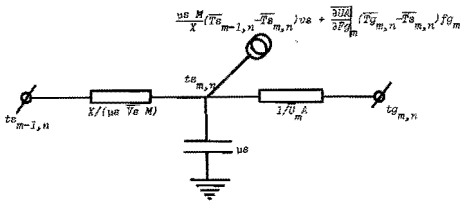

Figure 8.1 Network representation of equations (8.1)

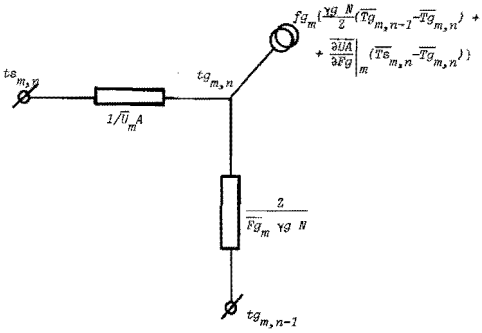

Figure 8.2 Network representation of equation (8.2)

coupling the networks of Figures 8.1 and 8.2, which results in the RC scheme of Figure 8.3. Such a network must be built for each elementary volume. Since there is no backmixing, the network of adjacent elementary volumes are coupled with the aid of buffer amplifiers. Altogether, $M \times N$ networks must be built and coupled.

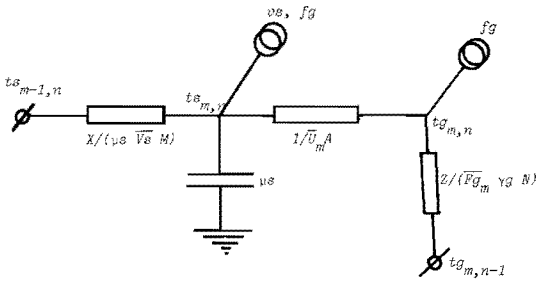

Figure 8.3 Coupled network representing representing equations (8.1) and (8.2)

The terms in (8.1) and (8.2) which take into account the effect of vs and fg disturbances must be simulated by appropriate current sources. However, implementation of current sources would make realisation of the network very complicated. If the flow dependence of the overall heat transfer coefficient U is neglected, the effect of velocity and flow variations may be incorporated in the network by means of the use of variable resistors achieved by inserting a fast transistor switch in series with the resistors Rs and Rg /36/. The linearisation procedure can be omitted in this case.

A simpler solution of the problem of including flow and velocity disturbances in the RC simulation is possible. Consider the network of Figure 8.4. Here $ts_{m-1,n}$, $ts_{m,n}$, $tg_{m,n-1}$, $tg_{m,n}$, vs and fg_m are voltages (variables) and the other quantities are constants. Application of Kirchhoff's current law in node 1 gives

$$\mu s \frac{dts_{m,n}}{dt} = \frac{ts_{m-1,n} - \beta s_{m,n}\, ts_{m,n}}{Rs_{m,n}} + \frac{tg_{m,n} - ts_{m,n}}{Rt_{m,n}} + \frac{vs - \beta v_{m,n}\, ts_{m,n}}{Rv_{m,n}} + \frac{fg_m - \beta f1_{m,n}\, ts_{m,n}}{Rf1_{m,n}} - \frac{ts_{m,n}}{Ra_{m,n}} \tag{8.3}$$

which can be written as

$$\mu s \frac{dts_{m,n}}{dt} = \frac{ts_{m-1,n} - ts_{m,n}}{Rs_{m,n}} + \frac{tg_{m,n} - ts_{m,n}}{Rt_{m,n}} + \frac{vs}{Rv_{m,n}} + \frac{fg_m}{Rf1_{m,n}} + \\ + ts_{m,n} \left[\frac{1 - \beta s_{m,n}}{Rs_{m,n}} - \frac{\beta v_{m,n}}{Rv_{m,n}} - \frac{\beta f1_{m,n}}{Rf1_{m,n}} - \frac{1}{Ra_{m,n}} \right] \tag{8.4}$$

This is identical with (8.1) if

$$\frac{1 - \beta s_{m,n}}{Rs_{m,n}} = \frac{\beta v_{m,n}}{Rv_{m,n}} + \frac{\beta f1_{m,n}}{Rf1_{m,n}} + \frac{1}{Ra_{m,n}} \tag{8.5}$$

and

$$\frac{1}{Rs_{m,n}} = \frac{\mu s \; Vs}{X/M} \tag{8.6}$$

$$\frac{1}{Rt_{m,n}} = \overline{U}_m A \tag{8.7}$$

$$\frac{1}{Rv_{m,n}} = \frac{\mu s}{X/M} \left(\overline{Ts}_{m-1,n} - \overline{Ts}_{m,n} \right) \tag{8.8}$$

$$\frac{1}{Rf1_{m,n}} = \overline{\left. \frac{\partial U}{\partial Fg} \right|_m} A \left(\overline{Tg}_{m,n} - \overline{Ts}_{m,n} \right) \tag{8.9}$$

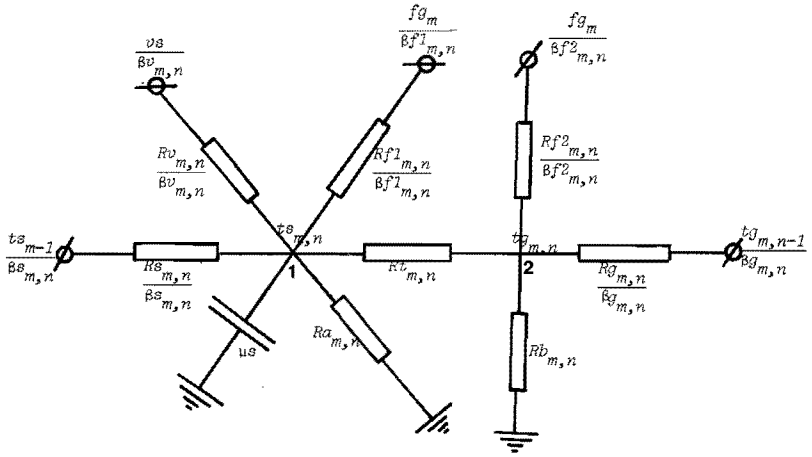

Figure 8.4 Coupled network representing equations (8.1) and (8.2) when only voltage sources are used

Kirchhoff's current law applied to node 2 gives

$$\frac{tg_{m,n-1} - \beta g_{m,n}\, tg_{m,n}}{Rg_{m,n}} + \frac{ts_{m,n} - tg_{m,n}}{Rt_{m,n}} + \frac{fg_m - \beta f2_{m,n}\, tg_{m,n}}{Rf2_{m,n}} + \\ - \frac{tg_{m,n}}{Rb_{m,n}} = 0 \tag{8.10}$$

which can be written as

$$\frac{tg_{m,n-1} - tg_{m,n}}{Rg_{m,n}} + \frac{ts_{m,n} - tg_{m,n}}{Rt_{m,n}} + \frac{fg_m}{Rf2_{m,n}} + \\ + tg_{m,n}\left[\frac{1 - \beta g_{m,n}}{Rg_{m,n}} - \frac{\beta f2_{m,n}}{Rf2_{m,n}} - \frac{1}{Rb_{m,n}}\right] = 0 \tag{8.11}$$

This identical with (8.2) if

$$\frac{1 - \beta g_{m,n}}{Rg_{m,n}} = \frac{\beta f2_{m,n}}{Rf2_{m,n}} + \frac{1}{Rb_{m,n}} \tag{8.12}$$

and

$$\frac{1}{Rg_{m,n}} = \frac{\gamma g\ \overline{Fg}_m}{Z/N} \tag{8.13}$$

$$\frac{1}{Rf2_{m,n}} = -\frac{1}{Rf1_{m,n}} + \frac{\gamma g}{Z/N}\left(\overline{Tg}_{m,n-1} - \overline{Tg}_{m,n}\right) \tag{8.14}$$

To simplify the simulation, the constants β are taken independent of m and n. Furthermore, $\beta f1 \triangleq \beta f2 \triangleq \beta f$, which makes possible the use of only one voltage source for the flow disturbance fg_m. If $\beta s = \beta g = \frac{1}{2}$, the coupling between the adjacent networks must be realised by means of buffer amplifiers with a gain factor $1/\beta s = 1/\beta g = 2$.

The resistors $Ra_{m,n}$ and $Rb_{m,n}$ are needed to make possible the use of uniform scaling factors βs, βg, βv and βf for all $M \times N$ networks. βs, βg, βv and βf can only fulfil (8.5) and (8.12) for $m=1,2,\ldots,M$ and $n=1,2,\ldots,N$, if βv and βf are so small that for each elementary volume positive resistances

$Ra_{m,n}$ and $Rb_{m,n}$ can be found. Generally, $Ra_{m,n}$ and $Rb_{m,n}$ will be different for the network of each elementary volume.

After an investigation into the (static) accuracy of the simulation scheme (see following section) it was decided to simulate the cooling section of the pellet-indurating plant by means of $M \times N = 13 \times 9 = 117$ networks as in Figure 8.4.

In the RC simulation only three types of electronic components are used, viz. resistors, capacitors and amplifiers. In choosing electronic components several objectives must be fulfilled such as high accuracy and low cost. A special point of importance is formed by the overall size of the RC simulator. To keep this within reasonable limits, it is necessary - because of the large number of networks - to use small electronic components. For resistors this is no problem. Integrated circuits can be used as small buffer amplifiers. In fact, the feasibility of building a special-purpose RC simulator originated with the availability of cheap small amplifiers.

The size problem was most serious with respect to capacitors. One of the final objectives of the RC simulation is to perform control experiments by coupling the RC simulator (the process) with the small digital computer (PDP-8I) of the Measurement and Control Group as a controller /16/. The time constants of the simulator must be large compared with the minimum sample and control-calculation period of the digital controller (about $1.2\ ms$). The typical input resistance of $2\ M\Omega$ of the amplifiers imposes a maximum value on the resistors. The only remaining possibility of making the RC time as large as necessary is to use large capacitances, which implies geometrically large-sized capacitors. The maximum size of the capacitors, however, is determined by the distance between two flip-chip modules. Hence, although, in principle, the scaling factors between heat and electrical resistance and real and simulated time can be chosen arbitrarily, feasibility reduces these degrees of freedom.

Apart from the size, a problem was formed by the price/accuracy dilemma. A choice was made for 5% inaccurate ¼W

Philips carbon resistors and 10% inaccurate Philips C280 metallised polyester capacitors and as buffer amplifiers the AD 741 C was found to be accurate enough. Some electrical characteristics of the amplifiers are given in Table 8.1.

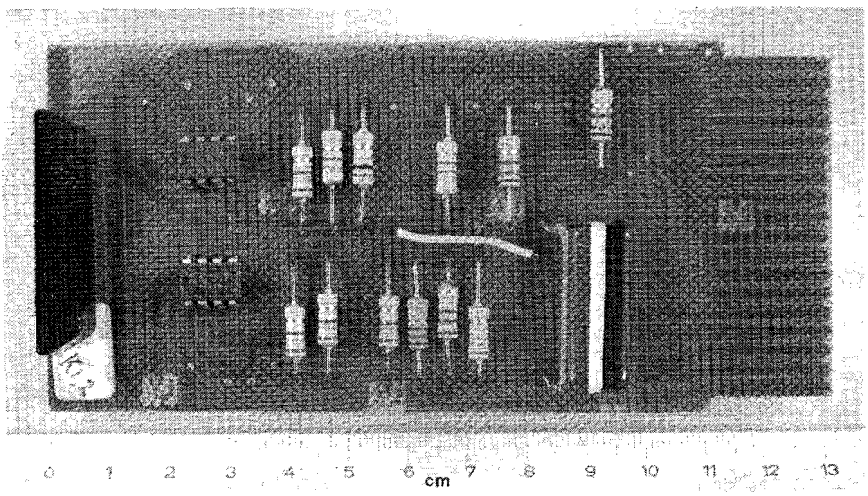

Figure 8.5 Single-width, single-height wired flip-chip module with electric components

For the special-purpose analog simulater a mounting panel was constructed which offered a way to build a complete system of up to 480 flip-chip modules into a 120×60 cm of rack space. As connector blocks the type H 800-W of DEC was used /19/. This is an 8-module moulded socket assembly. For each of the eight modules it provides an 18-pin connector with wirewrap pins. For the simulation of each of the 117 elements a single-width, single-height wired flip-chip module was used. On such a module the components, viz. resistors, capacitors and buffer amplifiers, can be soldered easily. A photograph of such a module is shown in Figure 8.5.

8.3 STATIC ACCURACY

Before the flip-chip modules were provided with resistances according to (8.5) to (8.9) and (8.12) to (8.14), the static accuracy of this backward-difference approximation was calculated. Introducing a step-disturbance in one of the

Table 8.1

Electrical characteristics of the AD741C

parameters	value	units
input offset voltage	1.0	mV
input offset current	20	nA
input bias current	80	nA
input resistance	2.0	MΩ
input capacitance	1.4	pF
offset voltage adjustment range	±15	mV
input voltage range	±13	V
common mode rejaction ratio	90	dB
supply voltage rejection ratio	30	μV/V
large signal voltage gain	200,000	V/V
output resistance	75	Ω
outpur short circuit current	25	mA
supply current	1.7	mA
power consumption	50	mW
transient response rise time	0.3	μs
overshoot	5.0	%
slew rate	0.5	V/μs

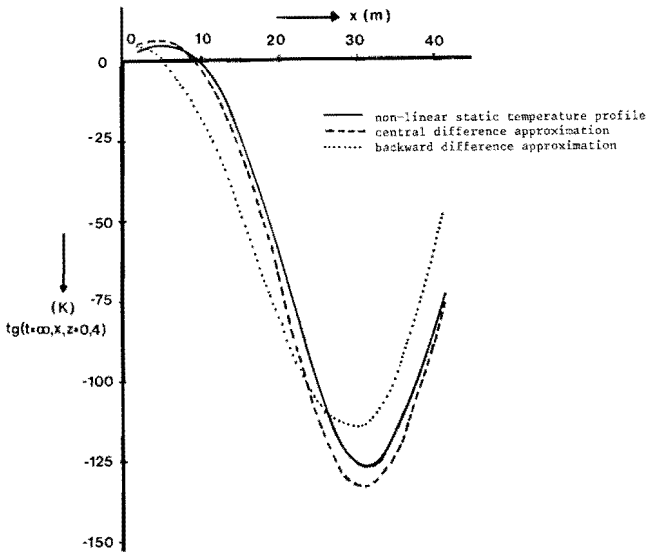

Figure 8.6 Static gas temperature change at $z = 0.4m$ after a +10% gas flow change

inlet quantities: gas flow rate, bed velocity, gas inlet temperature or pellet inlet temperature, the static pellet and gas temperature changes can easily be calculated. This was done digitally by means of the equations (8.3) with $\mu s \frac{dts}{dt} = 0$ and (8.10), using the values provided by (8.5) to (8.9) and (8.12) to (8.14). The correspondence of the static pellet and gas temperature changes obtained in this way (i.e. by applying backward differences for the derivatives with respect to x and z) with the more accurate static temperature changes (as defined in Section 5.3) is poor when compared with the static accuracy of the central-difference method which was used in all other simulations (Chapters 5 to 7). In Figure 8.6 this is illustrated by a static gas temperature change profile after a gas flow disturbance of 10%. The difference between the non-linear profile and the approximation is shown in Figure 8.7.

Simulation of the central-difference approximation of element (m,n) is only possible by means of RC elements when a large number of amplifiers is used. This would result in a much more complicated circuit than the one of Figure 8.4. A simulation scheme similar to Figure 7.1 is not feasible

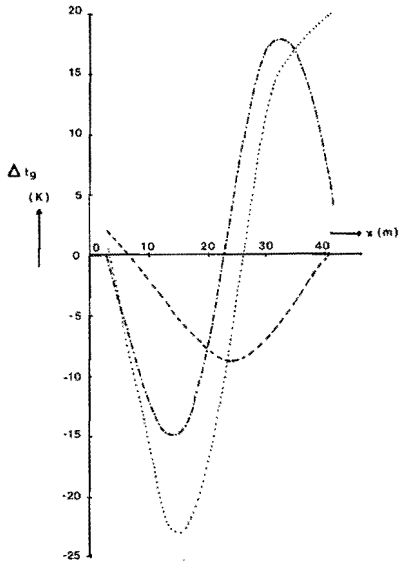

Figure 8.7 Difference between the static gas temperature change calculated with the non-linear static model and the gas temperatures change according to one of the following three difference approximations:

..... backward-difference approximation
-·-·- mixed central/backward approximation
— — — central-difference approximation

owing to the accuracy and the quality of the resistors, capacitors and amplifiers.

Some improvements of the static accuracy may be obtained by the use of central-difference values for the steady-state quantities $\overline{Ts}$, $\overline{Tg}$, $\overline{Fg}$, $\overline{U}$ and $\overline{\partial U/\partial Fg}$ instead of their backward-difference values. In this way, when partly applying a backward-difference approximation (viz. for the dynamic part of the simulation) and partly a central-difference approximation (viz. for the static part of the simulation), the following set of equations results from (8.1) and (8.2)

$$\mu s \frac{\partial ts_{m,n}}{\partial t} + \frac{\mu s\ \overline{Vs}}{X/M}\left(ts_{m,n} - ts_{m-1,n}\right) + \overline{U}_{m-\frac{1}{2}} A \left(ts_{m,n} - tg_{m,n}\right) =$$

$$= \frac{\mu s}{X/M}\left(\overline{Ts}_{m-1,n-\frac{1}{2}} - \overline{Ts}_{m,n-\frac{1}{2}}\right) vs + \left.\frac{\overline{\partial UA}}{\partial Fg}\right|_{m-\frac{1}{2}} \left(\overline{Tg}_{m-\frac{1}{2},n-\frac{1}{2}} - \overline{Ts}_{m-\frac{1}{2},n-\frac{1}{2}}\right) fg_m \qquad (8.15)$$

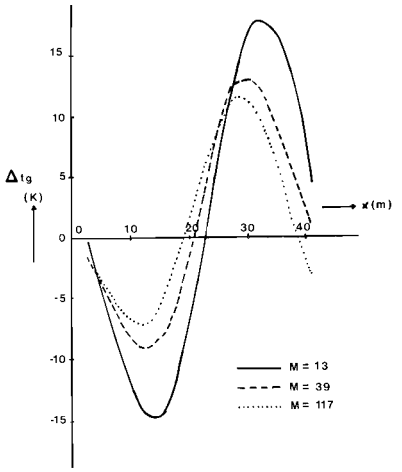

Figure 8.8 Difference between the static gas temperature change calculated with the non-linear static model and the gas temperature change according to the mixed central/backward-difference approximation for three different horizontal segmentations ($M=13,39,117$) after a 10 % disturbance in gas flow rate.

$$\frac{\overline{Fg}_{m-\frac{1}{2}}\,\gamma g}{Z/N}\,(tg_{m,n} - tg_{m,n-1}) + \overline{U}_{m-\frac{1}{2}}\,A\,(tg_{m,n} - ts_{m,n}) =$$

(8.16)

$$= \{\frac{\gamma g}{Z/N}\,(\overline{Tg}_{m-\frac{1}{2},n-1} - \overline{Tg}_{m-\frac{1}{2},n}) + \frac{\overline{\partial UA}}{\partial Fg}\Big|_{m-\frac{1}{2}}(\overline{Ts}_{m-\frac{1}{2},n-\frac{1}{2}} - \overline{Tg}_{m-\frac{1}{2},n-\frac{1}{2}})\}fg_m$$

The difference between the static temperature profile thus obtained and the more accurate profile coming from the non-linear model for a 10% flow disturbance is also shown in Figure 8.7. As can be seen from this figure, the mixed central/backward-difference approximation of (8.15) and (8.16) gives a somewhat better static correspondence with the non-linear static model result than the backward-difference approximation of (8.1) and (8.2). Similar results were found for other disturbances.

The following explanation is given for this effect. When using backward differences, the temperature inside element (m,n) is equal to the outgoing temperature. This rough approximation is made for the space-dependent and time-dependent variables ts and tg as well as for the space-dependent but time-

independent quantities $\overline{Ts}$, $\overline{Tg}$, $\overline{Fg}$, $\overline{U}$, $\overline{\partial U/\partial Fg}$ (steady-state values). In equations (8.15) and (8.16) this inaccurate backward-difference approximation is partly replaced (for the steady-state values) by a more accurate one, viz. the central-difference approximation. In this way the static behaviour of the RC simulation could be improved without changing the structure of the proposed RC circuit. With the modification the resistance values are determined by the following equations:

$$\frac{1}{Rs_{m,n}} = \frac{\mu s\ \overline{Vs}}{X/M} \tag{8.17}$$

$$\frac{1}{Rt_{m,n}} = \overline{U}_{m-\frac{1}{2}}\ A \tag{8.18}$$

$$\frac{1}{Rv_{m,n}} = \frac{\mu s}{X/M}\ (\overline{Ts}_{m-1,n-\frac{1}{2}} - \overline{Ts}_{m,n-\frac{1}{2}}) \tag{8.19}$$

$$\frac{1}{Rf1_{m,n}} = \left.\overline{\frac{\partial U}{\partial Fg}}\right|_{m-\frac{1}{2}} A\ (\overline{Tg}_{m-\frac{1}{2},n-\frac{1}{2}} - \overline{Ts}_{m-\frac{1}{2},n-\frac{1}{2}}) \tag{8.20}$$

$$\frac{1}{Ra_{m,n}} = \frac{1-\beta s}{Rs_{m,n}} - \frac{\beta v}{Rv_{m,n}} - \frac{\beta f}{Rf1_{m,n}} \tag{8.21}$$

$$\frac{1}{Rg_{m,n}} = \frac{\gamma g\ \overline{Fg}_{m-\frac{1}{2}}}{Z/N} \tag{8.22}$$

$$\frac{1}{Rf2_{m,n}} = -\frac{1}{Rf1_{m,n}} + \frac{\gamma g}{Z/N}\ (\overline{Tg}_{m-\frac{1}{2},n-1} - \overline{Tg}_{m-\frac{1}{2},n}) \tag{8.23}$$

$$\frac{1}{Rb_{m,n}} = \frac{1-\beta g}{Rg_{m,n}} - \frac{\beta f}{Rf2_{m,n}} \tag{8.24}$$

A finer horizontal segmentation improves the static accuracy of the RC simulation as is shown in Figure 8.8. A similar situation exists for the vertical segmentation in the z direction. However, finer segmentation involves a larger number of flip-chip modules with electronic hardware to be constructed. For this reason a choice was made for $M = 13$

and $N = 9$, the same segmentation as used in the other simulations (Chapters 5 to 7).

8.4 DYNAMIC ACCURACY

The analysis of the static accuracy of the RC simulation proved that the backward-difference approximation gives rather poor results. Therefore, the dynamic responses of the RC simulation had to be verified. The effect of the mixed backward/central-difference approximation on the dynamic behaviour was investigated. Because of the fact that the dynamic behaviour is mainly determined by the solid heat balance equation (8.1), the effect of the difference approximations will be analysed only for this equation and the influence of the z dependence will be omitted. Terms involving vs and fg disturbances are neglected for ease of discussion, but can be added without introducing extra difficulties.

Under these assumptions the solid heat balance reduces to (see (3.22))

$$\mu s \frac{\partial ts}{\partial t} + \mu s \overline{Vs} \frac{\partial ts}{\partial x} = \overline{U} A (tg - ts) \tag{8.25}$$

Backward-difference approximation with respect to the x coordinate results in

$$\mu s \frac{\partial ts_m}{\partial t} + \frac{\mu s \overline{Vs}}{X/M} (ts_m - ts_{m-1}) = \overline{U} A (tg_m - ts_m) \tag{8.26}$$

Introduction of a heat conduction or diffusion term into equation (8.25) gives

$$\mu s \frac{\partial ts}{\partial t} + \mu s \overline{Vs} \frac{\partial ts}{\partial x} - \mu s D \frac{\partial^2 ts}{\partial x^2} = \overline{U} A (tg - ts) \tag{8.27}$$

where D is the diffusion coefficient $[m^2 s^{-1}]$. Central-difference approximation of (8.27) with respect to the x coordinate results in

$$\mu s \frac{\partial ts_m}{\partial t} + \frac{\mu s \overline{Vs}}{2X/M} (ts_{m+1} - ts_{m-1}) - \frac{\mu s D}{(X/M)^2} (ts_{m+1} - 2\, ts_m + ts_{m-1}) =$$

$$= \overline{U} A (tg_m - ts_m) \qquad (8.28)$$

This equation can be rearranged as follows

$$\mu s \frac{\partial ts_m}{\partial t} + \frac{\mu s \overline{Vs}}{X/M} (ts_m - ts_{m-1}) + \overline{U} A (ts_m - tg_m) +$$

$$+ \left[\frac{\mu s \overline{Vs}}{2\, X/M} - \frac{\mu s D}{(X/M)^2} \right] (ts_{m+1} - 2\, ts_m + ts_{m-1}) = 0 \qquad (8.29)$$

When the term in square brackets equals zero, (8.29) is identical with (8.26), i.e. the central-difference approximation of the solid heat balance with diffusion equals the backward-difference approximation of the solid heat balance without diffusion. Therefore, the effect of using a backward-difference approximation instead of a central-difference one is the introduction of spurious diffusion /40/ with the diffusion coefficient

$$D = \frac{1}{2} \overline{Vs} \frac{X}{M} \qquad (8.30)$$

In view of what has been said in Section 2.3 about the occurrence of diffusion and dispersion, the dynamic behaviour of this backward-difference approximation may even better represent physical reality than the central-difference one ignoring D. This method has been used in chemical engineering design to evaluate the temperature and concentration profiles in tubular reactors, where the diffusion effects were extremely important, but could not easily be dealt with if the full model was used /46/.

The actual value of D may be so large that - according to (8.30) - a very coarse segmentation would be necessary, resulting in a very inaccurate simulation. This problem can be solved simply by the addition of resistances to the

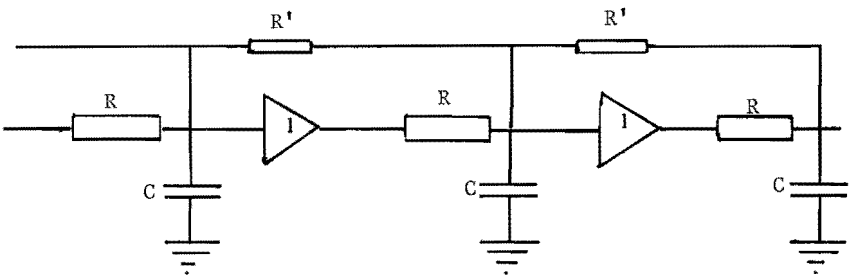

Figure 8.9 RC network simulating the transport and diffusion equations

original RC network, see Figure 8.9, in which for the sake of clarity a number of less important resistances have been omitted.

Additional heat transport into any other direction, e.g. by conduction, may be represented by connecting resistances to the appropriate nodes of the network elements of adjacent volumes. Finally, internal heat conduction inside the pellets may be represented by a circuit as shown in Figure 5.2.

8.5 TYPICAL SIMULATION RESULTS

In Figures 8.10 to 8.13 some dynamic responses of the RC simulation are presented. From these graphs it may be seen that compared with the dynamic responses found in Chapters 5 to 7 the wave fronts are smoothed out owing to the diffusive effect of the backward-difference approximation used in this simulation. This is seen very clearly in the solid temperature responses after a pellet inlet temperature step disturbance (figure 8.10).

The ultimate steady-state part of the step responses of Figures 8.12 and 8.13 show an interesting phenomenon: somewhere halfway in the bed (halfway the horizontal position x for Figure 8.12 and halfway the height z for Figure 8.13)

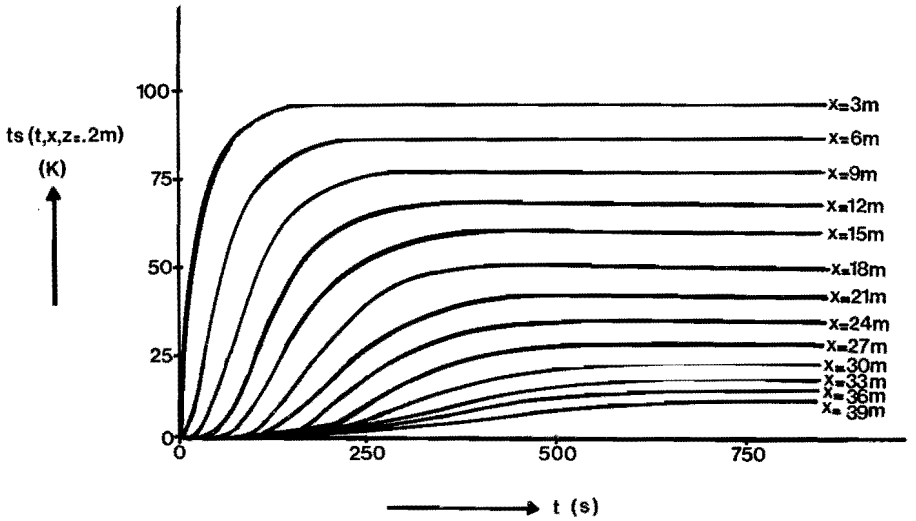

Figure 8.10 Pellet temperature responses at various horizontal position x and at height $z = 0.20\ m$ to a step disturbance in pellet inlet temperature of 100 K

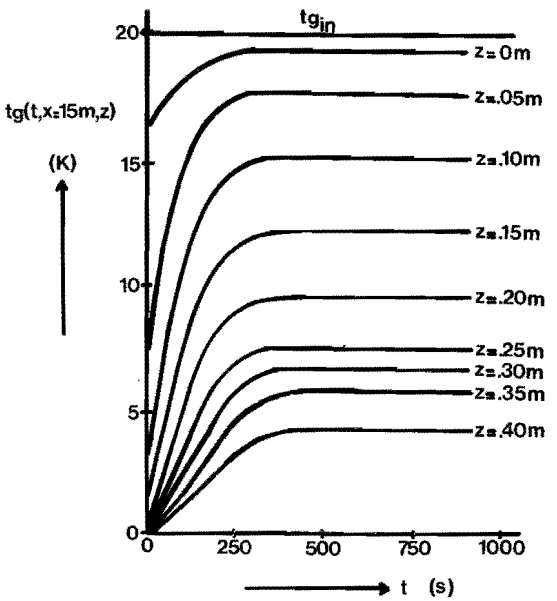

Figure 8.11 Pellet temperature responses at various heights z and at horizontal position $x = 15\ m$ to a step disturbance of gas inlet temperature of 20 K

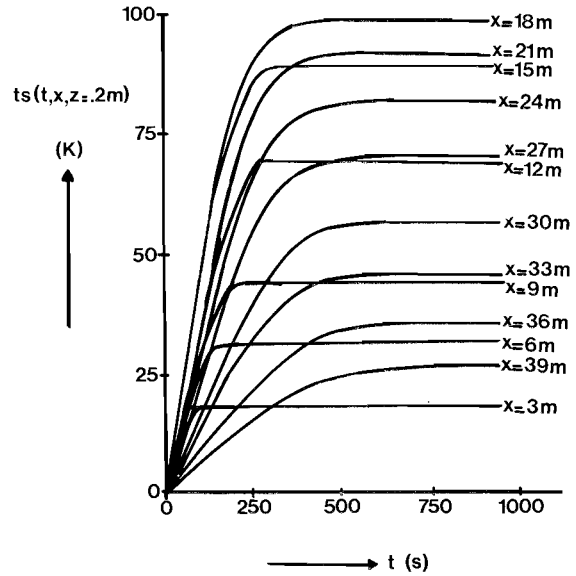

Figure 8.12 Pellet temperature responses at various horizontal position x and at height $z = 0.20\ m$ to a step disturbance in bed velocity of 10% $\overline{Vs}$

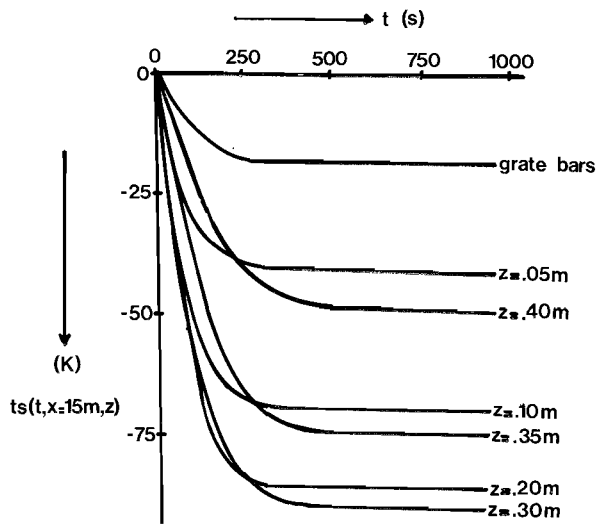

Figure 8.13 Pellet temperature responses at various heights z and at horizontal position $x = 15\ m$ to a step disturbance in gas flow rate of 10% $\overline{Fg}$

the responses show a maximum static amplification. These results are in accordance with the corresponding static accuracy profiles (see, for example, curve a in Figure 7.6). The reason why this effect only occurs after bed velocity or gas flow rate disturbances is that the effect of these disturbances is mainly determined by the gradient of the static temperature profiles (as shown in Figure 3.2) with respect to the height z or the horizontal position x. The maximum value of this gradient is halfway the cooling zone.

8.6 CONCLUSIONS

Because of its fully parallel operation the RC-network simulation is - in contrast to the other simulation techniques - very fast. The dynamic effect of a disturbance is simulated in all places of the bed in some milliseconds. This is of great advantage in trying and comparing different control schemes, calculating optimal controller settings and optimal sensor locations, etc.

A drawback of the RC simulation is that changing to another steady-state situation would involve the replacement of the majority of the resistors on the flip-chip modules, a cumbersome, time-consuming task. Therefore, it is advisable to postpone the calculation, selection and soldering of the resistors until the operating conditions of interest are well known.

Static accuracy is comparatively poor due to the use of backward-difference approximation methods which are needed in order to keep the analog scheme simple. Dynamically, spurious diffusion is introduced, which also may be present in the real pellet bed.

The total cost of the special-purpose analog simulator described in this chapter is about *f* 10.000,= in hardware for the cooling section of the pellet-indurating plant. This simulation has been set up for the whole plant and costs then about twice as much.

Chapter Nine

COMPARISON OF THE SIMULATION METHODS

9.1 GENERAL CONSIDERATIONS

By its very nature, a methodological comparison of simulation studies is never very satisfactory. For models are built and simulated for a *specific* purpose, whereas methodological studies aim at arriving at *general* conclusions. This difficulty arises because different models and simulation methods are used for different purposes. For example, start-up and shut-down problems may be studied by a non-linear model which is only accurate in the low-frequency range, whereas a model needed for feedback-control studies may be linear(ised) but must be accurate for higher frequencies.

An extra difficulty of the comparison is formed by the fact that in our simulations the applied method as well as the computer may be different. This is an uncommon situation: comparative studies in the literature mostly deal with different numerical integration methods implemented on the same machine. The few published comparisons between the effectiveness of different machines are limited to qualitative comments on obvious advantages and drawbacks.

The problem is also complicated by the past experience and the environment of the *user*. When a potential user is engaged almost continuously in simulation exercises, he may be expected to have a fairly broad expertise with regard to a variety of simulation methods. When his main mission is a rather different one - for example to (re)design processes and to 'shoot troubles' of any kind, if unavoidable even of a dynamic nature - it is not uncommon that he has learned to use only one method. Applicability and ease of adaptation of that method then are crucial requirements. And to finish with still another example: if the user is an electrical network specialist by training but

has never really managed to master a digital language like Algol 60, the RC-network simulation will have a strong appeal to him, not only as a means of simulation, but also - and perhaps even more importantly - as a means of grasping the process to be modelled as a whole, of gaining insight into its behaviour, of simplifying the model where possible, and of communicating about it with others who understand networks, in theory and practice.

Whether or not a specific kind of simulation equipment can be made available may turn out to be equally decisive. The availability of computer time or a computing budget is of comparable importance.

In spite of all these complications, which seem to prohibit a meaningful comparison, we will try to evaluate the various simulation methods. Our conclusions fall into two categories: (1) those relating to the elaborated example of a compartment of the pellet-indurating plant (described in Section 9.2) and (2) those relating to similar but somewhat different problems (described in Section 9.3).

The classical analytical solutions together with the double Laplace transform solution and the numerical-inversion solution of the equations describing a segment moving along with the pellet bed (as presented in Chapter 4) are only practicable (or only possible!) in the case of constant coefficients, uniform boundary conditions and linear partial-differential equations. Hence, although these methods may be very helpful for a theoretical point of view, for the actual solution of practical problems, where never all these requirements are satisfied together, these methods are of little use. Therefore, they will be left out of consideration and we will base our comparisons on the simulation methods described in the chapters 5 to 8.

9.2 CONCLUSIONS FOR THE CASE STUDY DESCRIBED IN THIS THESIS

Since for each of the elaborated simulation studies a good choice between the various possibilities of implementation has already been made in Chapters 5 to 8, the ultimate

comparison will mainly be a comparison between the various implementations with respect to the effectiveness of simulating the equations (3.22) and (3.23). We *had* to start from these rather simple linear model equations in order to be able to compare the four simulation methods at all.

In comparing the four simulation methods with respect to a number of criteria, such as static and dynamic accuracy, computation time with and without feedback, set-up time and flexibility, the results of the preceding chapters are summarised.

For the calculation of the dynamic behaviour of a compartment after an inlet disturbance in one of the input variables without coupling with other compartments or feedback-control action, digital simulation in the time domain, as described in Chapter 5, is most competitive because of high static and dynamic accuracy combined with short computation time as well as set-up time. When the aim of the simulation is to perform control studies or when the simulation is extended by taking heat- and mass-flow feedback into account, the digital simulation in the time domain looses attractiveness. The computation scheme becomes more complicated and the corresponding simulation time becomes so large that other simulation methods, like digital simulation in the frequency domain or RC-network simulation, may become preferable. For the frequency domain, this benefit is caused by the fact that the simulation time is not affected by the presence of feedback. Open-loop frequency response simulation results can directly be used in feedback studies, where the feedback may be caused by the process itself (coupling of interacting compartments) or by feedback controllers. Also the RC-network simulation, due to its high speed and fully parallel operation, is very suitable for extensive feedback and control simulation studies. Its main drawbacks are the inflexibility and the relatively poor dynamic accuracy.

It should be noted that the hybrid simulation, *as described in Chapter 7*, is no serious competitor for computation of the pellet-bed behaviour with or without feedback effects.

However, it must be admitted that this is due to the fact that we started from linearised process equations and that, hence, a CTDS-simulation method had to be chosen in order to make the simulation feasible. The relatively long set-up time (the patching and checking of the analog part of the simulation) and the required specialised knowledge together with the relatively limited flexibility (as compared with digital simulation) could only be compensated for by a much smaller computation time than the digital one. However, this was not the case, because at the time the hybrid studies were carried out, the large number of intermediate results had to be stored on disc memory and to be played back (owing to core-memory limitations).

Simulation in the frequency domain was only possible because of the linearity of the process equations (3.22) and (3.23). Digital and hybrid simulation can easily take non-linear effects into account. In principle, also in RC-network simulation non-linearities can be taken into account, but with a view to feasibility simple linear relationships are to be preferred in general, but sometimes its unique capability to "solve" sets of implicit equations in the same way as nature "solves" such problems, provides a peerless advantage.

9.3 GENERALITY OF THE CONCLUSIONS

The conclusions about the effectiveness of the various simulation methods are not limited to the simulation of pellet-indurating plants. Similar conclusions can be expected for other processes described by a comparable set of non-linear partial-differential equations of first order with respect to three or more independent variables. Hence, our conclusions are also of importance for simulation studies of processes like sintering plants, gas-liquid cross-flow heat exchangers or clinker coolers.

9.3.1 Linearisation

For the purpose of comparing the various methods of simulation, we had to linearise the equations. Due to the linearisation, only relatively small excursions from the given

steady-state operating condition are permitted. Hence, we focussed the simulation studies discussed in this thesis on the dynamics around a typical steady-state situation. Although it followed from the static accuracy tests of the various simulations that there were no large differences between the temperature profiles as predicted by the non-linear static model and by the linear dynamic model, it is clear that in this way only a certain class of control problems can be dealt with satisfactorily. Start-up and shut-down problems generally need a non-linear process model.

9.3.2 Space-dependent coefficients

An essential feature of the four simulation methods elaborated in Chapters 5 to 8 is their ability to deal with processes with *space-dependent* coefficients. Owing to the segmentation with respect to both space directions, the simulation methods could easily deal with non-uniform coefficients. In that way, also the interchange of the process with the environment (in the study of the pellet bed for example: the interchange between the bed and the grate bars of the transportation system) as well as non-uniform boundary conditions could be taken into account very easily. It should be noted, that for problems where the space dependence of the coefficients is less pronounced, quite different implementations might have been chosen on the various machines. For example, a time-lumped simulation would have been realised on the hybrid computer and even analytical solutions might have been applicable. Hence, the comparison of the various simulation methods is primiraly of importance for processes with coefficients that are significantly space-dependent.

9.3.3 Different assumptions

In general, the assumptions permissible in the derivation of a mathematical model will be different for other processes. An evaluation of the influence of the model assumptions on the simulation results is required in order to extend the validity of our comparative conclusions. Therefore, we will investigate the feasibility of the simulation methods under several

different assumptions.

Dispersive gas flow instead of plug-flow gas stream, or *heat conduction* in vertical and/or horizontal directions in the solid as well as in the gas introduces second-order differential quotients. Finite *conduction inside the pellets* even adds an extra dimension to the problem (see Section 2.3). As has already been shown in Section 8.4, RC-network simulation is very suitable for taking into account extra diffusion terms with respect to already existing independent variables as well as with respect to new coordinates. This is due to the fact that a passive ladder network merely consisting of resistors and capacitors represents the segmented version of the diffusion equation. In fact, RC-network simulation has more problems in simulating first-order transport equations (it then needs buffer amplifiers) than second order diffusion equations. In digital simulation and classical analog simulation just the opposite is true.

If one does not want to ignore the time constant introduced by the *heat capacity of the gas hold-up* in the bed which is small compared to the time constant of the solid material, an extra $\partial/\partial t$ term must be added. When there is a large difference between the time constants, the system of equations is a so-called stiff system. Digital simulation in the time domain will need much computer time since small integration steps are needed to account for the small time constant, and accuracy problems may then arise. Also hybrid simulation will use more computation time since the responses to be stored and played back must be sampled very frequently in order to take into account the high-frequency part of the responses of the stiff system. The RC-network simulation and the frequency-domain simulation can easily deal with stiff systems. In the RC network small capacitors must be added to the gas temperature node points and in the frequency-domain simulation it is sufficient to extend the calculations to higher frequencies.

The addition of a *chemical reaction* results in an extra transport equation like (2.53). Since this equation is essentially of the same type as the solid heat balance (2.52),

no new simulation problems arise because of the addition of the new equation. All simulations become more extensive, but not essentially different.

Heat transport by radiation needs the evaluation of the fourth power of the temperatures according to the Stefan-Boltzmann equation. Without linearising the equations, the frequency-domain simulation is not permissible any more. RC-network simulation becomes very complicated. For digital simulation in time domain, raising to the fourth power is no problem at all.

9.3.4 Other considerations

Simulation in the frequency domain may be preferable for *stabilising control* studies, in view of the extensive control theory available in frequency-domain terms.

The good *man-machine interaction* feature of the RC-network simulation may be an advantage for extensive simulation studies, e.g. the determination of optimal sensor location for the design of a feedback-control loop.

Incorporation of the simulation results obtained for a compartment of the process into a simulation of the whole plant is most easily performed by means of the frequency-domain simulation. In this case, the previously obtained results can be used directly without repeating the calculation. With RC-network simulation, where computation time is negligible, the hardware must be extended. For the digital simulation in the time domain as well as for the hybrid simulation the implementation must be adapted and the whole calculation repeated.

The ease of *changing parameter values* that are not very well known in advance often turns out to be an important factor in practice. Digital machines and also hybrid computers can easily perform such changes. The main drawback of the RC-network simulation is its inflexibility. Another value of a heat transfer coefficient means changing resistances. A change of the steady-state operating situation around which the process equations have been linearised is not feasible without changing or building another RC network.

As regards the *amount of time needed* to apply the various methods - an aspect that is closely related to *flexibility*, whatever the precise meaning of this term may be, - a distinction must be made between

- preparation time (set-up time), i.e. the time needed to adapt the method and its implementation to
  - a new problem
  - a problem reformulation (e.g. a revised assumption)
  - a change in operating conditions
  - a change in initial or boundary conditions
- computation time
- time needed to interpret the simulation results.

Digital simulation in the time domain is characterised by a relatively short set-up time and (for open-loop responses) a rather short computation time. Moreover, digital computation is very flexible.

Digital simulation in the frequency domain is characterised by a relatively short set-up time and a rather short computation time (giving all responses at once!) for open-loop as well as closed loop responses. It is also very flexible.

Hybrid simulation demands more set-up time (patching and checking of the analog part of the simulation), is less flexible than digital simulation, and was - in the implementation considered here - only somewhat faster than digital calculation.

RC-network simulation needs a long set-up time (design and construction of the flip-chip modules), a very short calculation time, but a very long time to adapt for other parameter values. The costs for the RC-network hardware will be of minor importance for an extensive simulation study. Realisation of an RC network for the whole pellet-indurating plant amounted to an investment of *f* 20.000,= in components.

In Table 9.1 a summary of the advantages and drawbacks of the four simulation methods is given for the circumstances considered in Chapters 5 to 8 as well under somewhat different conditions.

Table 9.1

COMPARISON OF THE VARIOUS SIMULATION METHODS

	digital simulation in the time domain	digital simulation in the frequency domain	hybrid simulation	RC-network simulation
Static accuracy	good	good	good	intermediate
Dynamic accuracy	good	intermediate	intermediate	poor
Computation time [+] (without feedback)	2 min[++]	4 min[+++]	1 min[++]	10 ms
Computation time (with feedback)	≈ 10 min	4 min	≈ 10 min	10 ms
Set-up time	short	short	intermediate	long
Flexibility	good	good	intermediate	poor
Accessibility of intermediate results	possible	possible	possible	good
Linearity required	no	yes	no	preferable
Incorporation of				
-diffusion	complicated	complicated	complicated	simple
-chemical reaction	possible	possible	possible	possible
-radiation[++++]	easy	impossible	possible	complicated
-accumulation of heat in the gas	complicated	possible	complicated	simple
Suitability for				
-overshoot calculation	good	poor	good	inaccurate
-feedback control studies	poor	good	poor	good
-start-up/shut-down studies	good	poor	good	poor
-(re)design studies	good	poor	good	poor

[+]) These computation times are - of course - highly dependent upon existing technology, but their ratio's tell the story.

[++]) for one complete response to a single disturbance

[+++]) for the frequency response of *all* process variables to *all* input variables (for 30 frequencies)

[++++]) if the Stefan-Boltzmann relation is not linearised

L I S T O F S Y M B O L S

A heat transfer area between gas and pellets per unit volume of the pellet bed $[m^{-1}]$

A_1 constant in (2.3)

A_2 constant in (2.3)

$\underline{\underline{A}}$ (2×5)-matrix (see (5.4))

$\underline{\underline{B}}$ (2×6)-matrix (see (5.22))

$\underline{\underline{C}}$ (2×4)-matrix (see (5.29))

C_l constant defined by (2.36)

Cs concentration of magnetite $[\text{mole } m^{-3}]$

$\underline{\underline{D}}$ (2×4)-matrix (see (6.18))

d_p diameter of the pellets

E activation energy $[\text{J mole}^{-1}]$

f function of x

Fg gas flow rate $[\text{kg } s^{-1}\ m^{-2}]$

G normalised dimensionless gas temperature

$G_{N,1}$ double Laplace transform solution of G according to (4.19)

$G_{N,2}$ single Laplace transform solution of G according to (4.40)

$G_{N,3}$ single Laplace transform solution of G according to (4.43)

$G_{N,4}$ numerical-inversion solution of G according to (4.52)

h heat transfer coefficient $[\text{J } K^{-1}\ m^{-2}\ s^{-1}]$

k rate coefficient $[s^{-1}]$

$k(x,s)$ kernel of integral transformation

k_0 velocity constant $[s^{-1}]$

l index in time direction

L number of time intervals

m index in horizontal x direction

M number of segments in horizontal x direction

n index in vertical z direction

N number of layers in vertical z direction

p Laplace variable [-]

p_l constant defined by (2.37)

q Laplace variable (demensionless in Ch.4 and $[s^{-1}]$ elsewhere)

r reaction rate $[\text{mole } m^{-3}\ s^{-1}]$

r distance from the center of the pellet [m]

R radius of the pellet [m]

R resistance

R^* overall resistance

S normalised dimensionless solid temperature

t time [s]

Tg gas temperature [^oC]

Ts pellet temperature [^oC]

u substituted variable (see (2.20))

U overall heat transfer coefficient [$J\ K^{-1}\ m^{-2}\ s^{-1}$]

U_0 temperature dependent coefficient (see (2.8))

Vs grate velocity [$m\ s^{-1}$]

x horizontal position [m]

z vertical position [m]

Z height of the bed [m]

α_k coefficients in Chepter 3

β_k coefficients in Chapter 3

γg specific heat of the gas [$J\ K^{-1}\ kg^{-1}$]

γs specific heat of the solid [$J\ K^{-1}\ kg^{-1}$]

ΔH heat of reaction [$J\ mole^{-1}$]

ΔP pressure drop over the bed [$N\ m^{-2}$]

ε void fraction of the bed [-]

θ residence time [s]

ηg viscosity of the gas [$kg\ m^{-1}\ s^{-1}$]

ζ dimensionless height

ζ^* fixed dimensionless height of a segment of the bed

κs thermal diffusivity of the pellet material [$m^2\ s^{-1}$]

λs heat conductivity coefficient of the pellet material [$J\ K^{-1}\ m^{-1}\ s^{-1}$]

μg heat capacity of the gas in the bed [$J\ K^{-1}\ m^{-3}$]

μs heat capacity of the pellets in the bed [$J\ K^{-1}\ m^{-3}$]

ρg density of the gas [$kg\ m^{-3}$]

ρs density of the pellet material [$kg\ m^{-3}$]

ϕ function of x and f

ψ function of f and ϕ

$\tau_{1,2}$ time constants according to (2.31) and (2.32) [s]

$\tau_{-,+}$ dimensionless time constants according to (4.29) and (4.30)

ω angular frequency [s^{-1}]

Subscripts

a average

0 initial

in inlet

out outlet

Superscripts

$\tilde{f}$ single Laplace transform of f

$\tilde{\tilde{f}}$ double Laplace transform of f

$\overline{F}$ steady-state value of F

RC-network symbols

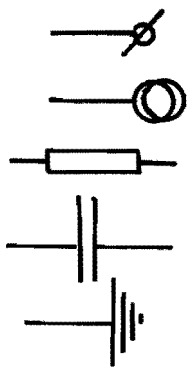

voltage source (with respect to earth)

current source

resistance

capacitance

earth

L I T E R A T U R E

1. Anzelius, A., "Uber Erwärmung vermittels durchströmender Medien", *Zeitschrift für Angewandte Mathematik und Mechanik* 6, 291 (1926)

2. Arora, A.K., "The simulation of a distributed parameter system on an analog computer", *Philips International Institute of Technology Studies*, report 394 (1971)

3. Aseltine, J.A., *Transform methods in linear system analysis*, McGraw-Hill, New York (1958)

4. Beijdorff, A.F., M. de Hes, "A hybrid computer model for a counterflow heat exchanger using CSDT-method", *Proceedings of the AICA/IFIP Congress on Hybrid Computation*, München (1970)

5. Bender, E., "Dynamic response of crossflow heat exchangers for variations in temperature and massflow", *Preprint 5th IFAC-congress*, Paris (1972)

6. Bender, E., private communication, see discussion on /5/ in *Proceedings of the 5th IFAC-congress*, Paris (1972)

7. Bellman, R., R.E. Kabala, J.A. Lockett, *Numerical inversion of the Laplace transform*, Elsevier, New York (1966)

8. Bosgra, O.H., J.P. Buis, "Hybrid computer solution of the hyperbolic equations describing forced-flow steam-generator dynamics", *Proceedings of the AICA/IFIP Congress on Hybrid Computation*, München (1970)

9. Bosgra, O.H., J.P. Buis, "Error analysis of a generalized method of lines for the hybrid solution of hyperbolic partial differential equations", *Proceedings of the AICA Conference on Hybrid Computation*, Prague (1973)

10. Brasz, J., P. van Exel, A. de Jongh, "A hybrid model for the transient behaviour of a pellet indurating plant", *Proceedings of the AICA Conference on Hybrid Computation*, Prague (1973)

11. Brasz, J., A.U. Khan, "Comparison of various ways of model building of distributed parameter systems", *Symposium on the use of computers in chemical engineering*, Usti nad Labem, Czechoslovakia (1972)

12. Brasz, J., A.U. Khan, "Comparison of various ways of model building of a regenerator", *AIChE Journal* 18, 1274 (1972)

13. Brasz, J., J.H. Voskamp, O. Rademaker, "The dynamic behaviour of a gas-solid cross-flow heat exchanger", *UKAC 5th Control Convention on "Modelling and Simulation for applied control systems"*, Bath University of Technology (1973)

14. Carter, C.E., E. Rose, "The simulation of an iron ore sinter strand process", *UKAC 5th Control Convention on "Modelling and Simulation for applied control systems"*, Bath University of Technology (1973)

15. Coughanowr, D.R., L.B. Koppel, *"Process systems analysis and control"*, McGraw-Hill, New York (1965)

16. Dekker, G., C.G.J. Buursen, "EROS, an Experimental Real-time Operating System", *Proceedings of the KIVI-Meeting on Computer Control*, Eindhoven (1973)

17. Dekker, L., "Applicability of hybrid computation", *Proceedings of the AICA/IFIP Congress on Hybrid Computation*, München (1970)

18. Deutsch, R., *System analysis techniques*, Prentice Hall, London (1969)

19. *Digital Control Handbook*, Digital Equipment Corporation, Maynard, Massachusetts (1968)

20. Douglas, J.M., *Process dynamics and control*, Prentice Hall, New Jersey (1972)

21. Eklund, K., "Linear drum boiler-turbine models", *Report 7117 Lund Institute of Technology, Division of Automatic Control*, Lund (1971)

22. Ergun, S., "Fluid flow through packed columns", *Chem. Eng. Progress* 48, 89 (1952)

22a. Fleuren, P.W.M., *"Het afkoelen van een gapakt bed"*, Internal THE communication, (1969)

23. Flierman, G.A., "A mathematical model of the blast furnace process", *ISI Preprint 123 of the conference on "Mathematical models in metallurgical process development"*, Iron and Steel Institute, London (1969)

24. Ford, R.L.,"Electrical analogues for heat exchangers", *Proceedings IEE* 103, Part B, 65 (1956)

25. Gilles, E.D., M. Zeitz, "Modal simulation of a distributed parameter system", *Simulation* 18, 179 (1970)

26. Grabbe, E.M., S. Ramo, D.E. Wooldridge (eds.), *Handbook of automation, computation and control*, Wiley (1959)

27. Harriott, P., *Process Control*, McGraw-Hill, New York (1964)

28. Hausen, H., "Uber die Theorie des Wärmeaustausches in Regeneratores", *Zeitschrift für angewandte Mathematik und Mechanik* 9, 173 (1926)

29. Hausen, H., "Uber den Wärmeaustausch in Regeneratoren", *Tech. Mech. Thermodynam.* 1, 219 (1930)

30. Hausen, H., "Näherungsverfahren zur Berechnung des Wärmeaustausches in Regeneratoren", *Zeitschrift für angewandte Mathematik und Mechanik* 11, 105 (1931)

31. Hempel, A.H., "Exact simulation of special first order partial differential equations", *Annales de l'Association Internationale pour le Calcul Analogique* 5, 196 (1963)

32. Henry, J.W., P.F. Smeaton, "Automatic control of a pelletizing plant", *Iron and Steel* 43, 303 (1970)

33. Hes, M. de, "Water-hammer in a closed circuit analysis with a hybrid computer", *Proceedings of the AICA/IFIP Congress on Hybrid Computation*, München (1970)

34. Jacobs, G.W.C., W. Krijger, "Buffering dry solids with speed control of a conveyor belt", *Revue A* 14, 35 (1972)

35. Jakob, M., *Heat Transfer*, Wiley, New York (1957)

36. Jørgensen, S.B., M. Kümmel, "An analog simulation technique for distributed flow systems", *Chem. Engng Sci.* 28, 647 (1973)

37. Kohlmayr, G.F., "Properties of transient heat transfer (single blow) temperature response function", *AIChE Journal* 14, 499 (1968)

38. Korn, G.A., "New techniques for all digital hybrid simulation", *Proceedings of the AICA/IFIP Congress on Hybrid Computation*, München (1970)

39. Kourim, G., "Die elektrische Nachbildung fer instationären thermischen Vorgänge beim Wärmeaustauscher", *Regelungstechnik* 5, 163 (1957)

40. Kümmel, M., "Analog simulation and control of a distributed system", *Chem. Engng Sci.* 24, 1055 (1969)

41. Lambert, J.D., *Computational methods in ordinary differential equations*, Wiley, London (1973)

42. Latenstein, A. van, J.M. van Langen, "Mischerzpelletierung in IJmuiden", *Stahl und Eisen* 92, 101 (1972)

43. Lebelle, P.A.M., J.J. Kooy, N.A. Hasenack, "The indurating process of pellets on a moving strand", *ISI Meeting on "Mathematical process models in iron and steel making"*, Amsterdam (1973)

44. Libsch, K.A., S.K. Tarby, "Magnetite oxidation in a travelling grate pellet Plant: a computer model", *Metallurgical Transactions* 4, 1347 (1973)

45. Masubuchi, M., "Dynamic response of crossflow heat exchangers", *Preprint 4th IFAC-congress*, Warszawa (1969)

46. McCann, M.J., "Control of distributed parameter systems", *Ph.D.thesis*, Imperial College, London (1963)

47. Mirsepassi, T., "An active-passive electric analog for the solution of transient response heat exchangers", *ISA Transactions* 4, 75 (1965)

48. Mitchell, A.R., *Computational methods in partial differential equations*, Wiley, London (1969)

49. Mozley, J.M., "Predicting dynamics of concentric pipe heat exchangers", *Ind. and Engng Chem.* 48, 1035 (1956)

50. Myers, G.E., J.W. Mitchell, R.F. Norman. "The transient response of crossflow heat exchangers, evaporators and condensors", *ASME Journal of Heat Transfer* 89, 75 (1967)

51. Nusselt, W., "Die Theorie des Winderhitzers", *Zeitschrift des Vereines deutscher Ingenieure* 71, 85 (1927)

52. Nusselt, W., "Die Beharrungszustand im Winderhitzer", *Zeitschrift des Vereines deutscher Ingenieure* 72, 1052 (1928)

53. Paris, J.R., W.F. Stevens, "Mathematical models for a packed-bed chemical reactor", *The Canadian Journal of Chemical Engineering* 48, 100 (1970)

54. Perry, J.H. (ed.), *Chemical Engineers' Handbook*, McGraw-Hill, New York (1963)

55. Rademaker, O., L.H. Goessens, J.H. Voskamp, A.C.P. Debie, "Dynamics and control of a clinker cooler", *Automatica* 6, 231 (1970)

56. Rademaker, O., J.E. Rijnsdorp, A. Maarleveld, *Dynamics and control of continuous distillation units*, Elsevier, Amsterdam (1975)

57. Rademaker, O., J.H. Voskamp, "Some notes on the temperature response of packed beds", *AIChE Journal* 21, 388 (1975)

58. Rosenberg, H.U. von, *Methods for the numerical solution of partial differential equations*, Elsevier, New York (1969)

59. Ross, H.U., A. Ohno, "Shrinkage of iron-ore pellets during agglomeration", in *Agglomeration*, W.A. Knepper (ed.), Wiley, New York (1962)

60. Schmidt, J.R., D.R. Clarke, "Analog simulation techniques for modeling parallel-flow heat exchangers", *Simulation* 17, 15 (1969)

61. Schuchmann, H., "On the simulation of distributed parameter systems", *Simulation* 18, 271 (1970)

62. Schumann, T.E.W., "Heat transfer: a liquid flowing through a porous prism", *J. Franklin Inst.* 208, 405 (1929)

63. Stangeland, B.E., A.S. Foss, "Control of a fixed-bed chemical reactor", *I&EC Fundamentals* 9, 38 (1970)

64. Stermole, F.J., M.A. Larson, "Dynamic response of heat exchangers to flow rate changes", *I&EC Fundamentals* 2, 62 (1963)

65. Szekely, J., R.G. Carr, "On nonisothermal flow of gases through packed beds" *Trans. of the Metall. Soc. AIME* 242, 918 (1968)

66. Vichnevetsky, R., "Use of functional approximation methods in the computer solution of initial value partial differential equation problems" *IEEE* C18, 499 (1969)

67. Vichnevetsky, R., "State of the art in hybrid methods for partial-differential equations", *Proceedings of the AICA/IFIP Congress on Hybrid Computation*, München (1970)

68. Voskamp, J.H., J. Brasz, W. Krijger, "Control analysis of a pellet indurating machine", *Iron and Steel* 45, 635 (1972)

69. Voskamp, J.H., J. Brasz, "Digital simulation of the steady-state behaviour of moving bed processes", *Measurement and Control* 8, 23 (1975)

S T E L L I N G E N

behorend bij het proefschrift van J. Brasz, 11-3-1977

1. Zonder warmtebalans is een mathematisch model ten behoeve van de regeling van een sinterbandproces niet zinvol.

   C.E.Carter, E.Rose, "Control investigations on a non-linear lumped-parameter model of a sintering process", 4th Int. Conf. on Digital Computer Applications to Process Control, IFAC/IFIP, Zürich, March, 1974

2. De nuldoorgangen die Bender [+]) tekent in het Bode diagram van de responsie van een gas-vloeistof kruisstroom warmtewisselaar voor de uittredende gas temperatuur op veranderingen in de intredende vloeistof temperatuur berusten op een foutieve interpolatie van een aantal berekende punten.

   [+]) *E.Bender, "Dynamic response of crossflow heat exchangers for variations in temperature and mass flow", Preprint 5th IFAC-congress, Paris (1972)*

3. In tegenstelling tot hetgeen Van der Grinten [+]) vermeldt, is de dynamica van de vloeistof- en de damp-stroom bij schoteldestillatiekolommen principieel verschillend. De vloeistofstroom moet beschreven worden met behulp van de gesegmenteerde versie van de advectieve transportvergelijking, en de dampstroom door de gesegmenteerde versie van de diffusievergelijking.

   [+]) *P.M.E.M. van der Grinten, Procesregelingen, Prisma Technica 40, Het Spectrum, Utrecht, 1970, pag. 72*

4. Door de introductie van kleine, goedkope IC-versterkers is analoge simulatie van processen met behulp van RC-netwerken weer een aantrekkelijk simulatie-alternatief geworden.

5. Indien het bijvoeglijk naamwoord "optimaal" letterlijk wordt genomen, wekt de term "optimale regeltheorie" (Engels: optimal control) ten onrechte hoge verwachtingen van de kwaliteit van de met behulp van deze theorie afgeleide regelingen.

6. De gewoonte in de procesdynamica om de massa- en energie-balansen direkt op te schrijven voor eindige volumina (segmenten, laagjes, etc.) zonder gebruik te maken van de limietovergang naar de bijbehorende partiële differentiaal vergelijkingen, kan het vinden van een efficiënte numerieke oplossingsmethode in de weg staan.

7. Bij het onderwijs in en in de toepassing van de regeltechniek dient uitgebreid apart aandacht te worden geschonken aan het statisch effekt van regelakties ("statisch regelen") alvorens wordt overgegaan tot een beschouwing over het dynamisch effekt van regelakties ("dynamisch regelen").

8. Voor het berekenen van de oplossingen van partiële differentiaal vergelijkingen met digitale rekenmachines is het gebruik van een specifieke oplossing gebaseerd op een eindige differentie methode vaak sneller en nauwkeuriger dan de numerieke evaluatie van klassieke analytische oplossingen.

9. Het is onjuist om, zoals Groenewold [+]) doet, een onderscheid te maken tussen mikro-, meso- en makro-risiko's op grond van de grootte van de schade van een ongeval ongeacht de bijbehorende kans van optreden.
[+])*H.J. Groenewold, "We moeten kernenergie-maar mag dat wel?", Wetenschap en samenleving 74/8 (1974)*

10. Plaatsing van commerciële advertenties voor boeken in wetenschappelijke tijdschriften dient onder verantwoordelijkheid van de tijdschrift-redaktie plaats te vinden of achterwege te blijven.

11. Een belangrijk en eenvoudig quantificeerbaar kriterium voor de maatschappelijke relevantie van universitair onderzoek is de plaats-baarheid in de maatschappij van afgestudeerden.

12. Het feit dat de zwaarte van sommige betrekkingen gecorreleerd is met het genus van de functie - zoals bijv. bij bibliothecaris/ bibliothecaresse, secretaris/secretaresse - is discriminerend en verwarrend.

J o o s t B r a s z was born in Amsterdam, The Netherlands, in 1945. He studied mathematics and physics at the Free University in Amsterdam from 1963 to 1970. From May 1970 till October 1974 he was employed at the Eindhoven University of Technology as a teaching and research assistent in the Measurement and Control Group of the Department of Technical Physics. Since 1974 he is with CTI/TNO (the Central Technical Institute of the Dutch organisation for applied physical research) as a scientific research fellow of the 50 MW Sodium Component Test Facility at Hengelo (Ov.).